Special Issues: The results from the first five-year 's term (2004 - 2008) of JAMSTEC

– Review –

Review of five years of activity at IFREE/JAMSTEC

Yoshio Fukao[1*], Shuichi Kodaira[1], Masataka Kinoshita[1], Yoshiyuki Tatsumi[1], Naohiko Ohkochi[1], Katsuhiko Suzuki[1], Daisuke Suetsugu[1], Takeshi Hanyu[1], Hiroko Sugioka[1], Shigeaki Ono[1], Kei Hirose[1], Takatoshi Yanagisawa[1], Yozo Hamano[1], Toshiya Fujiwara[1], Hiroshi Kitazato[1], Narumi Takahashi[1], Hide Sakaguchi[1]

The Institute for Research on Earth Evolution (IFREE) consists of five programs. During this five-year period, each program has pursued its own research targets, but at the same time each has made a considerable effort to work with other programs on subjects otherwise not easily approached. By selecting eight such subjects, we review our work in the 2004-2008 period.

Keywords : seismic imaging, arc evolution, ignious province, mantle plumes, subducted slabs, high-pressure experiments

Received 10 April 2009 ; accepted 11 May 2009

1 Institute for Research on Earth Evolution, Japan Agency for Marine-Earth Science and Technology

Corresponding author:
Yoshio Fukao
IFREE, Japan Agency for Marine-Earth Science and Technology
2-15, Natsushima, Yokosuka 237-0061, Japan
+81-46-867-9742
fukao@jamstec.go.jp

Introduction

This article is made up of eight chapters. Each chapter reports on work that has been done collaboratively among different programs. The headings of the chapters are as follows:

§1. Nankai trough seismogenic zone: New insights from seismic imaging, numerical simulation, and scientific drilling

§2. Arc evolution and continental crust formation: An integrated seismic and magmatological assessment at the Izu-Bonin-Mariana intraoceanic arc

§3. Links between Earth's internal activities and surface environment

§4. Mantle plumes beneath the South Pacific: Structure, flow pattern, and geochemical origin

§5. Tracing subducted slabs in the deep mantle

§6. Exploration of the central part of the Earth by high-pressure experiments and analog simulations

§7. Discovery of unknown phenomena in the deep ocean and on ocean floors

§8. Contributions of our research efforts to society and industry

The achievements reported here are closely linked to our efforts on developing technologies in observation and sampling, in analyses of observed and sampled data, and in digital and analog simulations and high-pressure experiments. Efforts in such directions will be reported as 26 original articles in a coming special volume of JAMSTEC-R titled “Development of sample analysis, seafloor observation, geophysical networking, and software development accomplished by the Institute for Research on Earth Evolution, 2004-2008.”

§1. Nankai trough seismogenic zone: New insights from seismic imaging, numerical simulation, and scientific drilling

1-1. Introduction

The Nankai Trough, where the Philippine Sea Plate is subducting beneath the Eurasian Plate, is considered unique because it has a well-investigated recurrence interval and displays rupture zone segmentation of magnitude 8-class earthquakes. For example, tsunami wave and seismic wave modeling studies have shown that the slip of the 1944 magnitude 8 Tonankai event propagated across the Tonankai segment but that no slip extended into the Tokai segment. Over the last five years, IFREE has been conducting intensive active-source seismic surveys in the rupture zones of the Tonankai and Nankai earthquakes. Rupture processes have been examined by numerical simulation in which results of the active-source studies was incorporated to create a realistic seismogenic zone model. In addition to those studies, IFREE took a leadership role in conducting seismogenic zone drilling by the Chikyu, and the first three expeditions were completed in 2008. Seismic imaging, numerical simulation, and scientific drilling will provide several new findings that will become breakthroughs to understanding the generation process of giant earthquakes in the Nankai Trough.

1-2. A cause of the Tokai slow slip revealed by active-source seismic study

A dense Global Positioning System (GPS) network detected an interseismic silent-slip event in the Tokai segment that involved about 2 cm of surface horizontal displacement. This slip was localized in a region of about 60×60 km in the coastal area of the Tokai segment. Similar silent-slip events have occurred in this region episodically over the past 30 years. Silent slips may have been reported in other subduction seismogenic zones, but no structural evidence for the cause of the slips has been documented.

In order to investigate the coseismic and interseismic slip phenomena in the Tokai segment, IFREE carried out an active-source seismic experiment along the 485-km-long onshore-offshore profile. The seismic velocity and reflectivity images show several regions of crustal thickening down to a depth of 45 km, which we interpreted as subducted ridges (Fig. 1-1). In the offshore part of the profile, we recognized subducting ridges at 300 km (the north ridge) and 350 km (the south ridge) with maximum thicknesses of 20 and 12 km, respectively. The ridge structures in the Tokai segment support the rupture propagation of the 1944 Tonankai earthquake. GPS data suggest a strongly coupled region where the back-slip rate is about 35 mm/year in the Tokai segment. The north ridge is situated in the area where strong coupling is predicted. The subducted crust beneath the Japanese island, according to the image, is a highly reflective interface from a depth of 25 to 45 km (Fig. 1-1). A slightly upward doming structure, 2 km high and recognized at 190 to 230 km (Fig. 1-1),

might be attributable to an even deeper ridge system. A landward-dipping zone with a high Poisson's ratio (more than 0.34) is located exactly at the highly reflective subducted crust (Fig. 1-2). Moreover, compilation of the seismic tomography results indicates that, in the Nankai seismogenic zone, the observed landward-dipping zone with a high Poisson's ratio exists only in the Tokai segment, which is where the subducted ridge system is inferred.

We conclude from our structural results and expected critical stiffness inferred from the seismic images that the Tokai silent slip was caused by the zone of high pore fluid pressure in the deeper portion of the locked zone. This zone of high pore fluid pressure is the result of dehydration of the subducted ridge, and it substantially extends the conditionally stable region. Episodic silent slip would make the recurrence interval in the Tokai

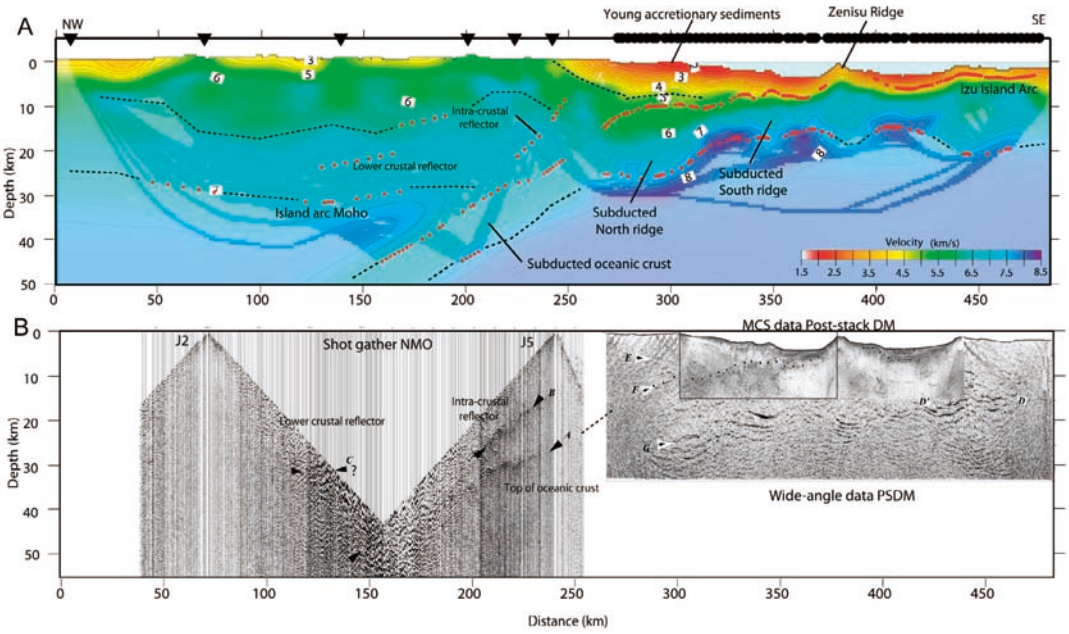

Fig. 1-1. A, seismic velocity image. B, seismic reflectivity image.

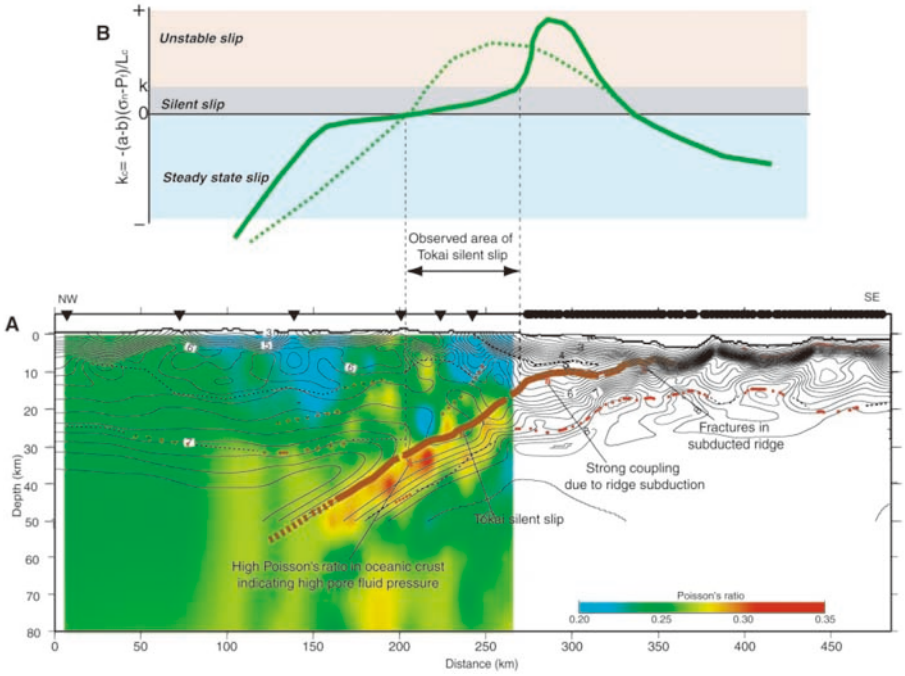

Fig. 1-2. A, Poisson's ratio structure obtained from earthquake tomography superimposed on the seismic velocity structure. B, expected variation of critical stiffness.

segment more complex, because episodic silent slip in the deeper part would cause an increase in shear stress in the strongly coupled region.

1-3. Seismic image of rupture boundary and numerical simulation for rupture synchronization

A giant earthquake occasionally occurs in a subduction zone owing to a simultaneous rupture in adjacent segments that have been previously ruptured by large earthquakes. However, it is still unknown whether a giant earthquake occurs coincidentally, or whether there is a causal factor controlling its generation. In order to image structural factors controlling the rupture segmentation, we acquired three-trough parallel wide-angle seismic profiles crossing the segmentation boundary off the Kii Peninsula (Fig. 1-3). The seismic images show the highly fractured oceanic crust at the seaward part of the segmentation boundary and the high velocity and density domed body in the overriding plate above the deeper part of the segmentation boundary. The highly fractured oceanic crust is identified by discontinuities of 2-3 km offsets at the top and bottom of the crust. The high-velocity ($Vp \approx 6.2$ km/s) body imaged shows it is 70 km in diameter and 8 km high. This body is situated immediately above the subducted oceanic crust and reaches nearly to the seafloor. We interpreted this body to be intruded igneous rock, which has been geologically suggested as the Shionomisaki igneous complex. Because of the expected large excess of normal stress and the shear strength at the high-velocity body, we deduce that there exists a strongly coupled patch at the deeper part of the segmentation boundary.

These two characteristic structures likely control rupture segmentation and synchronization. In order to quantitatively investigate the effects of these structural factors, we performed a numerical simulation on the basis of a rate- and state-dependent frictional law at the seismogenic interface. In this study, we applied realistic plate geometry and lateral variation of frictional parameters that are estimated by the seismic image we acquired. In the area where we found the high-velocity body, we applied a large (b - a)s, which indicates a strong coupling. In the highly fractured zone at the shallow part of the segmentation boundary, we set b = 0, which represents an uncoupled plate.

The numerical simulation incorporating those frictional

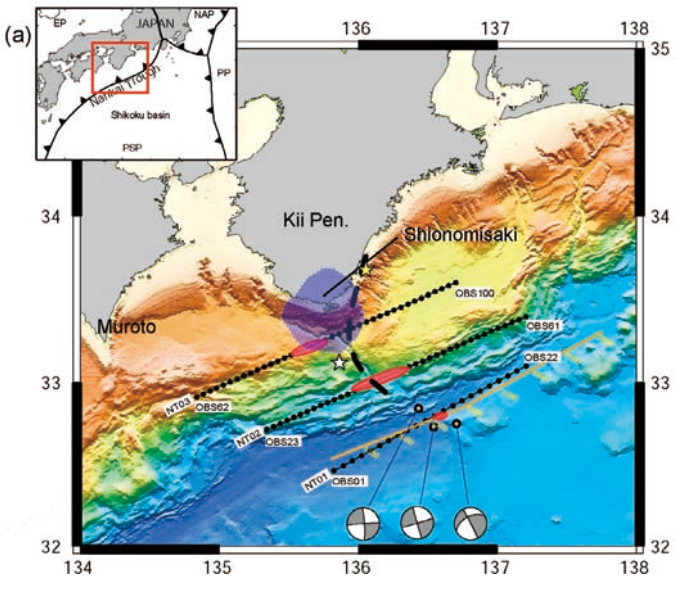

Fig. 1-3. Locations of the wide-angle seismic profiles and the MCS profile (yellow line). Red ellipses on the profiles indicate locations of highly fractured oceanic crust caused by the strike slip fault systems. Light blue patch at Cape Shionomisaki shows the high-velocity and high-density body imaged by this study and a gravity study. Earthquake focal solutions shown are obtained by microearthquake monitoring. White and yellow stars show epicenters of the 1946 Nankai and the 1944 Tonankai earthquakes. Black dots on the profiles indicate OBS locations.

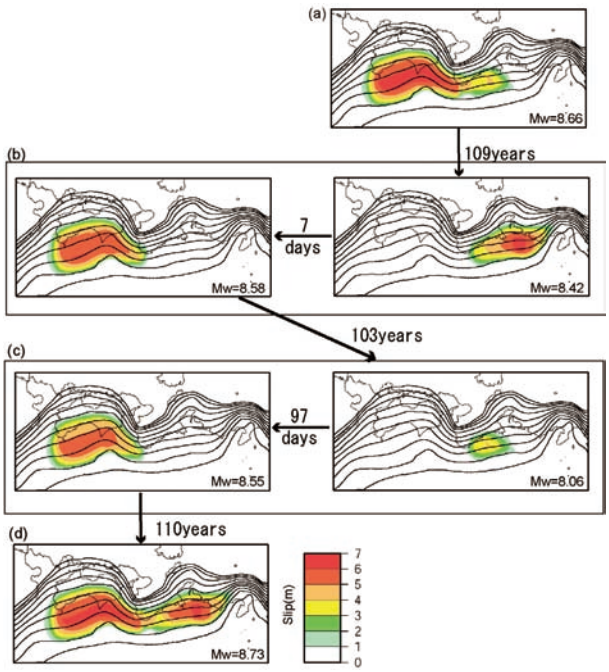

Fig. 1-4. Simulated earthquake history and distribution of earthquake slips whose velocity is more than 1 cmos-1, as obtained by numerical simulation. Rupture segmentations and sequence are (a) Tonankai + Nankai (Hoei type); (b) Tokai + Tonankai (right) and Nankai (left) (Ansei type); (c) Tonankai (left) and Nankai (right) (Tonankai/Nankai type); (d) giant earthquake (i.e., Tokai + Tonankai + Nankai). Mw, calculated moment magnitude.

variations explains the historic rupture patterns in the Nankai Trough (i.e. the rupture segmentations, the recurrence intervals, and the magnitude of the earthquakes) (Fig. 1-4). This result indicates that the structures we imaged in the segmentation boundary off the Kii Peninsula are the key factors in controlling the segmentation and synchronization of the rupture zones. Moreover, the numerical simulation shows the occurrence of a giant earthquake (moment magnitude 8.73) rupturing from the Tokai to the Nankai segment. Detailed analysis of a slip history in and around the segmentation boundary demonstrated that the two types of slow event prior to the giant earthquake are key phenomena for the synchronization of the rupture zones. The slow event or small earthquake occurs before the giant earthquake to release the slip deficit around the rupture nucleation point of the previous earthquake. This event accelerates the very slow event in the strongly coupled patch that reduces a degree of the coupling; consequently the earthquake rupture easily propagates through the segmentation boundary to generate the giant earthquake.

1-4. Coseismic behavior of a seismogenic fault: on-land analog study

The Shimanto and Nobeoka accretionary complexes have been studied in detail as ancient analogs of the Nankai accretionary margin and seismogenic zone.

Pseudotachylites occur in narrow dark veins less than a few millimeters thick, and their microstructure indicates rapid cooling of the frictional melt. Ujiie et al. (2007) suggested that the frictional melt occurred in an illite-rich slip zone with a minimum melting temperature of 1100°C, based on the composition of the pseudotachylite matrix and the characteristics of the unmelted grains and microlites in the matrix. They also inferred a large stress drop along the melted zone, causing an increase in slip rate and enhancing rupture propagation.

Kimura et al. (2007) divided the Nankai accretionary prism into outer and inner wedges and a transition zone; the transition zone shows a large critical taper with a steep surface slope, internal structure of out-of-sequence thrust, and step-down of décollement onto the sediment-oceanic crust interface. They suggest that the deformation and lithification process in the exhumed on-land accretionary complexes is indicative of the step-down of the plate boundary décollement occurring around the up-dip limit of the seismogenic zone.

Analyses of Chelungpu Fault rock for the 1999 Chi-Chi Earthquake were carried out, and knowledge of what happened to the fault gouge zone was greatly improved.

1-5. Nankai Trough Seismogenic Zone Experiments

The NanTroSEIZE Project

The IODP Nankai Trough Seismogenic Zone Experiment (NanTroSEIZE) is attempting to drill into, sample, and instrument the seismogenic portion of a convergent margin subduction zone fault or megathrust within a subduction zone where great earthquakes have repeatedly occurred. The fundamental goal of the NanTroSEIZE science plan is to create a distributed observatory spanning the up-dip limit of seismogenic and tsunamigenic behavior at a location where M > 8 subduction earthquakes occur, thus allowing us to observe the geodetic, seismologic, and hydrogeologic behavior of subduction megathrusts and the aseismic to seismic transition of the megathrust system.

This effort will involve the drilling of key elements of the active plate-boundary system at several locations

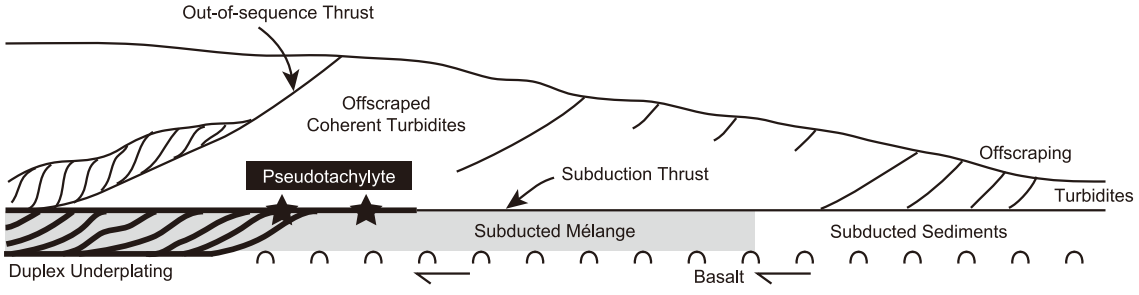

Fig. 1-5. Paleotectonic settings of the pseudotachylite-bearing fault zones (Ujiie et al., 2007).

off the Kii Peninsula of Japan, from the shallow onset of the plate interface to depths where earthquakes occur (Fig. 1-6 and 1-7). At this location, the plate interface and active megasplay faults, both of which are implicated in causing tsunamis, are accessible to drilling within the region of coseismic rupture in the 1944 Tonankai (M = 8.1) great earthquake. The science plan entails sampling and long-term instrumentation of (a) the inputs to the subduction conveyor belt; (b) megasplay faults at 3.5 km below the seafloor, which may accommodate a major portion of coseismic and tsunamigenic slip; and (c) the main plate interface at a depth of up to 6 km.

Studies related to the seismogenic zone along subducting plate boundaries have been lead by the IODP Task Force within IFREE. As well as overall design of the NanTroSEIZE project, preparation for the first drilling stage, including three expeditions, was conducted.

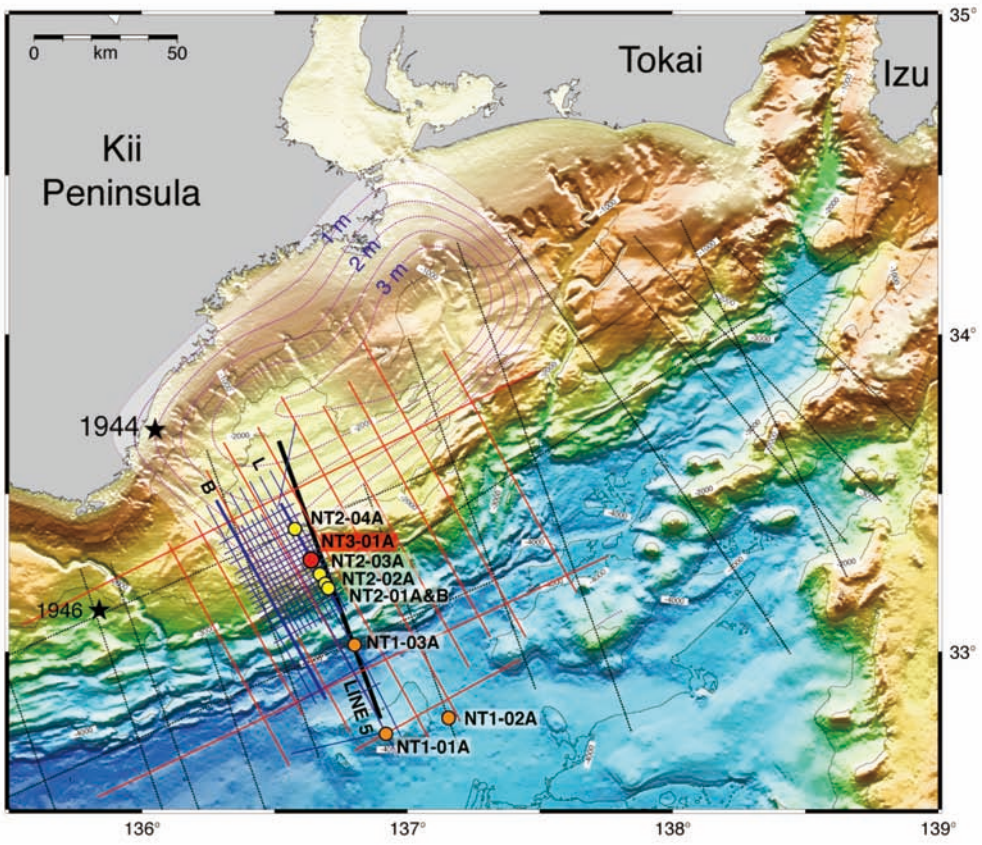

Fig. 1-6. Location of planned drill sites for NanTroSIEZE (colored circles) underlain by IFREE MCS lines and the asperity of the 1944 Tonankai event (Kikuchi and Yamanaka, 2003).

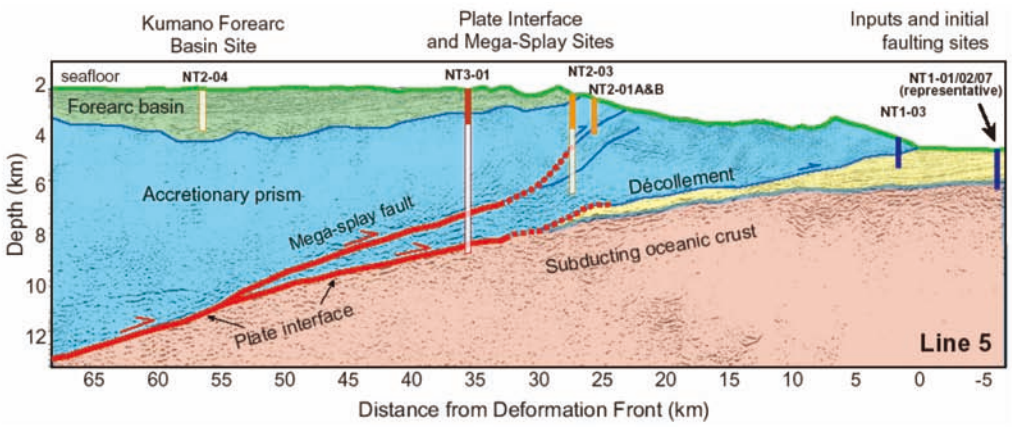

Fig. 1-7. Cross section of planned drill sites plotted on the seismic profile by Park et al. (2002).

Characterization around the drill sites

The Nankai Trough region is among the best-studied subduction zones in the world. It has a 1300-year historical record of recurring and typically tsunamigenic great earthquakes. Land-based geodetic studies suggest that the plate boundary thrust here is nearly 100% locked. Similarly, the relatively low level of microseismicity near the up-dip limits of the 1940s earthquakes (Obana et al., 2005; Fig. 1-8) implies significant interseismic strain accumulation on the megathrust; however, recent observations of very low frequency (VLF) earthquake-event swarms apparently taking place within the accretionary prism in the drilling area (Obara and Ito, 2005) demonstrate that interseismic strain is not confined to slow elastic strain accumulation.

Kasaya et al. (2005) carried out both land and marine magnetotelluric surveys across the coast of the Kii Peninsula and showed the conductive region of 10 Ω-m around the down-dip region of the plate boundary, implying that the pore fluid contributes to megathrust earthquakes. Kinoshita et al. (2008) suggested a possible thermal anomaly in the incoming plate in the Shikoku Basin off Kumano, based on their heat flow results.

Moore et al. (2007) imaged a megasplay thrust system along the Nankai Trough in three dimensions and mapped the splay fault geometry. The thrust geometry and evidence of large-scale slumping of surficial sediments (Fig. 1-9) show that the fault is active and that its activity has evolved

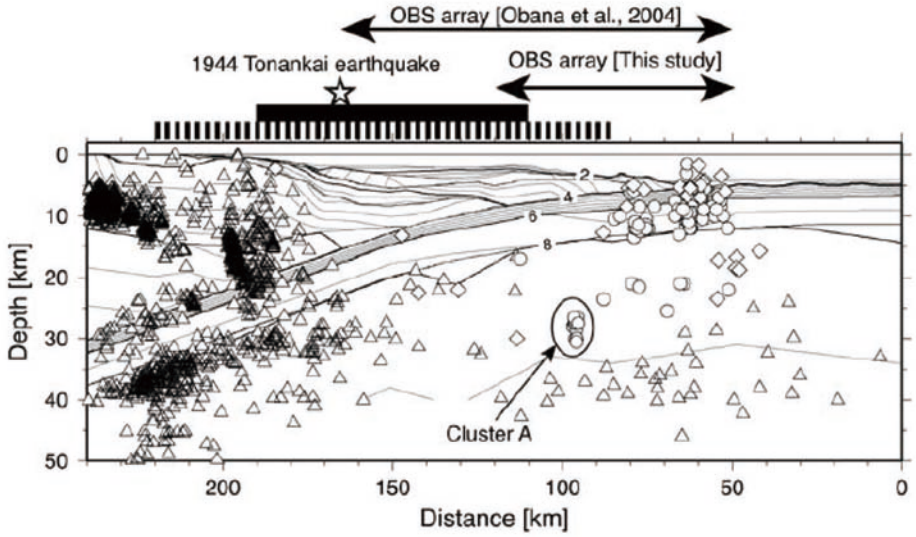

Fig. 1-8. Projected locations of hypocenters observed by the Japan Meteorological Agency (JMA) (open triangles) from January 2001 to July 2003, and two OBS experiments; Obana et al., (2004; open diamonds) and Obana et al. (2005; open circles) (Obana et al., 2005)

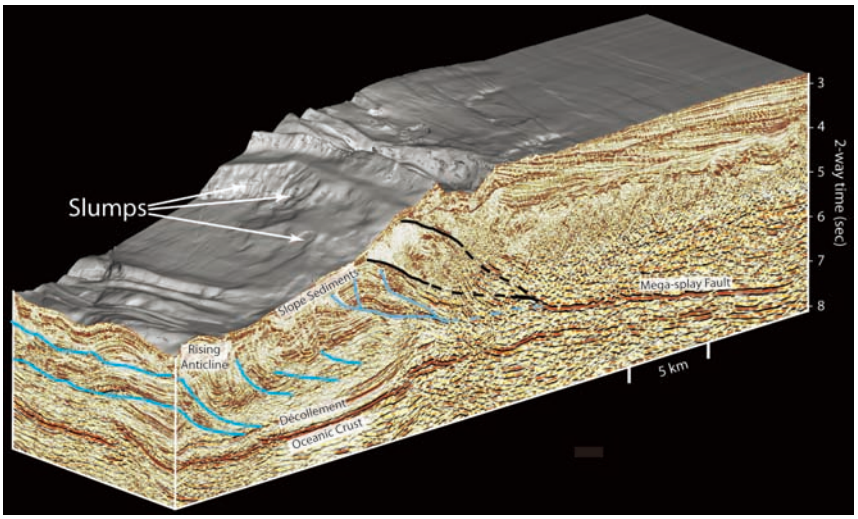

Fig. 1-9. 3-D seismic data volume depicting the location of the megasplay fault (black lines) and its relationship to older in-sequence thrusts of the frontal accretionary prism (blue lines). From Moore G. F., N. L. Bangs, A. Taira, S. Kuramoto, E. Pangborn and H. J. Tobin(2007), Three-dimensional splay fault geometry and implications for tsunami generation, *Science, 318*, 1128-1131. Reprinted with permission from AAAS.

toward the landward direction with time, contrary to the usual seaward progression of accretionary thrusts. They argue that the megasplay fault has progressively steepened, substantially increasing the potential for vertical uplift of the sea floor with slip, and concluded that slip on the megasplay fault most likely contributed to generating tsunamis.

Preliminary result from Stage 1 expeditions

The first stage of the IODP Complex Drilling Project NanTroSEIZE focused on characterizing the shallow portion of the Nankai accretionary prism and seismogenic zone off Kumano. In 2007-2008, a great number of core samples and logging/downhole measurement data were recovered at eight sites drilled by JAMSTEC's D/V *Chikyu* during three expeditions in which more than 70 scientists participated.

Primary targets for Stage 1 expeditions were the frontal thrust region, the midslope megasplay fault region, and the Kumano forearc basin region. Most excitingly, we found several lines of evidence that indicate recent/present activity of the megasplay and frontal thrust faults, although all drill sites were considered to be in the aseismic portion.

Although the interpretation is only preliminary as of this writing, some obtained results, such as borehole breakout images or core fractures, suggest a complex history and spatial variation in the stress field around the drill sites (Fig. 1-10); we believe that both the frontal thrusts and shallow megasplay have been active to the present age, contributing to the evolution of the accretionary prism and seismogenic zone, and to recent earthquake/tsunami generation. More studies on the data obtained, as well as the subsequent drilling operations from 2008, will further reveal the characteristics and dynamics of seismogenic behavior in this region.

Planning the next step: Borehole observatory

Monitoring of interseismic strain as well as seismic and hydrological parameters in the close vicinity of the seismogenic zone is one of our ultimate goals for NanTroSEIZE. The first step toward this goal starts with Stage 2 riser drilling in the Kumano forearc basin. Although it is essential for understanding the mechanism of great earthquakes to know how the interseismic (or even postseismic) strain is being accumulated or partitioned throughout the system, we still do not have the right tools ready to install. This riser hole is dedicated primarily to the installation of a geodetic/seismic/hydrological observatory that is under development at JAMSTEC.

We have been developing borehole observatory systems. Specifically, we are preparing for the first NanTroSEIZE borehole observatory to be installed in 2010, with a special emphasis on the integration of strain and pore pressure measurement.

§2. Arc evolution and continental crust formation: An integrated seismic and magmatological assessment at the Izu-Bonin-Mariana intraoceanic arc

2-1. Introduction

Continental crust occupies only 0.4% of Earth's mass. However, it contains the bulk of the incompatible lithophile elements and possesses differentiated compositions, quite distinct from the chondritic bulk of the Earth. Understanding how continental crust forms is thus essential for comprehending the evolution of the solid Earth. Continental crust has an average composition similar to andesites that typify magmatism at continental arcs. Largely for this reason, continental crust is believed to be created at convergent plate margins. However, modern-day mantle-

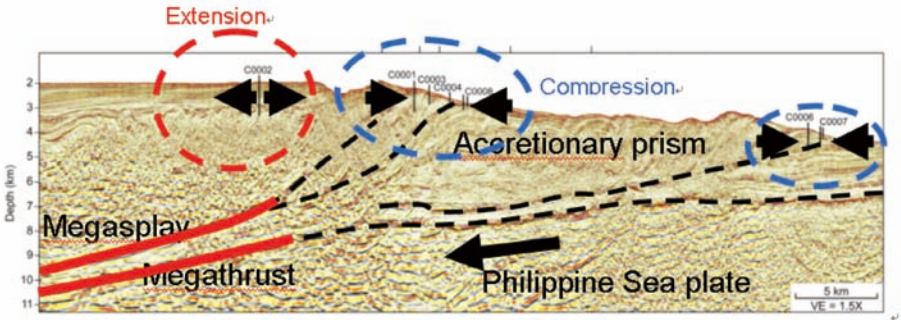

Fig. 1-10. NanTroSEIZE Stage 1 drill sites (C0001-C0008) and stress orientation direction inferred from LWD borehole breakout images (arrows).

derived magmatism in juvenile arcs is dominated by basalt. In order to overcome this apparent dilemma, we have conducted extensive geophysical and petrological surveys at the Izu-Bonin-Mariana (IBM) arc-trench system. The IBM, which extends 2800 km south from Honshu Island (Fig. 2-1), is a superb site for studying arc evolution and continental crust formation because it is a juvenile arc with a well-developed middle crust that exhibits Vp = 6.0-6.5 km/s, values identical to the average Vp of continental crust. We have thus conducted an integrated seismic and magmatological project toward comprehensive understanding of arc evolution and continental crust formation at the IBM.

2-2. Crust and mantle structure

Understanding crust and mantle structure is fundamental to solving key issues concerning processes that create continental crust in an intraoceanic arc setting. To obtain seismic images of the IBM Arc, IFREE conducted intensive active-source wide-angle seismic studies to examine structural variations of the IBM Arc. The seismic profiles we carried out widely cover the Izu-Bonin Arc and part of the Mariana Arc (Fig. 2-1). A cross-arc profile in the Mariana Arc provides general structural characters of each geological unit of the arc-back-arc system (Fig. 2-2): (1) slow mantle velocity of <8 km/s especially in the uppermost mantle, and deep reflectors

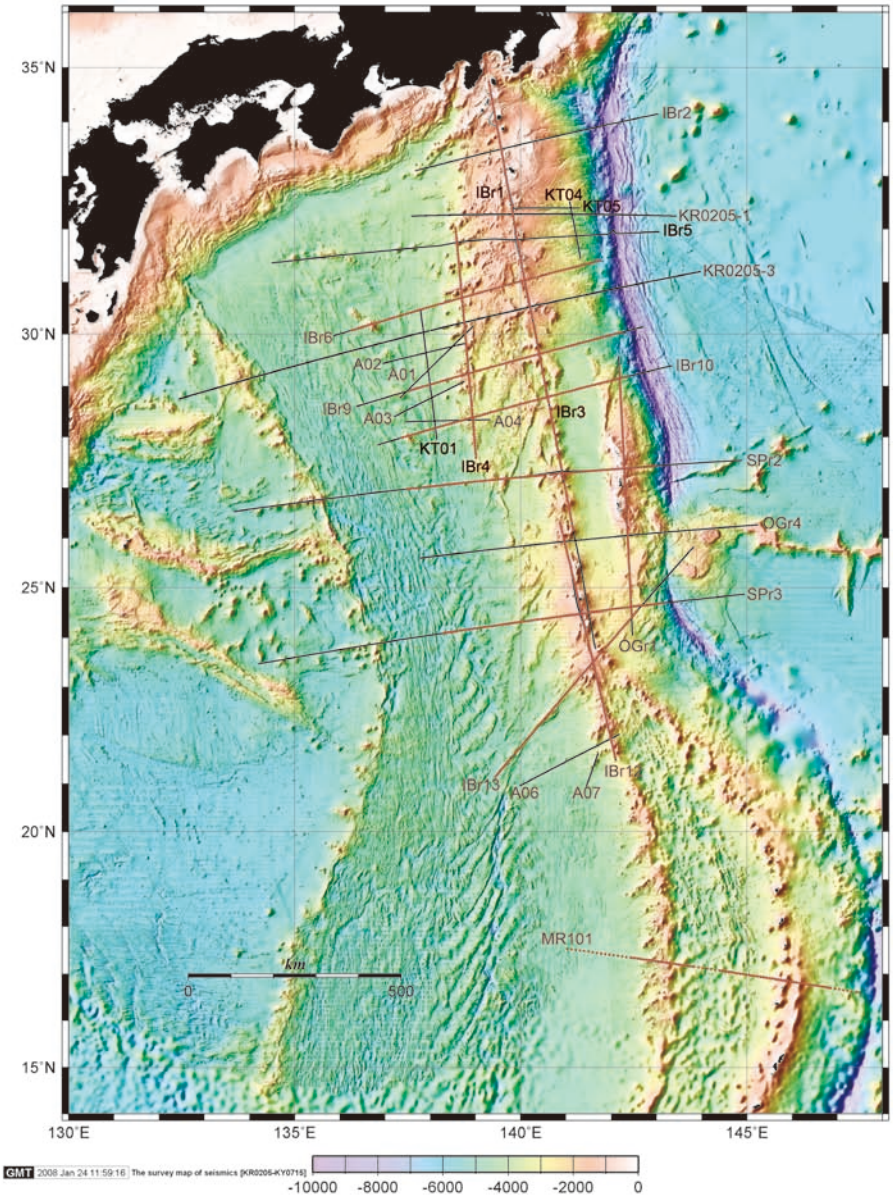

Fig. 2-1. IFREE's active-source seismic profiles at the IBM.

under the Mariana Arc and the West Mariana Ridge; (2) a deep reflector in the upper mantle beneath the relatively thick crust of the Mariana Trough axis; (3) distribution of lower-velocity lower crusts (6.7-6.9 km/s) beneath the volcanic front and adjacent to the Mariana Trough; and (4) high-velocity lower crust (7.2-7.4 km/s) beneath the boundary regions between the Mariana Arc and the Mariana Trench, and between the West Mariana Ridge and the Parece Vela Basin. Of the characteristics described above, petrological modeling described in the next section explained well the origins of the slow mantle velocity and the deep reflectors in characteristic (1).

Further seismological constraints on the evolution process of crust and mantle of the IBM Arc were obtained in a series of seismic profiles made along the arc. A 1000-km-long profile along the volcanic front from the Izu Peninsula to Iwo Jima provides unique along-strike images of arc crust and uppermost mantle to complement earlier cross-arc lithospheric profiles (Fig. 2-3). These reveal two scale (1000-10 km scale) variations, one at the scale of Izu vs. Bonin (thick vs. thin) arc crust and the other at the intervolcano (≈50 km) scale. These images show: (1) bulk composition of the Izu-Bonin arc crust is more mafic than typical continental crust; (2) middle crust with seismic velocities similar to continental crust lie predominantly beneath basaltic arc volcanoes; (3) bulk composition beneath basaltic volcanoes changes little at thick and thin arc segments;

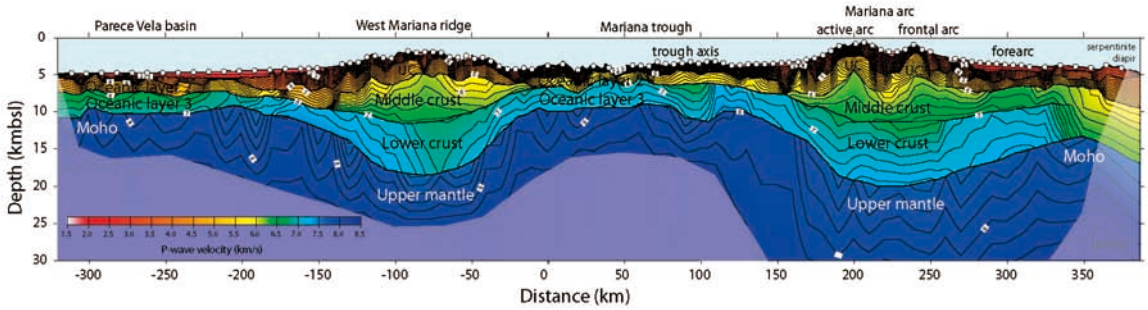

Fig. 2-2. Seismic velocity structure across the Mariana arc-back-arc system. Solid circles indicate ocean-bottom seismograph (OBS) locations. Numerals denote P-wave velocity (*Vp*) (km/s).

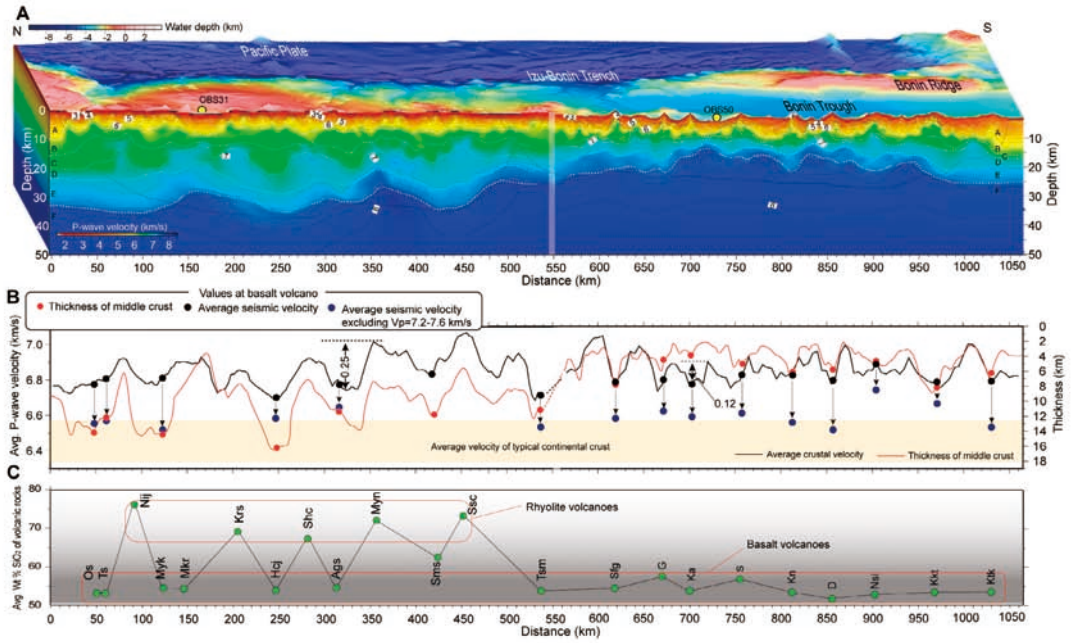

Fig. 2-3. A, Seismic velocity image along the volcanic front from the Izu to the Bonin arc obtained by seismic refraction tomography. B, Average crustal seismic velocity (black line) and thickness of the middle crust (*Vp* = 6.0-6.8 km/s) (red line), which is interpreted to be plutonic rocks of felsic to intermediate composition. Black and red dots indicate average seismic velocities and thicknesses, respectively, of the middle crust beneath basaltic volcanoes. Blue dots show average crustal seismic velocities beneath basaltic volcanoes, but excluding

and (4) a process to return lower crustal components to the mantle, such as delamination, is required for an arc crust to evolve into continental crust. Continued thickening of the Izu-Bonin crust, accompanied by delamination of the lowermost crust, can yield the velocity structure of typical continental crust.

One of the unique tectonic processes in the Izu-Bonin Arc is a repeated rifting process, which may be preserved in the back-arc/rear-arc area. A profile along the rear arc of the Izu Arc revealed new seismological evidence of a past rifting process. A resultant seismic image of the rear arc shows marked variations of crustal thickness along the seismic profile: thin (10-15 km) crust in the northern part, three discrete thick (20-25 km) crustal segments in the central part, and a moderately thick (≈ 15 km) crust in the southern part (Fig. 2-4). These variations are mainly attributed to thickness variations of the middle crust having seismic velocity of 6.0-6.8 km/s. This variation of crustal thickness does not correlate with seafloor topography, which is characterized by post-Miocene across-arc seamount chains. It does correlate well with crustal variations observed along the present-day volcanic front of the Izu-Bonin Arc. These findings suggest that the magmatic activity that created the across-arc seamount chains had little effect on the rear-arc crust and that the main part of the rear-arc crust was created before the rear-arc separated from the volcanic front. By correlating the structural variations along the rear-arc (i.e. the variation of the average seismic velocity as well as the thickness of the middle crust) and those along the present-day volcanic front, we found that the direction of rifting to separate the rear-arc (paleo-arc) from the present-day volcanic front was north-northeast.

2-3. Arc evolution via crust-mantle transformation across the transparent Moho

The evolution of arc crust and subarc mantle in the Izu-Bonin-Mariana (IBM) intraoceanic arc system was examined by petrological modeling of arc magma generation and differentiation. Characteristic seismic structural features of the IBM Arc highlighted in this modeling include the presence of (1) a middle crust with a *Vp* of 6.0-6.5 km/s; (2) a 6.5-6.8 km/s *Vp* layer at the top of the lower crust; (3) a high-velocity (*Vp* = 6.8-7.2 km/s) lower crust; and (4) an uppermost mantle exhibiting rather low velocities (*Vp* = 7.4-7.7 km/s) (Fig. 2-5).

The formation of the middle crust, which is considered to have an intermediate composition, was explored via two models: (a) a mantle-derived basalt model involving anatexis of the initial mafic lower crust or mixing of mantle-melting-derived basaltic magma with crust-melting-derived felsic magma; and (b) a mantle-derived andesite model involving differentiation of boninitic magma. In

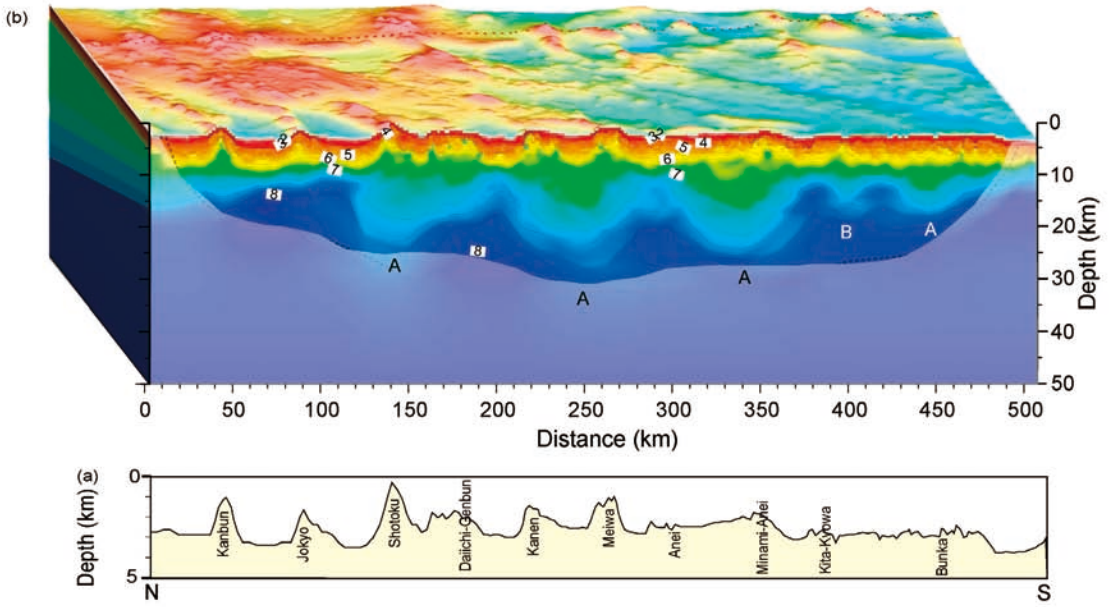

Fig. 2-4. (a) Seafloor topography along the profile. The names of the seamounts close to the profile are labeled.
(b) Final seismic velocity image. The shaded area indicates a poorly resolved area identified by the checkerboard test.

order to examine the crust/mantle structure, end-member compositions appropriate for the IBM Arc were used, including representative basalt, rhyolite, andesite, tonalite, and peridotite, together with an experimentally inferred melting/crystallization regime (Table 2-1).

The *Vp* calculated for the inferred composition for each layer of the IBM crust on the basis of the basalt model is consistent with the observed values, whereas the andesite model cannot account for the characteristic *Vp* of the middle crust, the uppermost lower crust, and the uppermost mantle (Fig. 2-6).

The results further suggest that the volume of mafic restite and cumulates that are crustal residues resulting from the evolution of middle and upper arc crust is at least three to nine times greater than that of the seismically defined IBM lower crust (Fig. 2-7). One possible explanation that could overcome this apparent dilemma is that mafic to ultramafic crustal components are transformed to subarc mantle. During this process, the subarc Moho is chemically transparent and permeable to the crustal components. The subarc Moho could be the boundary between the remaining initial basaltic arc crust (above) versus melting residues or restites (below). If so, the Moho represents the former melting front during crustal anatexis (Fig. 2-8). This crust-mantle transformation, which transfers the mafic to ultramafic component to the mantle, could play the major role in the creation of mature and differentiated arc crust from the mafic initial arc crust (Fig. 2-8). It should be further stressed that a density inversion may be caused by garnet stabilization at the base of the low-velocity upper mantle restite layer (light blue in Fig. 2-6). This gravitational instability may result in the delamination of the overlying dense mafic, restitic component, which would contribute to formation of a deep-mantle geochemical reservoir.

The model proposed here provides a comprehensive explanation for the crust/mantle structure of the IBM Arc, the temporal development of arc crust, and the general formation of continental crust. It should be stressed, however, that this model depends strongly on inferred compositions of the upper crust and middle crust. In order to test the model and to further develop the concept of arc evolution, direct sampling from both the entire upper crust and the middle crust of the IBM Arc must be achieved.

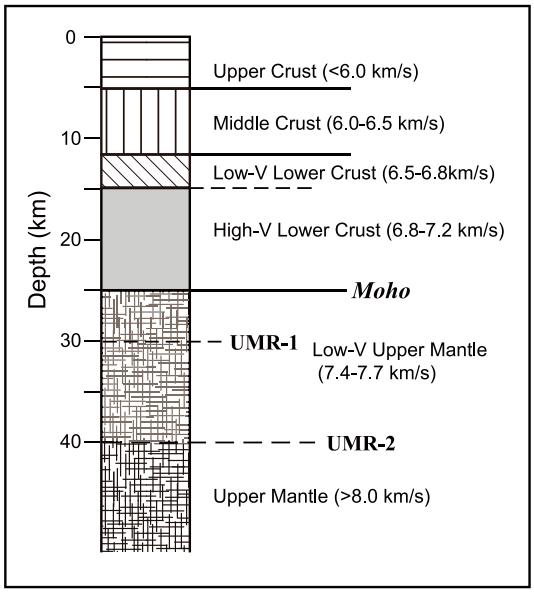

Fig. 2-5. Generalized seismic velocity structure in the IBM after Suyehiro et al. (1996), Takahashi et al. (2007a, b), and Kodaira et al. (2007). The subarc Moho in the IBM is identified based on a combination of the distribution of seismic reflectors, the velocity jump across (from 6.8-7.2 to 7.4-7.7 km/s), and the continuity from the well-defined "normal" Moho beneath the back-arc basins of the IBM. Seismic reflectors are also observed within and at the base of the low-velocity domains in the uppermost mantle (UMR-1 and UMR-2).

Table 2-1. Compositions of magmas, cumulate, and restites

	PM	CM	DB	AMA	AMM	DBN	PBN	FMI	RTA	RTFI	UCFM	RTFA	RTFM	RTFB	HB
SiO_2 (wt.%)	47.8	40.1	50.0	60.0	60.0	60.1	57.7	75.0	45.7	47.2	75.0	53.6	53.6	53.7	45.4
TiO_2	0.6		0.8	0.6	0.6	0.2	0.3	0.3	0.9	0.9	0.3	0.7	0.7	0.1	
Al_2O_3	14.9		19.1	18.1	17.1	12.9	11.1	14.0	19.5	19.7	13.0	20.3	18.8	12.9	
FeO*	10.9	13.4	10.2	6.8	6.9	7.9	8.8	2.0	11.7	11.1	2.2	8.8	8.9	10.3	5.7
MgO	14.9	46.5	6.0	3.1	3.7	8.9	12.3	0.2	7.2	6.6	0.2	4.3	5.2	12.6	48.9
CaO	9.5		12.1	7.6	8.5	7.3	7.8	3.0	14.0	13.1	3.3	9.4	10.7	9.1	
Na_2O	1.2		1.6	3.3	2.8	2.2	1.6	4.5	0.9	1.3	4.8	2.7	1.9	1.1	
K_2O	0.2		0.2	0.5	0.5	0.5	0.4	1.0	0.1	0.1	1.2	0.2	0.2	0.3	
Total	100.0	100.0	100.0	100.0	100.0	100.0	100.0	100.0	100.0	100.0	100.0	100.0	100.0	100.0	100.0
H_2O			0.1	0.3	0.3	5.0	5.0								

PM, primary magma; CM, cumulate; DB, differentiated basalt produced by 22% separation of cumulate from PM; AMA, andesitic magma produced by 30% melting of DB; AMM, andesitic magma produced by mixing between DB and FMI; DBN, differentiated boninite; PBN, primitive boninite; FMI, felsic magma produced by 10% melting of DB; RTA, restite after AMA production; RTFI, restite after FMI production; UCFM, felsic magma produced by 20% melting of AMA , AMM, or DBN; RTFA, restite after UCFM production from AMA; RTFM, restite after UCFM production from AMM; RTFB, restite after UCFM production from BON.

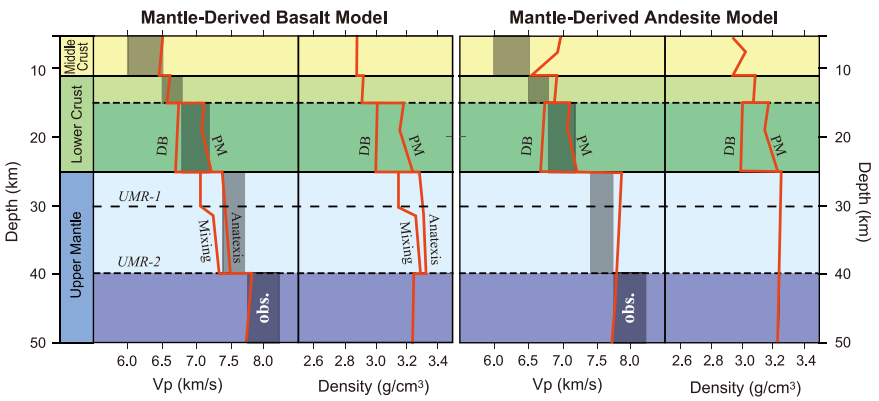

Fig. 2-6. *Vp* and density calculated for the inferred lithologies in sub-IBM crust and mantle (red lines) along a moderate-T geotherm. The mantle-derived basalt model, especially the anatexis model, provides *Vp* consistent with the observed *Vp* (dark regions; obs.). The mantle-derived andesite model exhibits *Vp* higher than the observed values for the middle crust, the top layer of the lower crust, and the uppermost mantle layers. The density inversion is predicted within the uppermost mantle in the basalt model. DB, differentiated basalt; PM, primary basalt.

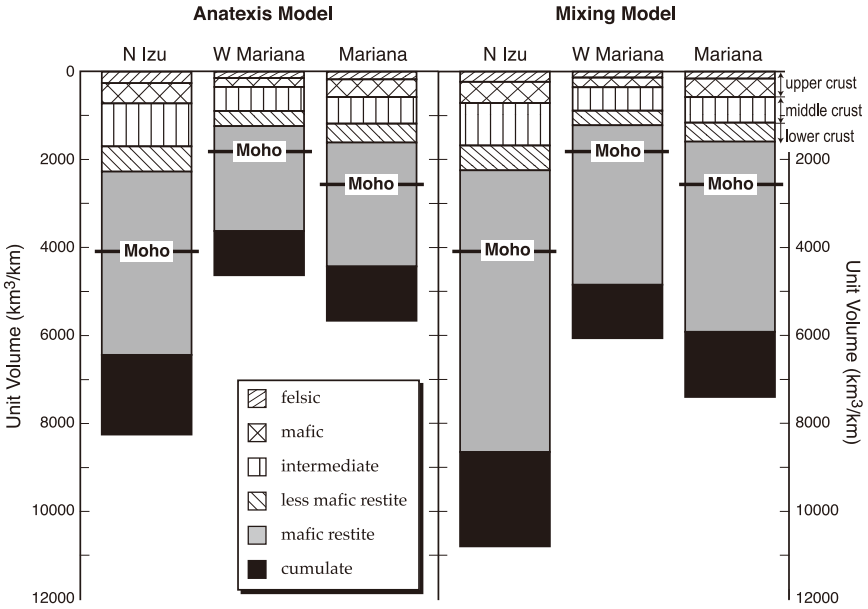

Fig. 2-7. Unit volume of each layer of the IBM crust across three cross-arc sections: Northern Izu, Western Mariana, and Mariana. Volumes of mafic restite and cumulate layers are calculated based on the observed volume of upper and middle crust and the low-velocity (less marif) layer at the top of the lower crust. The seismically determined Moho is located within the mafic restite/cumulate layer, thus the "crustal excess" is distributed in the upper mantle beneath the Moho in the IBM system.

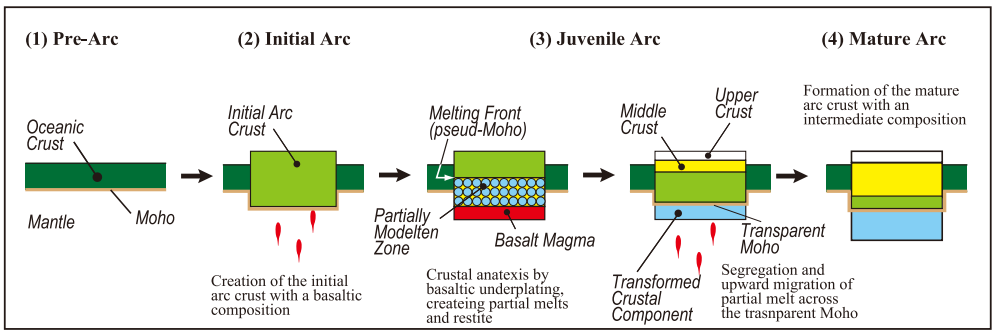

Fig. 2-8. A model of arc crust evolution. Incipient arc magmatism replaces the preexisting oceanic crust to create the initial basaltic arc crust. Successive arc magmatism causes anatexis and differentiation of the arc crust, along with upward migration of intermediate melts across the pseudo-Moho and transformation of mafic crustal component into the mantle. This finally creates mature arc crust with an intermediate composition similar to average continental crust.

§3. Links between Earth's internal activities and surface environment

Over at least the last 3.5 billion years, Earth's history has been punctuated by massive volcanism. It generated large volumes of predominately mafic magmas that were emplaced onto the Earth's surface by processes and mechanisms largely unknown and unrelated to seafloor spreading or subduction. These formed large igneous provinces (LIPs) that were usually accompanied by catastrophic environmental change. Environmental effects associated with LIP formation include global warming, biological mass extinctions, and variations in ocean and atmospheric chemistry, including oceanic anoxic events (OAEs), which are characterized by deposition of organic-rich black shales. Therefore, the mantle geodynamic processes that produce LIPs have potentially profound effects on the Earth's biosphere and climate. These massive volcanisms are recorded in oceanic sediments and sedimentary rock. One successful research effort is related to the Earth's surface environment around OAE-1a and OAE-2, which occurred around 94 and 124 Ma, respectively, when volcanic activities were also enhanced.

The mechanism connecting LIP emplacement and OAE formation in the Cretaceous has been investigated with multidisciplinary collaboration among members of IFREE-4 and IFREE-5. Of these collaborations, a project measuring carbon, lead, and osmium isotopic compositions of a sedimentary sequence around OAE-1a (the Selli Event) provided strong evidence that LIP formation ultimately triggered OAE (Tejada et al., revised; Kuroda et al., in prep.). Based on age determinations of basaltic rock, it has long been known that the timing of the formation of the Ontong Java Plateau (OJP), the largest LIP ever formed, is 126-119 Ma, which is close to the timing of OAE-1a (≈124 Ma). Therefore, it has been discussed whether or not the events are mechanically connected.

We first determined osmium isotopic composition ($^{187}Os/^{188}Os$ ratio) for the sedimentary sequence that includes OAE-1a black shale deposited in the western Tethys with temporally high resolution. At the lowest level of OAE-1a black shale, we observed a sharp, large negative shift of Os isotopic compositions down to 0.16 (Fig. 3-1) throughout the OAE-1a sequence, suggesting that the isotopic composition of Os dissolved in seawater substantially decreased during that time. The marine Os

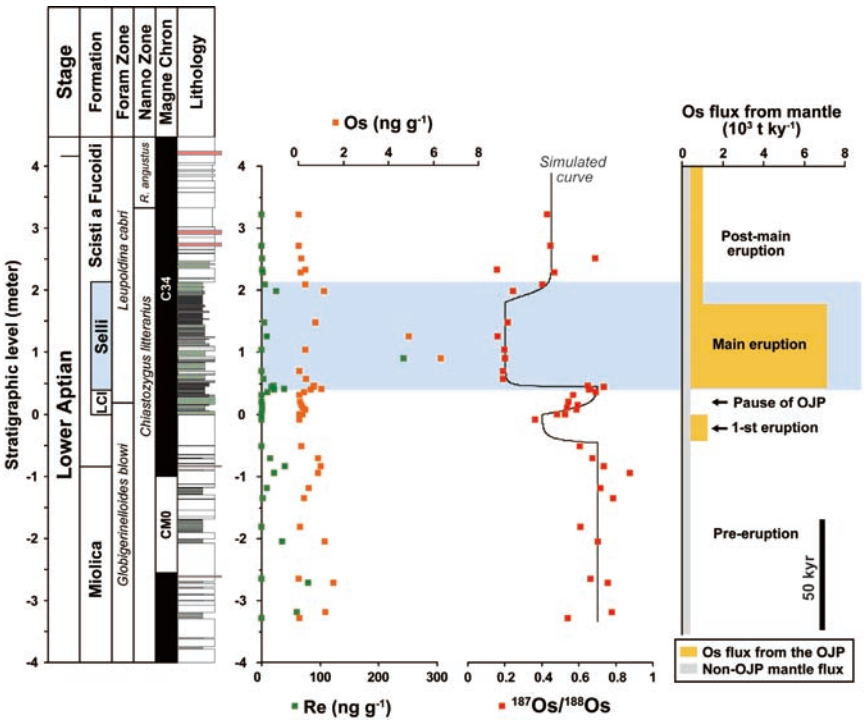

Fig. 3-1. Osmium (red) isotopic compositions, Os (orange) and Re (green) abundance in the sedimentary sequence from central Italy (Tejada et al., accepted). OAE-1a (the Selli Event, blue zone) around 124 Ma is temporally correlated with a negative isotopic excursion of Os, which may be related with the eruption of the Ontong Java Plateau, a large igneous Pacific province. Estimated Os flux from the mantle based on a one-box model is shown in the right diagram.

isotopic record is a function of changes in the balance among three major sources of inputs to the ocean and an output to sediment. The mantle and cosmogenic inputs are unradiogenic with an Os isotopic composition of 0.12-0.13. This implies that the extensive volcanism (probably associated with the OJP formation) simultaneously occurred with the formation of OAE-1a. Based on the simple one-box model calculation, more than 2×10^6 t Os had to be released from the mantle to the ocean.

This observation/interpretation is consistent with what we have done at OAE-2 (94 Ma) using lead and carbon isotopic compositions (Kuroda et al., 2007). Around 94 Ma, Caribbean/Madagascar LIPs expelled a large amount of magmas in a short period of time. Therefore, our efforts during the last several years led us to the conclusion that the massive volcanisms associated with LIP emplacement should have caused significant perturbation of biogeochemical cycles in the atmosphere-ocean system.

Although our observations strongly imply that LIP emplacement ultimately triggered OAE, we still do not understand how we can connect these events. Extensive emission of CO_2 and eolian dust to the ocean-atmosphere system associated with the massive volcanism, and subsequent climatic change, may be an important process to bridge these events. One-dimensional ocean modeling is being constructed and evaluated for the above process (Misumi, 2007).

During the mid-Cretaceous, OAEs repeatedly occurred, and organic-rich black-colored sediments (i.e. black shales) were widely deposited. We have intensively studied biomarker (i.e. organic molecules originating from a specific group of organisms) composition in the black shales to reconstruct the oceanic environment during the OAEs. During the last several years we have developed a novel method for isolating/purifying alkyl porphyrins, tetrapyrroles derived from chlorophyll nuclei from the sediment (Fig. 3-2; Kashiyama et al., 2007a), for assigning chemical structures with nuclear magnetic resonance and X-ray crystallography (Kashiyama et al., 2007b), and for determining both carbon and nitrogen isotopic compositions of these molecules (Kashiyama et al., 2008; Ogawa et al., patent pending). Since these molecules contain four nitrogen atoms, they carry crucial information on the nitrogen cycle in the euphotic zone of the water column.

In fiscal 2007, we extensively applied the method to Cretaceous black shales to understand the surface ocean ecology and environment during the OAEs. The nitrogen isotopic compositions of most alkyl porphyrins from black shales in OAE-1a and OAE-2 range from -8 to -2 per mil (Fig. 3-3). The isotopic results strongly suggested that the diazotrophic (i.e. N2-fixing) cyanobacteria were major drivers to fertilize the euphotic zone of the surface ocean during the OAEs (Ohkouchi et al., 2007; Ohkouchi et al., 2008; Kashiyama et al., 2008). Furthermore, we observed abundant highly branched isoprenoids (HBI) derived from rhizosolenid diatoms in these black shales. These observations along with other varied geological evidence lead us to hypothesize that the symbiosis between diazotrophic cyanobacteria (*Richelia* spp.

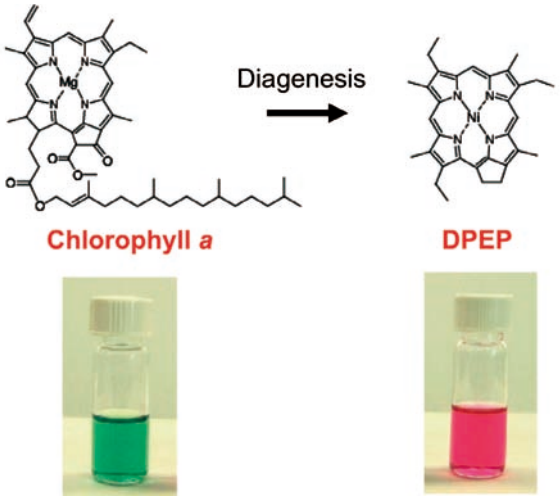

ig. 3-2. Chemical structure of chlorophyll a and porphyrin diagenetically derived from the nucleus of chlorophyll *a*. Photos of isolated chlorophyll *a* from modern higher plants (left, lower) and porphyrin (Deoxoerythroetioporphyrin) from Cretaceous black shale (right, lower) are also shown.

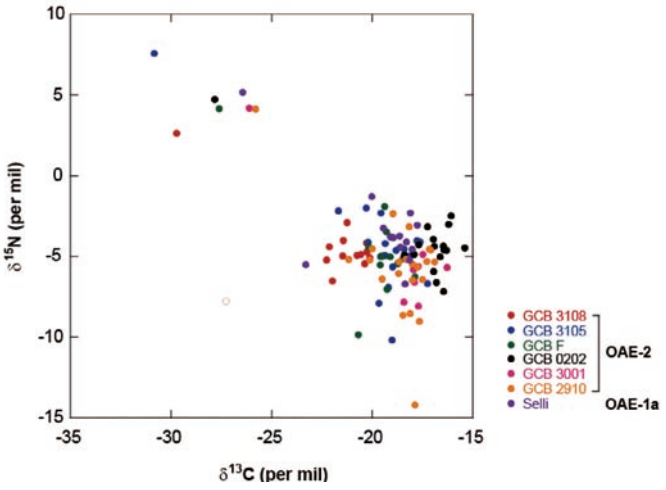

Fig. 3-3. Carbon and nitrogen isotopic compositions of various species of alkyl porphyrins isolated from OAE black shale samples (OAE-1a and OAE-2) collected from central Italy. The nitrogen isotopic compositions of most porphyrins range -5 to -3 per mil, suggesting they are derived from an N_2-fixation process.

or *Hemiaulus* spp.) with rhizosolenid diatoms may have played an important role in the biological productivity in the stratified oligotrophic ocean during the OAEs. Furthermore, in collaboration with CDEX in JAMSTEC, we are currently planning a D/V *Chikyu* cruise to evaluate drilling technologies for recovering chert/shale (hard/soft) sequences. Despite many drilling efforts by DSDP/ODP during the last 30 years, they largely lack Cretaceous strata, especially for OAE black shales, because of very low recovery due to the laminated chert sequences. Therefore, a novel drilling technology is essential for investigating Cretaceous OAEs in the pelagic Pacific Basin, which is as yet largely unexplored. We plan to overcome the low-recovery problem by using the state-of-the-art drilling technology of the D/V *Chikyu*. The influence of oceanic environments related to the formation of the Ontong Java Plateau, the largest LIP ever found and which formed simultaneously with the OAE-1 and the onset of the Cretaceous superchron, will be a primary focus of this drilling.

§4. Mantle plumes beneath the South Pacific: Structure, flow pattern, and geochemical origin

4-1. Introduction

The South Pacific region is characterized by a superswell elevated up to 700 m in a 3000 km × 3000 km area and a concentration of midplate volcanoes called hot spots. These hot spots include Society, Macdonald, Marquesas, Pitcairn, and Arago, which form island chains with a short age progression of 4-6 Ma. They produce oceanic island basalt (OIB) with enriched mantle signatures, suggesting an origin deep in the mantle. This region experienced massive eruptions that produced large oceanic plateaus such as Ontong Java in the mid-Cretaceous Period. These phenomena all suggest the presence of major hot mantle upwelling, which leads to the hypothesis of a superplume in the deep mantle beneath the South Pacific, but its size, origin depth, and even presence remain controversial. We review recent progress on the South Pacific mantle plumes made by IFREE.

4-2. Seismic image of the superplume and narrow plumes

So far, knowledge of the detailed structure of the mantle beneath the South Pacific has been limited mainly because of a lack of seismological data to investigate the mantle. Seismic stations have been sparse in the area due to its remoteness and oceanic environment. To obtain a better seismic image of the superplume, we conducted a Japan-France cooperative research project: The Japanese side (IFREE and ERI/University of Tokyo) and the French side (LDG, UPF, CNRS, and IPGP) deployed 20 temporary broadband seismographs on the seafloor and on islands in the South Pacific, which enabled the highest spatial resolution that has ever been achieved for the mantle structure beneath the region (Fig. 4-2a). We obtained an upper-mantle S-velocity model with surface wave tomography, topography of the 410-km and 660-km discontinuities with a P-wave receiver function method, and a lower-mantle P-velocity model with P-wave travel time tomography. The seismic image thus obtained (Fig. 4-1) indicates that large-scale low-velocity anomalies, on the order of 1000 km in diameter, called a superplume, are located from the bottom of the mantle to 1000 km in depth, and small-scale low-velocity anomalies, on the order of 100 km in diameter, are present above it. A comparison of seismic images and recent mantle convection studies by laboratory and numerical experiments indicates that the superplume may be a hot and chemically distinct mantle dome and that the small-scale anomalies may be narrow plumes generated from the top of the dome. The experiments show that the secondary plumes are generated in a sporadic manner and do not last long, which may explain the short age progressions for the hot spots in this region. The secondary plumes should entrain chemically distinct superplume materials, which may be the origin of the enriched mantle signature found in the South Pacific OIB. The superplume or dome may be oscillating vertically, as shown in the laboratory experiment, which should cause cyclic volcanic activity in the South Pacific. The massive volcanic activity responsible for the large oceanic plateaus in the Cretaceous Period may have occurred when the superplume rose to the shallow upper mantle, and the relatively quiet conditions at present may be because the superplume is located deep in the lower mantle.

4-3. Seafloor swell dynamically supported by mantle plumes

The South Pacific seafloor has swells associated with the hot spots, the wavelength of which is several hundred kilometers. The origin of the swell is not well understood.

It may be due to dynamic support by mantle plumes or due to plate reheating by plumes. The high-resolution seismic model obtained by the seafloor deployment of broadband stations described above enabled a quantitative discussion on the relationship between the swell topography and a mantle flow pattern. We calculated mantle flow pattern expected from a 3-D density model of the mantle in order to ascertain whether the swell can be attributed to dynamic support by mantle plumes. The density model was obtained from the upper-mantle S-velocity model shown in Fig. 4-1 using an appropriate conversion factor. We used a two-layered viscosity model composed of a highly viscous lithosphere and a less viscous (by two orders) asthenosphere. Instantaneous mantle flow was then calculated by solving the conservation equations of mass and momentum under the Boussinesq approximation. The topography dynamically induced by mantle flow (dynamic topography) was obtained from the computed mantle flow. We obtain an excellent correlation between the observed and the modeled dynamic swells (Fig. 4-2), which indicates the hot-spot swells are dynamically supported by mantle plumes. Fig. 4-3 shows the modeled flow pattern with locations of active volcanism. It appears that some hot spots are located directly beneath the ascent of a mantle plume (e.g., Society) and others are not (e.g., Macdonald). The latter hot spots may be generated due to a lateral flow under the lithosphere induced by the ascent of mantle plumes. The buoyancy fluxes of the mantle plumes, which represent the strength of a plume, were also computed from the mantle flow model. The buoyancy fluxes obtained from the flow model are consistent with those obtained from swell morphology at the surface. From the buoyancy flux, we can infer that the mantle plumes beneath the Society hot spot and the Macdonald hot spot are significantly stronger than other plumes, suggesting a deeper origin. The present study indicates that a direct link exists between the surface observations (hot-spot swells) and mantle flow.

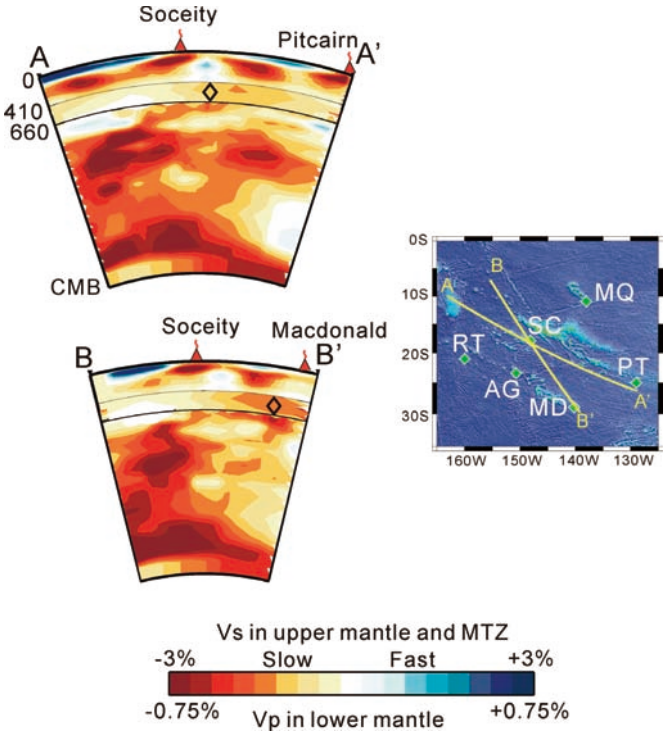

Fig. 4-1. Cross sections of seismic structure in the entire mantle. S-wave velocities are shown for the upper mantle (0-66 km). S-waves at depths of 410-660 km are taken from a global model by Ritsema and Heijst (2000). P-wave velocities are shown for the lower mantle (660-2900 km). Velocity scales are ±3% in the upper mantle and ±0.75% in the lower mantle. Diamonds plotted in the MTZ indicate the locations of significantly thinned MTZ. Positions of the profiles are given in the right-bottom panel. Circles plotted in the MTZ (410-660 km) are locations of MTZ thickness estimated near the profiles within 2.5°, where red and blue represent thicker and thinner than the global average, respectively, and the size is proportional to the deviation from the average.

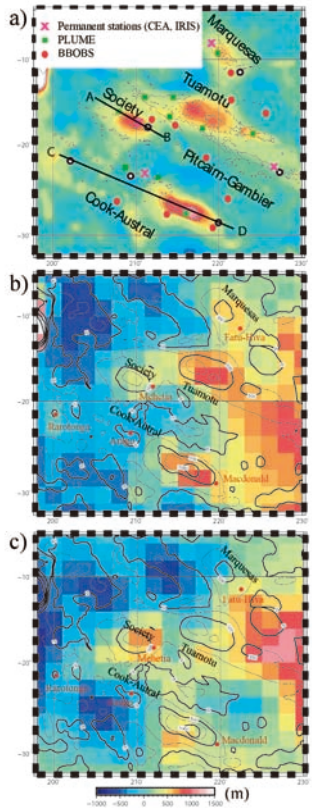

Fig. 4-2. French Polynesia swells: (a) The color map represents the observed swells. The open circles represent the location of active volcanism. The AB and CD profiles are used to make depth cross sections. Red and green symbols denote BBOBS and PLUME stations, respectively, and pink crosses are permanent stations. (b) Observed swells with age correction and 2° × 2° sampling. The original swells (a) are shown with isocontours. The red dots represent the location of active volcanism. (c) Dynamic topography.

4-4. Geochemical origin of hot spot magma

French Polynesia is a unique place from a geochemical point of view for the following reasons. First, volcanic rocks from several hot spots show large variations in isotopic and trace element compositions, suggesting that the source region of the mantle plumes beneath French Polynesia includes several mantle reservoirs (endmembers), such as HIMU, EMI, and EMII. Second, volcanoes on a single hot-spot track show temporal compositional changes, indicating small length-scale heterogeneity in the source regions. In order to elucidate the processes that form those mantle reservoirs and the modes of mass transport, storage, and mixing of the materials in the convecting mantle, we need to refine geochemical constraints on the mantle reservoirs by applying novel analytical techniques on hot-spot volcanic rocks.

Here, we present one of the studies on the HIMU endmember, which is characterized by extremely radiogenic Pb isotopes. The HIMU rocks were collected from Mangaia, Rurutu, and Tubuai in the Cook-Austral Archipelago. In addition to conventional whole-rock analyses, clinopyroxene and olivine separates were used for Sr-Nd-Pb-Hf and for Os isotopic measurements, respectively. We found that isotopic data obtained from clinopyroxene display clear correlation trends in Sr-Nd-Hf isotopic space (Figs. 4-4a-c), which could not be observed by whole-rock analyses. Clinopyroxene crystallized earlier and thus preserved less modified isotopic information in contrast to whole rocks, which may have been modified by shallow-level contamination by oceanic crust, sediment, or seawater. The clinopyroxene data obtained demonstrate that the HIMU magmas were produced by mixing between two components, HIMU and the depleted mantle (Fig. 4-4). Nd and Hf isotopic compositions of HIMU should be less radiogenic (more enriched) than previously thought, because the HIMU endmember should be more unradiogenic than the observed lavas. Os isotope data using olivine also provide a tight constraint on HIMU. Os isotopic compositions of magmas are uniform irrespective of Os content and other radiogenic isotopic compositions, and therefore this value is indigenous to the HIMU source (Fig. 4-4d).

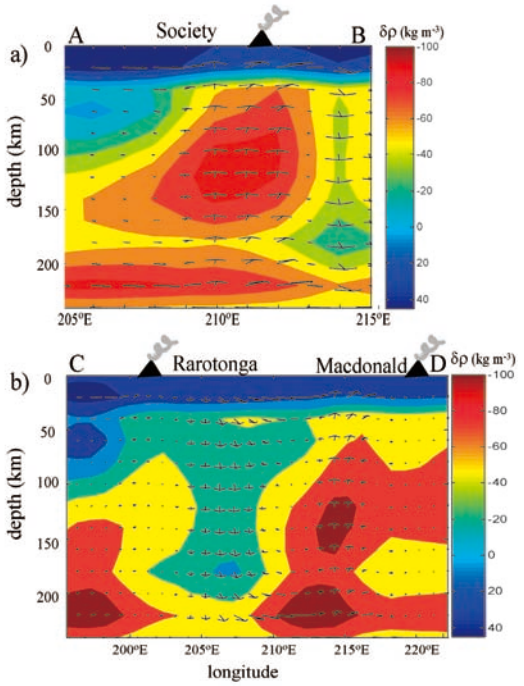

Fig. 4-3. Flow pattern. Depth cross section along the AB (a) and CD (b) profiles displayed in Fig. 2a. The color map represents density anomalies, and arrows are the convection driven by them. The schematic volcanoes represent active volcanism emplacement.

The main body of the volcanic edifice of oceanic islands exists under water and is not accessible by on-land surveys. In order to investigate the detailed geological and geochemical evolution during the growth of volcanoes, submarine surveys were conducted by a manned submersible, the *Shinkai 6500*, at Rurutu, Tubuai, and Raivavae. Although data are limited to whole-rock samples, preliminary results demonstrate that some submarine samples show distinctly more depleted Pb-Sr-Nd-Hf isotopic compositions than subaerial ones (Fig. 4-4c). This indicates that compositions of the magma source were temporally changed, not only along a hot-spot track but also within a single volcano. Isotopic compositions of both subaerial and submarine rocks can be accounted for by mixing of the depleted mantle and HIMU source, with an increasing proportion of the HIMU source against the depleted mantle toward the later-stage volcanism.

The most likely source for HIMU so far proposed is subducted ancient oceanic crust. However, the Os isotopic evidence is not consistent with this model if the HIMU source is oceanic crust itself. Os concentration in oceanic crust is three orders lower than in mantle peridotite, contrasting with Hf and Pb concentrations that differ by up to one order between them. Mixing between oceanic crust and mantle during upwelling, therefore, establishes a highly curved mixing trajectory in the Hf-Os isotopic space, which does not fit the data (Fig. 4-4d). The magmas that are uniformly enriched in Os isotopes with various Hf and Pb isotopic compositions require two mixing components, both of which had comparable Os/Hf and Os/Pb. This

condition can only be achieved by a HIMU source composed of hybrid material between oceanic crust and peridotitic mantle that had been generated prior to shallow mixing with the depleted mantle.

Nd-Hf isotopic relationships further constrain the origin of the HIMU source. The data define a convex mixing trajectory in Nd-Hf isotopic space, indicating that Nd/Hf of the HIMU source should be higher than that of the depleted component by a factor of three or more (Fig. 4-4c). Oceanic crust has almost equivalent Nd/Hf to the depleted mantle. Partial melting of oceanic crust (eclogite) can increase its Nd/Hf by a factor of two to three, but hybridization of the oceanic crustal melt with peridotite, as suggested above, reduces the Nd/Hf ratio below three times the Nd/Hf of the depleted mantle. This constraint suggests that the Nd/Hf ratio of the oceanic crust should be more effectively differentiated than expected by partial melting in eclogite facies.

One of the possible processes to account for this could be that oceanic crust was partially molten in garnetite facies at greater depth, because garnet is able to fractionate Nd/Hf by a factor of up to 6. In this model, recycled oceanic crust in garnetite facies partially melts in an upwelling plume at the bottom of the upper mantle or in the transition zone, and then this melt mixes or reacts with peridotite to form hybrid material. This model requires a reduction of the solidus of oceanic crust by several hundred degrees at great depth. The presence of originally contained carbonate or diffusively added water from a hydrated transition zone may enhance partial melting of recycled oceanic crust, although such melting processes have been less constrained at this stage.

An alternative model is the partial melting of oceanic crust with perovskite residue in the lower mantle, as partition coefficients of Nd and Hf display a significant contrast by one order. Partial melting of oceanic crust is most likely above the core mantle boundary where subducted cold slabs are reheated, and this melt would mix with surrounding mantle to form the HIMU source. Postperovskite may also play a role for differentiating subducted material, which remains to be proved by future work on determining partition coefficients of this phase.

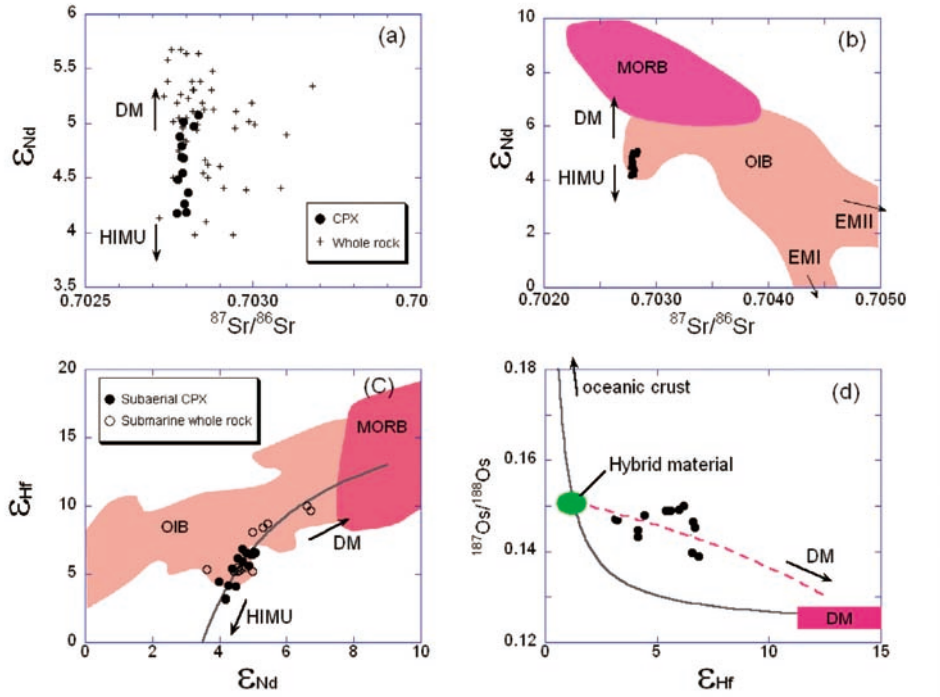

Fig. 4-4. (a) Sr-Nd isotopic compositions of clinopyroxene samples from three islands with HIMU isotopic characteristics. Previous whole-rock data are also shown for comparison. Clinopyroxene data demonstrate a clear correlation trend between Sr and Nd isotopes. (b) Sr and Nd isotopic compositions of clinopyroxene samples in comparison to the variations of OIBs and MORBs. The HIMU magmas are explained by mixing of HIMU source and depleted mantle (DM). (c) Nd-Hf isotopic compositions of (subaerial) clinopyroxene samples and submarine whole-rock samples. Submarine samples extend the range of isotopic compositions of the HIMU islands. Again, all the data are aligned on a mixing trajectory with convex curvature between HIMU and DM. The best-fitting mixing line (solid line) indicates Nd/Hf of the HIMU source is three times greater than that of DM. (d) Hf and Os isotope ratios of clinopyroxene and olivine samples, respectively. Solid-state mixing lines between oceanic crust and DM (solid black line) do not fit the data. Hybrid material formed by mixing/reaction of oceanic crust melt and solid peridotite (green seed) will have an Os/Hf ratio that is comparable to DM (peridotite), therefore mixing of melt derived from the hybrid material and DM should draw a near-straight mixing trajectory, which reasonably accounts for the data.

§5. Tracing subducted slabs in the deep mantle

5-1. Introduction

A gigantic downward flow of mantle convection is taking place in the northwestern Pacific by simultaneous subduction of the Pacific Plate, Indo-Australian Plate, and Philippine Sea Plate. Tracing deeply subducted slabs of these oceanic plates is a key to understanding the nature of mantle convection and the linkage between the deep and shallow mantle. Our approach in this direction is interdisciplinary, involving observational, experimental, and numerical approaches. The observational approach is strongly oriented to ocean-bottom observations. Much of the work at IFREE on this subject has been conducted through the Deep Slab Project (2004-2008) supported by Japan's Ministry of Education, Culture, Sports, Science, and Technology in collaboration with researchers at universities. Here we report the progress at IFREE on this subject during this five-year period.

5-2. Observational approach

5-2A. Ocean-bottom observations for subducted slabs and the surrounding mantle

During this five-year period, a long-term geophysical experiment was conducted in the Philippine Sea and the western Pacific Ocean by using 16 broadband ocean-bottom seismometers (BBOBSs) and 16 ocean-bottom electromagnetometers (OBEMs). Fig. 5-1 shows the locations of the BBOBS and OBEM sites. This experiment was performed in three phases, each consisting of a one-year deployment, resulting in a three-year continuous data set available from October 2005 to November 2008. The BBOBS is equipped with a broadband sensor (CMG-3T) with a leveling unit, and it records three components of seafloor motion at a sampling rate of 100 Hz using a 24-bit AD converter. The OBEM measures three components of geomagnetic field variations using a fluxgate magnetometer and two horizontal components of electrical field variations using two mutually orthogonal pairs of electrodes separated by 5 m. The OBEM also measures seafloor tilt. This was the world's longest-term and largest-array-size BBOBS and OBEM experiment. The outline of this experiment is reported by Shiobara et al. (2009). Part of the data retrieved from this experiment has already been analyzed and reported by Isse et al. (2009), Shito et al. (2009), Seama et al. (2007), and Isse et al. (2006). In addition to these newly retrieved data, we also analyzed the BBOBS data and the submarine-cabled geopotential data obtained in past experiments in the same region. The results are reported by Koyama et al. (2006), Suetsugu et al. (2005), Isse et al. (2004), and Fukao et al. (2004).

5-2B. Other seismological and electromagnetic studies for subducting slabs and the surrounding mantle

We have also conducted extensive tomographic studies

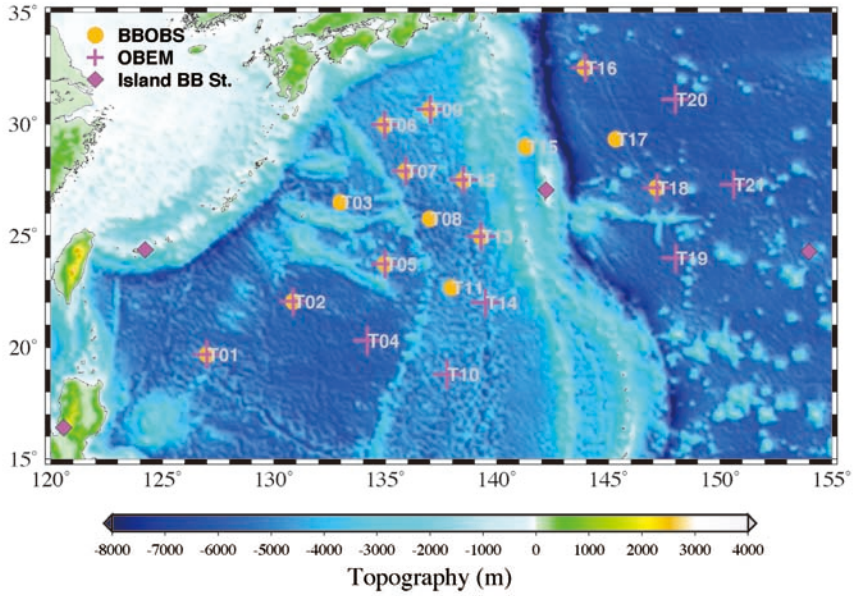

Fig. 5-1. Location map of BBOBS (orange circles) and OBEM (pink crosses) sites through the three-year observational term. Red diamonds show broadband seismic stations on islands [modified from (1)].

and other types of seismological and electromagnetic studies using the data from existing observational networks. Topics include disturbance of the temperature field by a subducting slab and its impact on the postspinel phase transition. Topics also include an attempt to determine water content in the mantle transition zone where a subducted slab is trapped. The results of these studies are reported by Obayashi et al. (2006), Ichiki et al. (2006), Suetsugu et al. (2006), Tono et al. (2005), Niu et al. (2005), and Gorbatov et al. (2005).

5-3. Numerical simulation of mantle convection involving slab subduction

In this field, two complementary approaches are taken at IFREE. One is to simulate mantle convection that can explain observational features of the globe to infer what is dynamically occurring within the Earth. Another is to simulate mantle convection to understand its elementary processes. Work along the latter approach has been conducted using JAMSTEC's Earth Simulator. Fig. 5-2 refers to one of the results of this work, showing the effect of the postspinel transition at 660 km depth on the Rayleigh-Bénard convection within the three-dimensional spherical shell of a model mantle with uniform viscosity. Depending on the basal Rayleigh number of the system and the Clapeyron slope of the phase transition, three modes of mantle convection pattern appear. Pattern change occurs from the one-layered to the two-layered mode through the intermittent mode. The diagram indicates the existing ranges of the three modes. The ranges of the seismological Clapeyron slope and the basal Rayleigh number for the mantle are shown by arrows along the vertical and horizontal axes, suggesting that the Earth's mantle convection is in the intermittent mode state, a feature consistent with the seismological observations that subducting slabs tend to be stagnant in the mantle transition zone. The references related to this subject are given in Yoshida and Nakakuki (2009), Yoshida (2008a, b), and Yanagisawa et al. (2005).

5-4. High-pressure experiments for deeply subducting slabs and the surrounding mantle

A major target of high-pressure experiments on this subject was to infer the behavior of the MORB component of a subducted slab in the lower mantle. Experiments were conducted to determine phase relations, mineral chemistry, and density of MORB composition in comparison with normal mantle composition under temperatures and pressures corresponding to the whole lower mantle, including the D" layer. According to these studies, the postperovskite transition of MORB composition starts at a pressure lower than the transition pressure for pure $MgSiO_3$ perovskite and ends near that pressure; thus, former MORB

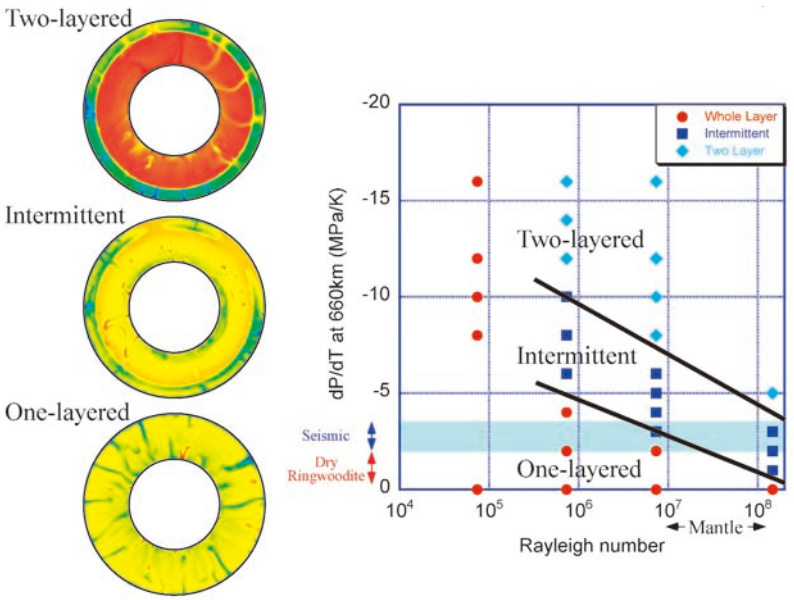

Fig. 5-2. Three modes of mantle convection pattern [modified from Yanagisawa and Yamagishi (2005)]. Left: Pattern change from the one-layered to the two-layered mode through the intermittent mode. Right: Existing ranges of the three modes in the Clapeyron slope versus the Rayleigh number diagram for a uniform-viscosity mantle with three-dimensional (3-D) spherical shell geometry. The phase transition occurs at 660 km depth. The Rayleigh number is defined for the system component heated from below. Half of the heating comes from the internally heated system component. The ranges of the "seismological" Clapeyron slope and the basal Rayleigh number for the mantle are shown with arrows along the vertical and horizontal axes, respectively.

crust is denser than the average lower mantle at all depths greater than ≈720 km, including the D" layer. Fig. 5-3 shows a comparison of the density profile of MORB composition with the PREM reference Earth model in the entire pressure range of the lower mantle. The density profile along an assumed geotherm indicates that the crustal part of the subducted slab remains denser than the surrounding lower mantle, even if it is thermally assimilated to the surrounding lower mantle, and thus may eventually accumulate in the D3 layer to differentiate its chemical nature from the rest of the mantle. The references related to this topic are given by Tateno et al. (2009), Ono (2008), Ohta et al. (2007), Ono (2007), Mibe et al. (2007), Hirose et al. (2005), and Ono et al. (2005).

5-5. Synthesis of the results obtained in different disciplines for stagnant slabs

A stagnant slab is a subducted slab of oceanic lithosphere subhorizontally deflected above, across, or below the 660 km discontinuity. This phenomenon has now been widely recognized beneath subduction zones around the circum-Pacific and in the Mediterranean. Collaboration of seismic and electromagnetic observations, mineral physics measurements, and geodynamic modeling has begun to provide a consistent picture of stagnant slabs, as briefly outlined above. A synthesis was attempted along with the Deep Slab Project (2004-2008) and the results are reported by Fukao et al. (2009).

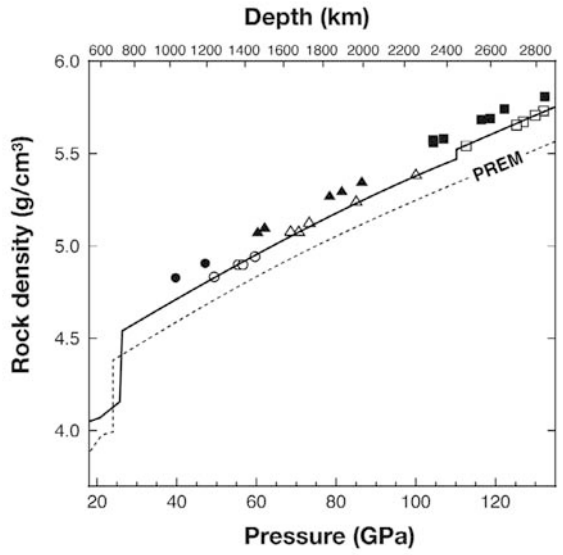

Fig. 5-3. Rock density of midocean ridge basalt (MORB) crust in the lower mantle [modified from (25)]. Dashed line indicates the PREM density. The subducted MORB is denser than the surrounding mantle except between the 660 km boundary and 720 km depth. The density contrast is ≈3% at the base of the mantle.

§6 . Exploration of the central part of the Earth by high-pressure experiments and analog simulations

6-1. High-pressure experiments towards understanding processes at the base of the Earth's mantle

6-1-1. Introduction

Seismic observations have shown that the region above the core-mantle boundary, called the D3 layer, contains strong seismic anomalies. The seismic discontinuity, anisotropy, and an anticorrelation between the observed shear and bulk sound velocities have been reported. Recent seismological study suggested that the shear-wave discontinuity at the top of the D" layer corresponds to the phase transition in mantle minerals. Mineralogists tried to confirm this phase transition with high-pressure experiments. However, they failed to identify it because of difficulties in experiments at extremely high pressures and temperatures corresponding to the bottom of the lower mantle.

We have developed experimental techniques that can reproduce the P-T conditions corresponding to the D" layer and further to the inner cone (see also the next section) as a power user at JASRI/SPring-8 (Fig. 6-1-1).

Fig. 6-1-1. SPring-8, the world's largest synchrotron facility (left), and the laser-heated diamond-anvil cell equipped with an X-ray diffraction system at the BL10XU beam line (right).

6-1-2. Discovery of a new silicate phase, postperovskite

The Earth's lower mantle is believed to be composed mainly of (Mg,Fe)SiO_3 perovskite, with lesser amounts of (Mg,Fe)O and $CaSiO_3$. But it has not been possible to explain the many unusual properties of the D" layer, which occupies the lowermost ≈150 km of the mantle, with this mineralogy. In order to overcome this apparent dilemma and further to understand the processes occurring at the core-mantle boundary, in situ X-ray diffraction measurements of $MgSiO_3$ were performed at high pressure and temperature similar to the conditions at the D" layer. Results demonstrate that $MgSiO_3$ transforms from perovskite into a layered $CaIrO_3$-type postperovskite phase (Figs. 6-1-2, 6-1-3) (Oganov and Ono, 2004; Murakami et al., 2004).

The density discontinuity at the transition is ≈1%, which agrees with that expected by the seismology. The predicted shear wave discontinuity is ≈1.5%, consistent with the ≈1% suggested by seismological study. We predict a very small discontinuity for the compressional wave velocity, < ≈0.3%, explaining why it was so seldom found at the top of the D" layer. One mystery of D", the anticorrelation between the shear and bulk sound velocities, can also be quantitatively explained by the postperovskite transition. This new mineral, with its layered structure, is likely to have rheology completely different from that of perovskite, with possible implications for mantle convection. If the lattice-preferred orientation for postperovskite is assumed, the significant seismic anisotropy of the D" layer, which indicates that horizontally polarized shear waves are faster than the vertically polarized ones, can be explained. In regions of upwelling convective streams (e.g., the central Pacific), slip planes formed by the deformation would be predominantly vertical. This estimated anisotropy is consistent with seismic observations in such regions. Another interesting feature of this transition is that the Clapeyron slope is very large, ≈8 MPa/K. The core-mantle boundary pressure of 136 GPa implies that at temperatures above 4000-4500 K, postperovskite would be less stable than perovskite (Fig. 6-1-4).

The discovery of the new phase transition and the investigations of its physical properties were performed in pure $MgSiO_3$. A similar transition was also confirmed in natural compositions, pyrolite or basalt. This indicates that the new transition is a key to understanding the fate of a subducted slab. The estimated net density of the basalt rock is larger than that of the surrounding mantle estimated by seismic observations. The density difference is small at less than 0.05 g/cm^3. However, our estimation indicates that the density crossover, which was predicted by previous studies, is not likely to occur in the lower mantle, as the density difference between the subducted

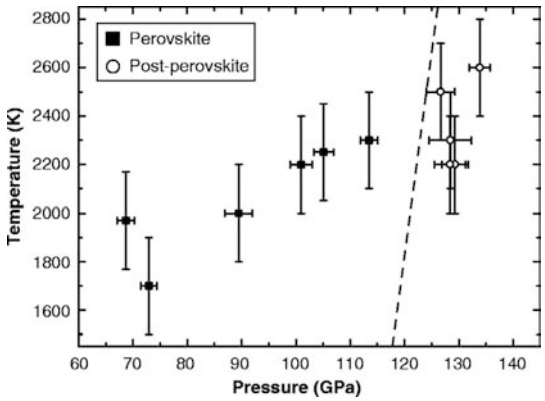

Fig. 6-1-3. Phase diagram of $MgSiO_3$. Solid squares and open circles indicate the stabilities of *Pbnm* perovskite and the postperovskite phase, respectively. A broken line shows the transition boundary proposed by Sidorin et al. to explain the D3 discontinuity by a solid-solid phase transition.

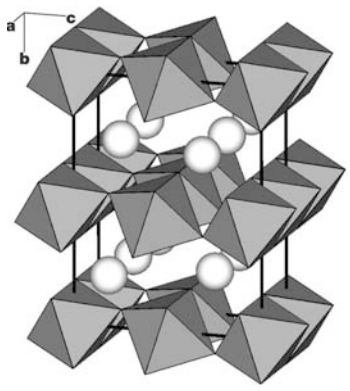

Fig. 6-1-2. Structure of the postperovskite phase of $MgSiO_3$ (calculated at 120 GPa). SiO_6 octahedrons and Mg atoms (spheres) are shown.

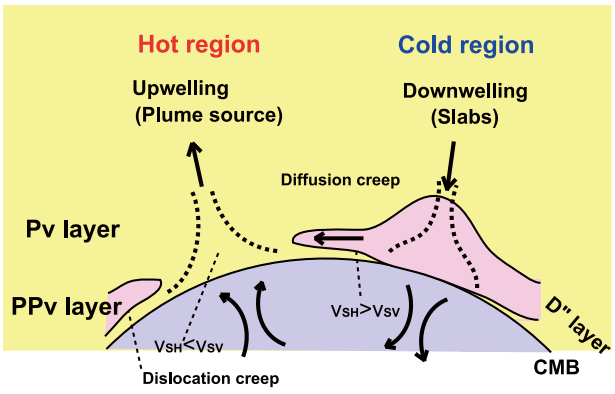

Fig. 6-1-4. Schematic illustration of the processes occurring at the base of the lower mantle.

basalt and the surrounding mantle is nearly constant as depth increases. Therefore, the subducted slab may descend into the base of the lower mantle.

The postperovskite structure has been confirmed in many oxides. One of these oxides, alumina, led to an important implication for the structure of electrical conductivity in the mantle. It is known that measured changes of a few milliseconds in the length of Earth's day on decadal timescales are attributed to the exchange of angular momentum between the solid mantle and fluid core. To explain the length-of-day type of variations, several mechanisms have been proposed. One of them is the electromagnetic coupling between the core and a weakly conducting mantle. However, this model was considered unrealistic because the electrical conductivity of perovskite can not support it. Recently our study showed that postperovskite type alumina has a high electrical conductivity compared with perovskite. This led to the determination of the electrical conductivity structure of the lower mantle. The electrical conductivity of postperovskite favors the electromagnetic coupling mechanism to understand the observed changes in the length of Earth's day.

6-1-3. Mantle-core interaction

The Earth's iron-rich liquid outer core should be in chemical equilibrium, at least with the base of the mantle, which primarily consists of perovskite/postperovskite and magnesiowüstite. We examined the solubility of oxygen in molten iron coexisting with magnesiowüstite to 94 GPa and 3120 K by using a laser-heated diamond-anvil cell and an analytical transmission electron microscope. The results demonstrate that oxygen solubility decreases with pressure below 64 GPa but increases at higher pressures (Fig. 6-1-5). Combining these experimental results with previous partitioning data between perovskite/postperovskite, magnesiowüstite, and molten iron, we calculated the chemical composition of the liquid outer core in the Mg-Si-Fe-O system. Our calculations show that the outer core contains significant amounts of silicon and oxygen at 135 GPa and 4000 K, which account for at least a 9% core density deficit from pure iron. Both silicon and oxygen should be the primary light elements in the Earth's core, consistent with the chondritic Earth model. The bottom of the mantle in contact with such liquid iron alloy is significantly depleted in FeO.

6-2. Experiments at pressures beyond 135 GPa: Towards the center of the Earth

6-2-1. Introduction

A number of problems remain unsolved in the Earth's iron-rich metallic core. This is in part because the pressure and temperature (P-T) conditions of the core are greater than 135 GPa and ≈4000 K, and experiments in such extreme conditions are difficult. It has been known since the early 1950s that the liquid outer core is less dense than pure iron or iron-nickel alloy by about 10%. The light alloying element(s) such as sulfur, silicon, oxygen, carbon, and hydrogen should therefore be incorporated in the outer core, but the identification of light element(s) is still highly controversial. The crystal structure of iron metal at the solid inner core conditions is also not known yet, which makes interpretation of seismological observations difficult. The temperature of the core may best be estimated from the melting temperature of iron alloy at the inner core boundary (the boundary between the solid and liquid core), but current estimates include an uncertainty of more than 2000 K, partly because the melting temperature depends strongly on the light alloying element. The buoyancy of liquid after partially crystallizing the solid at the inner core boundary is important to drive convection in the outer core, but it also depends on which light element is incorporated.

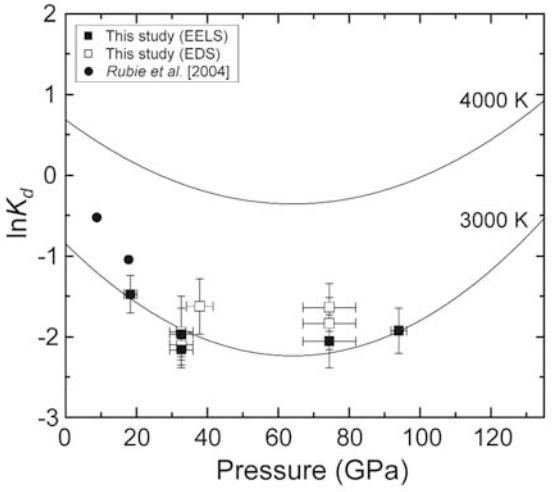

Fig. 6-1-5. Partitioning of oxygen between molten iron and magnesiowüstite. Open and solid squares are based on the EDS and EELS analyses, respectively. The previous data obtained with the multianvil apparatus are extrapolated to 3000 K (Rubie et al., 2004) and shown by circles.

6-2-2. Development of cutting-edge technology

In order to understand these enigmatic issues, advances in high P-T laboratory experiments are necessary. The high-pressure group at IFREE has developed laser-heated diamond-anvil cell (DAC) techniques to generate higher P-T conditions. In addition, developments at synchrotron facilities play another key role in such high P-T experiments. The BL10XU beam line of SPring-8, the world's largest synchrotron facility, is dedicated to X-ray diffraction (XRD) measurement of a tiny sample at high P-T in the DAC (typically 20 μm in diameter and 10 μm in thickness) using very intense X-rays. We have been a power user of BL10XU since 2003. Our new power-user proposal for the next five years (2009-2013) has very recently been approved. We have been working extensively on such synchrotron XRD measurements at high P-T. At the same time, we have expanded the maximum P-T conditions of the XRD measurements year by year (Fig. 6-2-1). When IFREE started a joint project with JASRI/SPring-8 in 2002, the maximum pressure at mantle temperatures for in situ angle-dispersive X-ray diffraction (XRD) measurements was <100 GPa, which corresponded to the depth of the middle lower-mantle. With technical improvements in pressure and temperature generation within the diamond-anvil cell and XRD measurements, we can now reproduce 300 GPa. Our group is now competing with other groups in conducting higher P-T experiments. The latest experiments have been conducted above 300 GPa and 4000 K at SPring-8. This is already close to the conditions at the Earth's inner core boundary (330 GPa and ≈5000 K).

6-2-3. Phase transition of silica

The high-pressure behavior of silica has long been of great interest, owing to its wide range of implications in geophysics, materials science, and solid-state physics. Si is tetrahedrally coordinated by O in silica polymorphs at relatively low pressures. Stishovite (a rutile-type SiO_2 phase) forms above ≈10 GPa with an increase in the coordination number of Si from 4 to 6. Previous experimental studies have shown that stishovite undergoes a second-order structural phase transition to a $CaCl_2$-type phase around 70 GPa and 1600 K. It further transforms to an a-PbO_2-type phase above 121 GPa and 2400 K without change in the coordination number of Si. In addition, a number of metastable silica phases with 6-coordinated Si have been reported below 120 GPa. Recent theoretical calculations have predicted a phase transition from the a-PbO_2-type to a pyrite-type structure around 200 GPa. However, no experimental studies of silica have been made at such multimegabar pressures because of

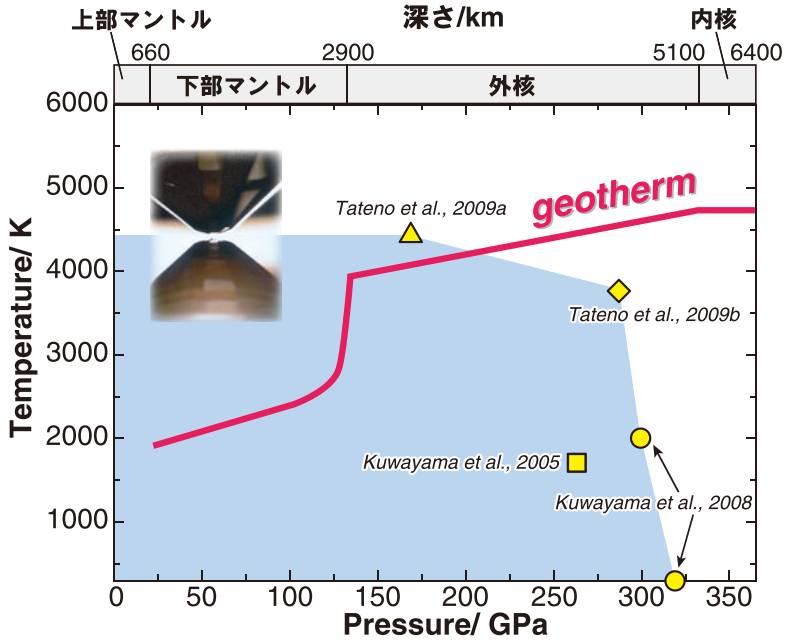

Fig. 6-2-1. The Earth's geotherm (red solid line) and the latest conditions achieved with the LA-DAC system by IFREE at SPring-8 (stars and blue-hatched region). Other symbols show conditions obtained by other groups.

substantial difficulties in both compression and heating.

With technical development of generating higher P-T conditions, we have determined a series of phase transition boundaries in SiO_2 (Fig. 6-2-2). Silica adopts rutile-type structure (stishovite) above 10 GPa and undergoes transformations twice in the Earth's lower mantle. The cubic pyrite-type SiO_2 phase was predicted by theory more than 20 years ago, and we finally succeeded in synthesizing it above 270 GPa.

Silica is the most abundant oxide component in the Earth's crust and mantle, but the pressure required for the pyrite type is greater than that found in the Earth's mantle. Nevertheless, it is also one of the most important oxide components in other planets of our solar system. Theoretical modeling of the interiors of ice-giant planets suggests that both Uranus and Neptune may have a rocky core at pressures about 800 GPa and below, and therefore pyrite-type silica might be an important constituent of these planets. Moreover, silicates are significant oxide components in extrasolar systems. During the formation of terrestrial planets, pressures may exceed 260 GPa and thus include the pyrite-type silica phase.

6-2-4. Structure and composition of the Earth's core

Iron is believed to be a major component of the Earth's core because it is the most abundant element that satisfies seismologically observed densities. Based on cosmochemical models and the studies of iron meteorites, it is generally accepted that the core contains a substantial amount of nickel as well. The high-pressure behavior of iron-nickel alloy is therefore essential for interpreting seismic observations and understanding the nature of the Earth's core. It has been a matter of extensive debate, however, simply because of the substantial difficulties in both compression and heating the materials.

We have investigated the phase relations of iron and

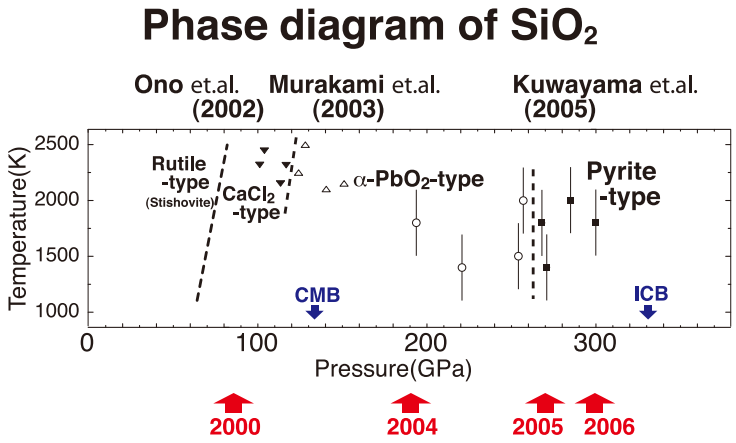

Fig. 6-2-2. Phase diagram of SiO_2 determined by IFREE. With development of advanced technology for high-pressure experiments (red arrow with year), new phases for SiO_2 have been discovered.

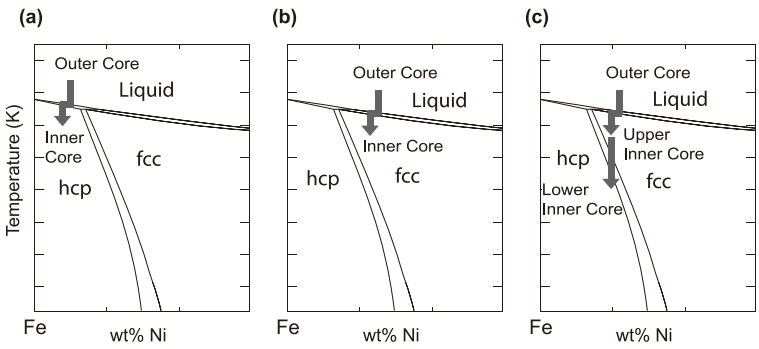

Fig. 6-2-3. Schematic phase diagrams of iron-nickel system at the pressure of the inner core boundary. (a) If the Ni content in the outer core is less than that of the fcc-hcp-liquid triple point, the inner core could be composed of the hcp phase. (b) If the nickel abundance in the outer core is larger than that of the triple point, the fcc phase should be first crystallized at the inner core boundary. (c) The fcc phase may transform to hcp structure at the deep inner core with secular cooling.

iron-nickel alloys with 18 to 50 wt% Ni up to over 300 GPa using a laser-heated diamond-anvil cell. Synchrotron X-ray diffraction measurements show the wide stability of hcp iron up to 300 GPa and 4000 K without phase transition to dhcp, orthorhombic, or bcc phases (Kuwayama et al., 2008). Our experiments also showed that the incorporation of Ni significantly expands the stability field of the face-centered-cubic (fcc) phase, suggesting that the inner core possibly includes the fcc phase, depending on the Ni content in the core. The geometry of the temperature-composition phase diagram of iron-nickel alloys suggests that the hcp-fcc-liquid triple point is located at 10 to 20 wt% Ni at the pressure of the inner core boundary. The fcc phase could crystallize depending on the nickel and silicon content in the Earth's core as both are fcc stabilizers (Fig. 6-2-3).

The properties of iron-light element compounds are also of great interest. Sulfur is one of the most plausible light alloying elements to exist in the Earth's core. Our group recently discovered several new FeS polymorphs (FeS VI and VII phases) through both experiments (Ono et al., 2006; Sata et al., 2008) and theory (Ono et al., 2008). The solubility of Si in solid iron has important implications for the light element in the inner core but has been controversial. Our recent study on Fe-Si alloy demonstrates the positive-pressure effect on the solubility of Si in hcp iron. Sata et al. (unpublished data) examined the compression behavior of iron compounds including FeO, FeSi, FeS, and Fe_3C at the core pressure range. A comparison of these compressibility data with the seismologically determined density profile in the core constrains the chemical composition of the core.

6-3. Visualization of turbulent thermal convection in liquid metal under a uniform magnetic field

6-3-1. Introduction

The convective flow in the outer core of the Earth is supposed to be extremely turbulent, because molten iron has very low viscosity and the spatial scale is large. It is important for outer core dynamics that the flow behaves turbulently under the influence of rotation and magnetic field. In many numerical dynamo simulations, the values of the Prandtl number (*Pr*) and magnetic-Prandtl number (*Pm*) are set around 1, but these values for liquid metals are actually much smaller than 1. Laboratory experimentation using liquid metal is a useful way to study a turbulent flow system with such low *Pr* and *Pm*, although it is difficult to realize self-sustained dynamo action.

We focused on Rayleigh-Bénard convection of liquid metal under an external magnetic field. The system is not rotating. Visualizing the flow pattern and its fluctuations is a desirable way to understand any type of flow. Liquid metals are opaque fluids, so optical methods of flow visualization cannot be applied. We improved the Ultrasonic Velocity Profiler (UVP) method to measure the fine-scale velocity field of the flow occurring in liquid metals. The principle of this method is as follows. A series of ultrasonic pulses emitted from an ultrasonic transducer is reflected by the particles suspended in fluid and is received by the same transducer. Position information is given by the time of flight from emission to reception of the ultrasonic pulse, and velocity information is obtained by analyzing the Doppler shift of the received echo signal. If the numerical density of the particles is large enough, ultrasonic pulses are reflected everywhere along the line of the passing pulse. Thus this method can measure the instantaneous velocity profile along the line. By scanning the measurement lines, we can visualize the whole flow pattern existing in the container.

Our aim in this study is to achieve a direct velocity measurement for convection in liquid metal and to look at the characteristic pattern, whether there exists any mean flow with large-scale structure, and furthermore, in which way the external uniform magnetic field deforms the structure and character of the turbulence of the flow.

6-3-2. Apparatus and method

We use liquid gallium as the working fluid in our experiment. The horizontal scale of the square container is 200 mm, and the height is 40 mm. The transducers for ultrasonic measurement are fixed on side walls, so the horizontal component of the flow velocity at each line is measured with this system. ZrB_2 powder is used as tracer particles because it has neutral buoyancy in liquid gallium. The melting temperature of gallium is 29.8°C, so the upper plate cooling temperature is fixed at 32.0°C, and the lower plate heating temperature is raised to 60.0°C. *Pr* of gallium around this temperature is 0.03, and *Pm* is $\approx 10^{-6}$. The Rayleigh number (Ra) is 10^3-10^5.

A Helmholtz coil system is used to impose a uniform magnetic field on the container. We can set the horizontal or

vertical magnetic field with an intensity of up to 20 mT. The diameter of the coil is 700 mm, and uniformity of the magnetic field around the container is assured. The maximum Hartmann number (*Ha*) realized in this system is about 100. Three components of the magnetic field are monitored outside of the container by a magnetometer. Temperature is measured at some points inside the liquid gallium by small-sized thermistors. Fig. 6-3-1 shows the container for convection and the overall setup of the system.

6-3-3. Results

We measured the horizontal flow velocity in liquid metal with stepwise increase of the external magnetic field. We observed obvious changes in flow characteristics depending on the direction and intensity of the magnetic field. Fig. 6-3-2 is an example of the time series of velocity measurement at four lines in the container.

With zero magnetic field, many fluctuations are observed, reflecting the turbulent behavior of the flow. The flow is also characterized by periodic behavior (slanting red and blue patches in Fig. 6-3-2), which is the oscillation of the organized structure in the turbulence. We found that its period is comparable to the circulation time of the mean-flow, and gets shorter with the increase of *Ra*.

With increase of the horizontal magnetic field (*Bh*), the flow is reorganized as a two-dimensional roll with its axis becoming parallel to the direction of the magnetic field, and small fluctuations decrease ($7.5 < Bh < 12.5$ mT in Fig. 6-3-2). At the same time, fluctuation with a much longer timescale is observed, which is characterized by the reversal of the flow direction of the two-dimensional roll. The reversal occurs randomly, and it may provide insight into outer-core dynamics.

Under a much stronger magnetic field ($Bh > 15$ mT in Fig. 6-3-2), the flow pattern becomes a steady two-dimensional roll without any fluctuation.

In Fig. 6-3-3, we can clearly summarize these styles of flow behavior by two parameters: *Ra* and applying a horizontal magnetic field.

6-3-4. Discussion

When we apply a horizontal magnetic field along the roll axis of this convecting system, the fluctuating components are reduced and the two-dimensionality of the roll structure is enhanced. The reduction rate of the fluctuation depends on the intensity of the magnetic field applied. We think that the criterion for the reduction is described by the comparison of two time scales, Joule dissipation time (t_{JD}) and circulation time (t_U). U is the typical flow velocity. If $t_{JD} < t_U$, then strong reduction of fluctuation may occur. This can explain the *Ra* dependence of our result, that a stronger magnetic field is necessary to stop the fluctuation of the roll for higher *Ra* (for larger U).

When we apply a vertical magnetic field, the flow velocity and frequency of the periodic behavior reduces as the apparent *Ra* of the system becomes smaller. This is easily understandable because the critical *Ra* increases with the intensity of the vertical magnetic field, and then the effective *Ra* for the fluid decreases.

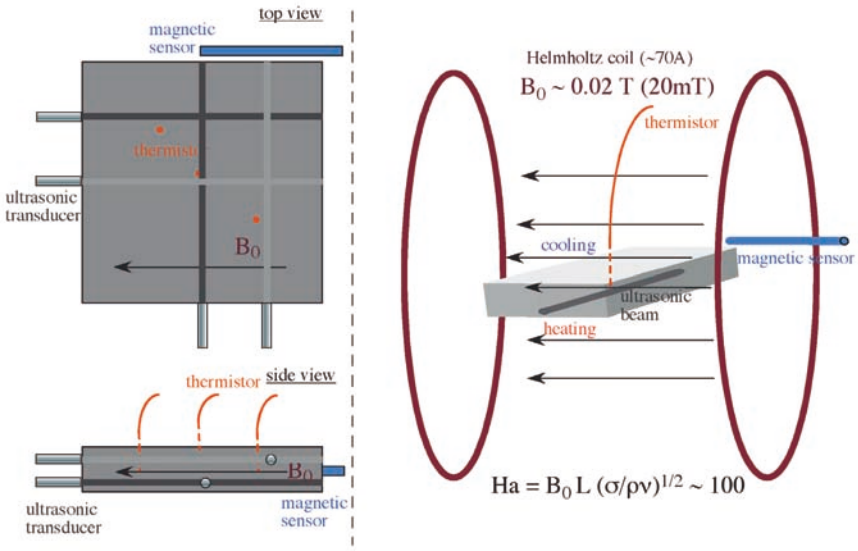

Fig. 6-3-1. Setting for the convection system with an external magnetic field.

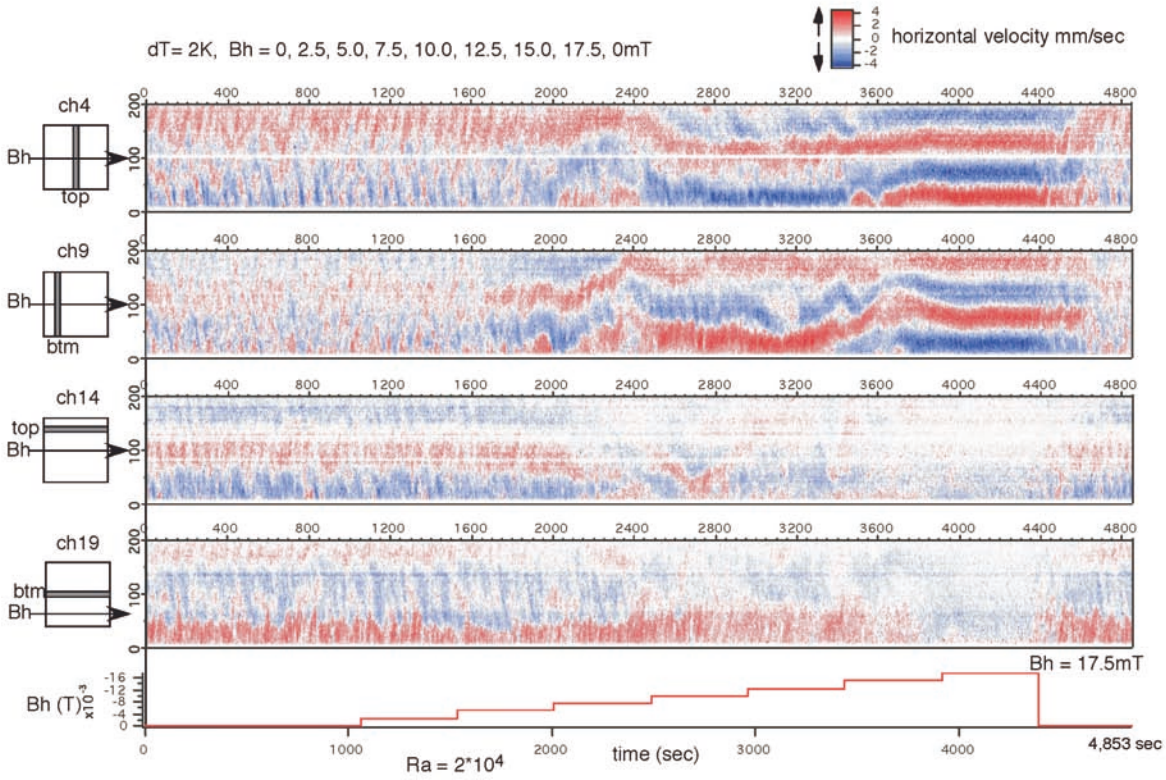

Fig. 6-3-2. Measurement of the horizontal flow velocity with stepwise increase of the horizontal magnetic field.

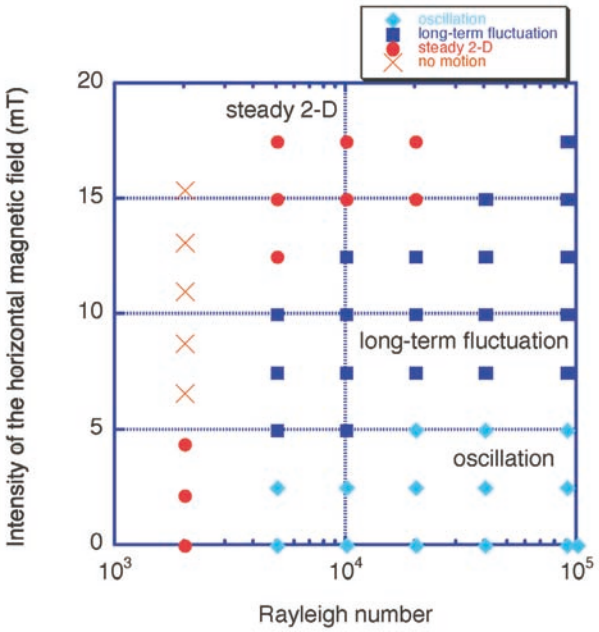

Fig. 6-3-3. Observed style of the convection pattern in liquid metal under a horizontal magnetic field.

§7. Discovery of unknown phenomena in the deep ocean and on ocean floors

7-1. Seafloor geomagnetic observatory detects tsunami signals from the Kuril earthquakes

7-1-1. Introduction

It is generally known that electric and magnetic fields are generated within ocean currents moving through the earth's magnetic field due to electromagnetic (EM) induction. The theory of EM induction (Longuette and Higgins, 1956; Sanford, 1971; Chave and Luther, 1991) indicates that observations of motionally induced electric and magnetic fields can reveal large-scale flow structures that are difficult to obtain by other methods. Specifically, observation of tsunami propagation in offshore areas would be very important to precisely predict the arrival times and accurate tsunami heights at the seashore. Compared to the standard method, simultaneous measurements of electric and magnetic fields are superior in detecting the arrival direction and the particle motion of tsunami flow at a single station, which can not be obtained with a pressure gauge. Recently, it was found for the first time that electromagnetic (EM) time series from a seafloor observatory in the northwest Pacific contained clear signatures of tsunami-induced EM variations.

7-1-2. Observation of tsunami signals

We have been operating a seafloor electromagnetic observatory in the northwest Pacific (NWP: 41.1° N, 159.95° E, water depth = 5816 m) since August 2001 (see Fig. 7-1-1). The seafloor apparatus of the observatory observes and records the absolute geomagnetic total force, three components of the geomagnetic fields, and two horizontal components of the geoelectric fields along with the instrument's orientation and tilts. The apparatus installed about two years ago was recovered, and a new apparatus was installed during the KR07-08 cruise. The data sets for the period from 23 July 2005 to 29 April 2007 were safely recovered at that time and are being used for the study of secular variation of geomagnetic fields. During the period of observation, two large tsunami earthquakes occurred in the Kuril Islands, on 15 September 2006 and on 13 March 2007. Tsunamis from these earthquakes were observed along coastal areas of Japan. The epicenters of these earthquakes were close to the present station (700-

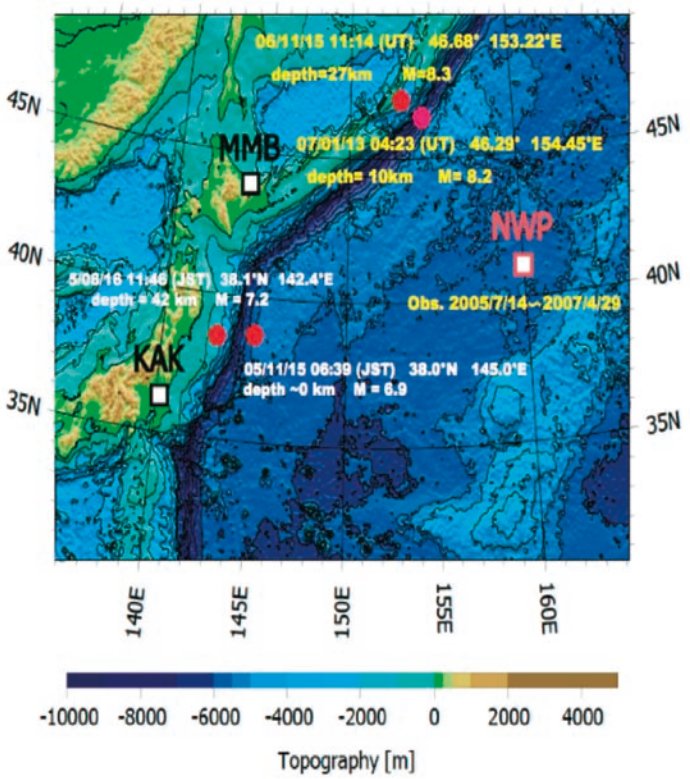

Fig. 7-1-1. Location of the NWP seafloor observation site and the two large Kuril Islands earthquakes.

800 km from the NWP).

Just after the recovery of the records, it was found that the time series of the three components of the magnetic fields (*Bx*, *By*, *Bz*) and the two horizontal components of the electrical field (*Ex*, *Ey*) from the observatory all contained clear signatures of tsunami-induced EM variations. Fig. 7-1-2 shows the records of the five components of the EM field corresponding to the 2006 Kuril Islands earthquake. The signals start about 50 minutes after the arrival time of the seismic waves detected by the tiltmeter installed with the seafloor observatory. This delay time is consistent with the theoretical estimate of tsunami propagation across the northwest Pacific. The amplitude of the tsunami signal's magnetic field is ≈1 nT, the electrical field is ≈0.5 μV/m, and the dominant period of the signals is about 15 minutes. These signal levels are much higher than the noise level of the EM fields, as shown in Fig. 7-1-2.

From these EM signals, various properties associated with tsunami propagation can be obtained. Since the source electric current due to tsunami propagation flows parallel to the tsunami front, the magnetic field due to this electric current is perpendicular to the tsunami front. Hence *Bx* and *By* can be combined to estimate the direction of the propagation direction of the tsunami wave. Based on this principle, the tsunami arrival direction was estimated to be about 320°, which is consistent with the direction of the epicenter of the earthquake from the NWP. And since the EM variations are motionally induced signals, these EM signals have information about the particle velocity of seawater due to tsunami propagation. Based on the formulation given by Sanford (1971), two horizontal components of particle motion (*Vx*, *Vy*), averaged over the entire water depth, can be expressed from the two perpendicular pairs of (*Ex*, *By*) and (*Ey*, *Bx*) as shown below.

$$\bar{V}_x = \frac{1}{F_z}\left((1-\lambda)E_y + \frac{2B_x}{\mu\sigma_1 H}\right)$$
$$\bar{V}_y = \frac{1}{F_z}\left(-(1-\lambda)E_x + \frac{2B_y}{\mu\sigma_1 H}\right) \quad (1)$$
$$\lambda = \frac{\sigma_2(H_s - H)}{\sigma_1 H}$$

where *Fz* is the vertical component of the geomagnetic field, *H* and *Hs* are the depth of the sea bottom and the lower boundary of the sedimentary layer below the sea bottom, and σ_1 and σ_2 are the electrical conductivities of seawater and the bottom sedimentary layer, respectively. Assuming λ is much smaller than 1, the vertically averaged particle velocities, *Vx* and *Vy*, are calculated from (*Ey*, *Bx*) and (*Ex*, *By*), and as shown in Fig. 7-1-3, the coordinate system is rotated to parallel (X-component) and perpendicular (Y-component) directions to the propagation direction of the tsunami wave.

As shown in Fig. 7-1-3, the maximum amplitude of particle motion along the propagation direction is ≈1

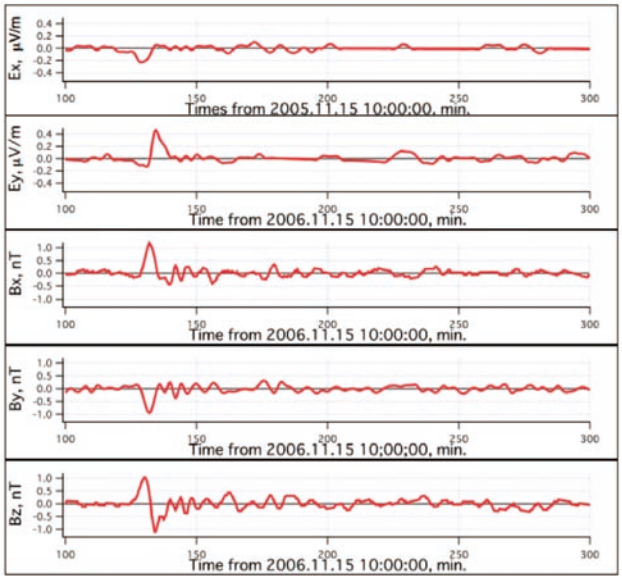

Fig. 7-1-2. Variation of two horizontal components of the electrical fields (*Ex* and *Ey*) and three components of the magnetic fields due to 2006 Kuril Islands earthquake.

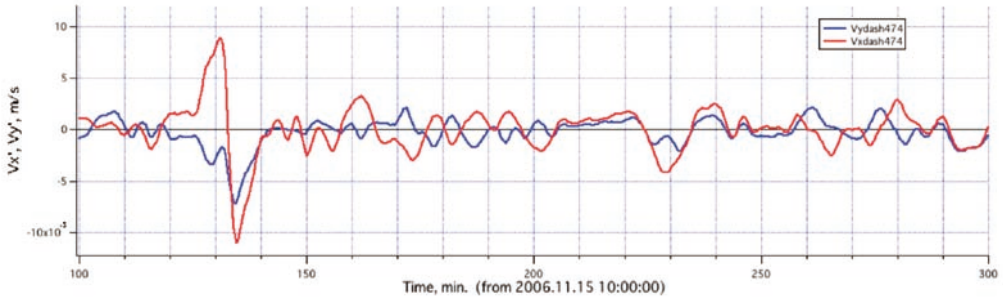

Fig. 7-1-3. Variation of vertically averaged particle motions due to the 2006 Kuril Islands earthquakes. Velocities along and perpendicular to the tsunami wave's direction of propagation are shown.

mm/s. Using long-wave approximation, the amplitude of 1 mm/s at a water depth of 5816 m corresponds to about 30 cm of sea-level change. Finally, it should be noted that the tsunami-induced vertical magnetic component (*Bz*) can be used as a precursor of tsunami arrivals since *Bz* attains maximum *T/4* earlier than the change of the water depth, where *T* is the period of the tsunami wave.

7-2. Discovery of new volcanism at a petit-spot

7-2-1. Discovery of a petit-spot

In 1997 basalts were sampled on a seaward slope of the Japan Trench at ≈7300 m water depth. These basalts were unexpectedly young (^{40}Ar-^{39}Ar age dating: 5.95 ± 0.31 Ma) alkali basalts (Hirano et al., 2001). Noting that there are no known hot spots in the vicinity, this substantial discovery suggests that unknown intraplate volcanism occurs and new volcanoes are built on the ≈130 Ma old Cretaceous Pacific Plate, that is, cool and thick oceanic lithosphere.

In 2004 we extended the survey area to the southeast (≈120˚) upstream of the Pacific Plate motion (e.g., DeMets et al., 1990). The area is up to ≈600 km away from the trench, and it is supposed to be the birthplace of the ≈6 Ma basalts. As a result of the survey, we found small knolls, a few km in diameter and ≈100 m in relative height, on the abyssal plane (≈6000 m water depth). Highly vesicular alkali basalts collected from the small knolls indicate <1 Ma age (Hirano et al., 2006). Noble gas isotopic data suggest the source mantle of alkali basalts is similar to that of MORB rather than that of OIB. The origin of these rocks is inferred to the base of the lithosphere or asthenosphere ≈90 km below the seafloor (Hirano et al., 2006). The lava contains abundant mafic xenocrysts and xenolith fragments of basalts, dolerites, gabbros, and mantle peridotites, which are typical of the oceanic lithosphere (Abe et al., 2006). The intraplate volcanism was termed “petit-spot.”

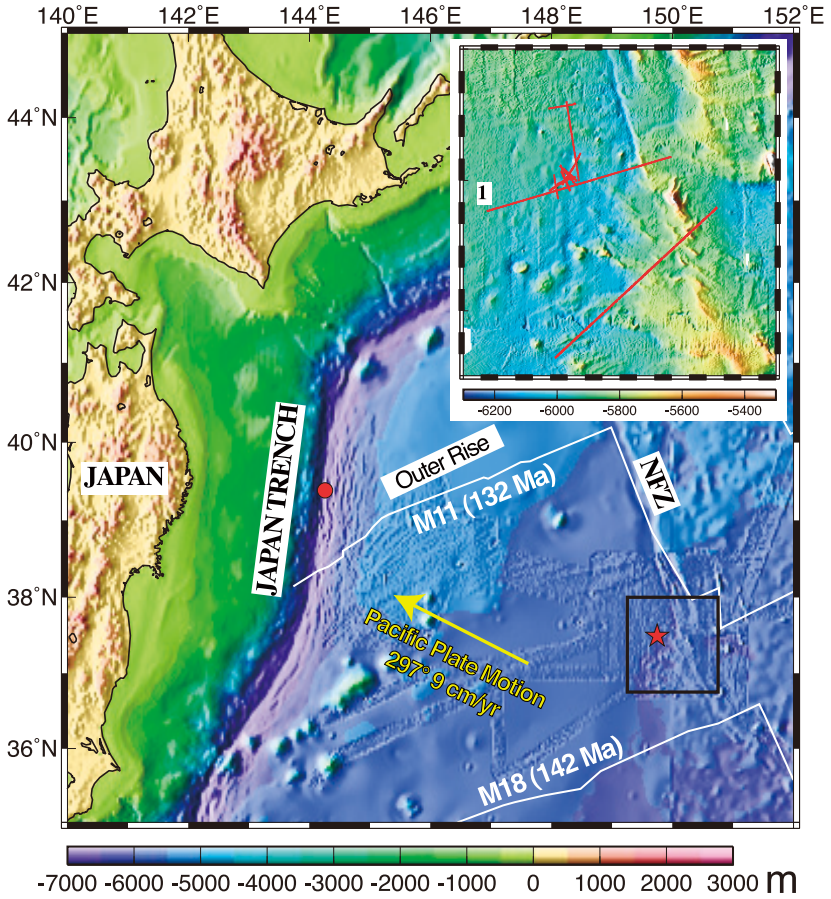

Fig. 7-2-1. The black square is the petit-spot area. The circle is the sampling site where the ROV *Kaiko* has collected ≈6 Ma basalts. The star is the petit-spot volcanoes where we collected <1 Ma basalts. Solid white lines indicate crustal age-identified magnetic isochrons. NFZ: Nosappu Fracture Zone. The inset is swath bathymetry of the survey area. Solid lines delineate seismic survey lines.

7-2-2. Interdisciplinary survey of the petit-spot

Petit-spot volcanism will help scientists better understand the thermal/mechanical structure of the oceanic lithosphere and the magma production process in the shallow upper mantle, and also the evolution and modification of old oceanic crust/lithosphere. Therefore we have conducted interdisciplinary surveys (Abe et al., 2005; Baba et al., 2007). These surveys were expanded to a broad area in the northwestern Pacific since additional ^{40}Ar-^{39}Ar ages obtained were 4.23 ± 0.19 Ma and 8.53 ± 0.18 Ma (Hirano et al., 2006).

This work is being conducted in collaboration with the Tokyo Institute of Technology, the Ocean Research Institute and the Earthquake Research Institute of the University of Tokyo, Chiba University, and Tsukuba University, as well as with other research programs in JAMSTEC.

7-2-3. Scienti fic results

In 2005 we conducted a seismic reflection survey to evaluate the subsurface volume of magma and the structure of lava flows and/or sills of the petit-spot volcanoes and found that this young basalt pooled in between sedimentary layers and oozed to the surface through cracks and vents (Fujiwara et al., 2007).

The *Shinkai 6500* submersible dives were performed at some of the petit-spot knolls. The basin surrounding the knolls was fully covered with soft pelagic sediment. In contrast, pillow lavas and robes outcropped along the slope of the knolls. The outcrops were limited around summits (Machida et al., 2005). Sampled rocks indicate the volcanic edifice consists of porous (up to 60% porosity) alkaline lavas. Rock sampling was also conducted in the Japan Trench sites. Basaltic lavas from volcanic knolls are highly vesicular (10-40%). Less vesicular (0-20%) lavas and cherts were collected on fault scarps, where probably deeper parts of the volcanic knolls and/or sills were exposed by horst-graben normal faulting.

Since 2005 ocean bottom electromagnetometers (OBEM) for the magnetotelluric soundings (MT) have been deployed. The acquired electromagnetic field

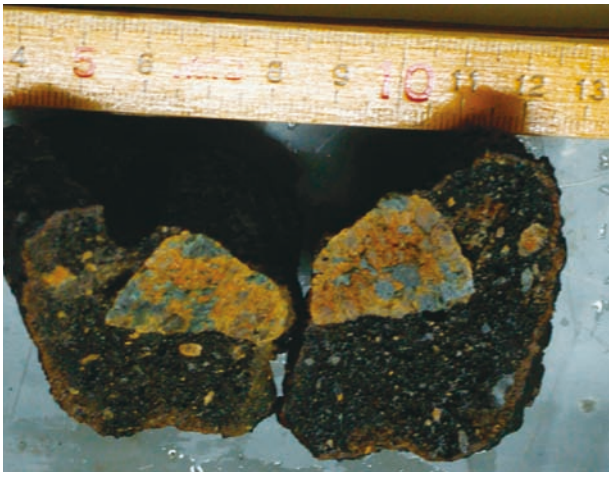

Fig. 7-2-2. Large mantle xenoliths (lherzolite) obtained from the petit-spot volcanoes.

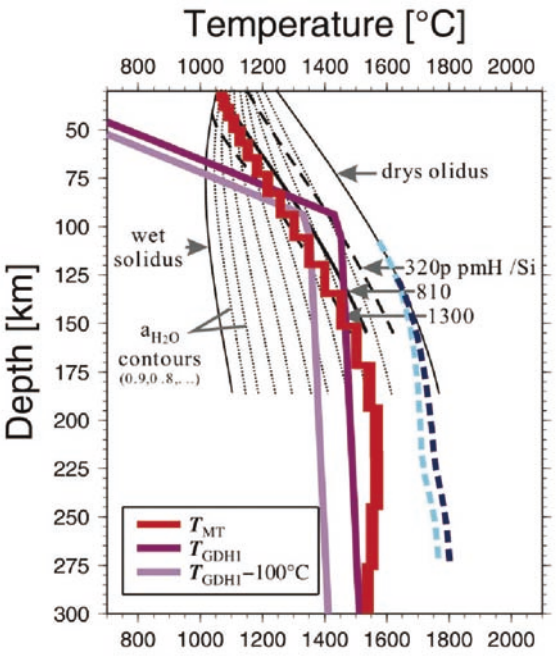

Fig. 7-2-3. Temperature calculated from electrical conductivity (red line). Neither the dry nor the wet case, the temperature exceeds the corresponding solidus.

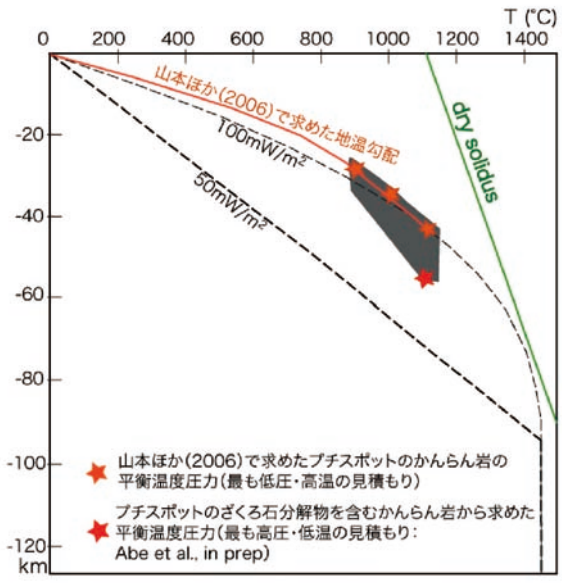

Fig. 7-2-4. Geothermal gradient estimated from sampled mantle xenoliths (orange line). Stars are estimated temperature at the estimated depths.

variation data were analyzed, and the MT responses, which were the transfer function between the electric and magnetic fields, were obtained. The responses indicated that the lateral heterogeneity in electrical conductivity was less significant beneath the survey area. A one-dimensional inversion study shows that the data require a peak in conductivity (0.05 S/m) at about 200 km depth. The mantle temperature may be calculated from the conductivity using experimental results. The electrical conductivity model does not support melt generation in the asthenosphere under the assumption of pyrolitic mantle composition (Baba et al., 2007).

Broadband ocean-bottom seismometers (BBOBS) were deployed around the petit-spot volcanic field from 2007 to 2008. Seismic attenuation and travel-time anomalies in the lithosphere/asthenosphere beneath the petit-spot region were measured to infer physical properties of the region using waveform data from regional earthquakes within the Pacific slab in the Tohoku subduction zone. The relation between attenuation and travel time anomaly is consistent with predictions based on the thermal effect. We anticipate that the present asthenosphere beneath the petit-spot is under normal conditions according to the age (Shito et al., 2008). Local seismicity will provide constraint on the magma eruption processes of a petit-spot.

On the other hand, the thermal gradient in the oceanic lithosphere estimated from mantle xenoliths shows discordance with standard thermal models. Equilibrium temperature of the peridotite varied 850-1130°C at a depth of 30-45 km, and the geotherm was higher than models such as GDH1 (Abe et al., 2006).

High average heat flow (70-90 mW/m^2) was observed at some sites on the abyssal plane seaward of the Japan Trench, while very low heat flow (<20 mW/m^2) was observed in the vicinity of the small knolls of the petit-spot. That requires the existence of some heat sources and hydrothermal circulation in the upper part of the oceanic plate (Baba et al., 2008).

The petit-spot provides a unique window for mantle source material beneath the oldest part of the Pacific Plate. To investigate the geochemical features of the upper mantle unrelated to plumes in the northern hemisphere, Machida et al. (2009) determined Sr, Nd, and Pb isotopic compositions of basalts and proposed that recycled material from an ancient subduction system or crustal delamination resides throughout the upper mantle of the Pacific Ocean as minor blobs. A model of "small-scale recycled material melting" consistently explains geochemistry and noble gas isotopic composition of magma, and the volume of petit-spot volcanism.

Swath bathymetric and backscattering data were collected during our research cruises. New petit-spot knolls were discovered around the Sanriku outer-rise earthquake hypocentral region (Abe et al., 2007). Hirano et al. (2008) pointed out that such petit-spot-like intraplate volcanism may be ubiquitous in areas of front sides of trench outer rises, and thus widely spread throughout old-age oceanic plates. The detailed bathymetry depicts small knolls, seamounts, and detailed tectonic fabrics. Koike (2009) suggested that some seamounts were of intraplate volcanic origin based on bathymetry and gravity anomaly analyses.

7-3. The deepest part of the oceans as a paradise for primitive protists (single-celled eukaryotes)

Geographic distribution of marine organisms is mainly controlled by physicochemical conditions of the oceans such as temperature, salinity, dissolved oxygen concentration, and other environmental factors. It is also controlled by the history of the Earth, such as changes in the relative configuration of continents and oceans in the past. Submarine topographies, which are formed in connection with the movement of lithospheres, should also give clear constraints for distribution of benthic organisms that dwell deep in the sea. Deep trenches are chiefly formed along plate subduction zones. Most deep trenches revealed to be more than 10,000 m deep are distributed in the western part of the Pacific Ocean. What kinds of benthic organisms dwell in the deep trenches? Very little research has been carried out on trench communities, even though deep trenches have extreme environmental conditions with darkness, low temperature, high hydraulic pressure, and oligotrophy, because we require special gear to reach deep trenches of more than 10,000 m water depth.

We had the chance to visit Challenger Deep in the Marianas Trench, the deepest point of the world's oceans, with the ROV *Kaiko* that belongs to JAMSTEC during the KR02-11 cruise. We succeeded in collecting a push core sample from Challenger Deep.

A total of 432 foraminifera (=449 per 10 cm^2) were picked out from the >32-μm fraction of a sediment core (0-

1 cm layer) collected using the *Kaiko* remotely operated vehicle. This population density is similar to our shallower (7088-7761 m) trench sites and higher than at many shallower abyssal sites. Except for 4 individuals of the multichambered agglutinated genera *Leptohalysis* and *Reophax*, the assemblage was dominated by delicate, soft-walled species, all of them new to science (Todo et al., 2005). Most (85%) of these 428 specimens were organic-walled allogromiids, typically brown in color and with tubular morphologies, in some cases subdivided into two or more elongate or globular chambers. Such a high proportion of organic-walled allogromiids is very unusual; in most deep-sea environments they constitute 5-20% of the living assemblage (Gooday et al., 2008b). The only previous study of foraminifera from a comparable water depth reported 4 stained (living) individuals belonging to the agglutinated genus *Lagenammina*. Foraminifera with calcareous walls cannot exist at this great depth because the water is strongly undersaturated in calcium carbonate.

The Challenger Deep assemblage most resembles the fauna at a shallower site in the Marianas Trench (Stn. 40, 7123 m water depth). Here, *Nodellum*- and *Resigella*-like allogromiids were also common, albeit less so (44.7% of the assemblage) than at Challenger Deep. Psammosphaerids, however, were much more abundant (37%) and the assemblage more diverse (57 species).

Fig. 7-3-1. Twelve foraminiferal species found at Challenger Deep in the Marianas Trench.

Samples from two northwest Pacific trenches (Kuril and Japan) yielded a small number of *Nodellum/Resigella*-like species, suggesting that the dominance of these forms in the Marianas Trench (including Challenger Deep) may reflect the more oligotrophic setting compared to the northwest Pacific, rather than water depth.

Analysis of small subunit ribosomal DNA gene sequences indicated that single-chambered noncalcareous taxa form a series of deep-branching evolutionary lineages, representing the basal radiation from which more complex multichambered groups arose. They include the only foraminifera to have invaded freshwater and terrestrial habitats. Our results indicate that these primitive groups are also important components of benthic communities in the deepest ocean trenches, suggesting that they are more adaptable than other foraminiferans to extreme pressures. Similar forms are widespread in the abyssal deep sea and abundant at 7800 m water depth in the Atacama Trench, but they are never such a dominant faunal component. Challenger Deep may have developed to its present depth during the past 6-9 million years. Its very distinctive foraminiferal fauna probably represents the remnants of abyssal assemblage that was able to adapt to the steady increase in hydrostatic pressure over this time period. In total, seven species and one genus were described as new to science (Gooday et al., 2008a; Kitazato et al., in press).

§8. Contributions of our research efforts to society and industry

8-1. Contribution to the Japanese continental shelf survey: To specify areas of Japan's extended continental shelf

8-1-1. Introduction

Japan submitted particulars related to its extended continental shelf to the Commission on the Limits of the Continental Shelf in 2008. Here we describe the background as an introduction by citing from the Executive Summary of Japan's Submission to the Commission on the Limits of the Continental Shelf (2009).

Japan signed the United Nations Convention on the Law of the Sea (hereinafter referred to as “the Convention”) on 7 February 1983 and ratified it on 20 June 1996. The Convention entered into force for Japan on 20 July 1996. According to Article 76 of the Convention, Article 4 of Annex II of the Convention, and the decision adopted by the 11th Meeting of States Party to the Convention, Japan is under obligation to submit particulars of the outer limits of its continental shelf beyond 200 miles from the territorial sea baseline to the Commission on the Limits of the Continental Shelf set up under Annex II of the Convention along with supporting scientific and technical data by 12 May 2009. Japan intended to establish the outer limits of its continental shelf beyond 200 miles from the territorial sea baseline in seven regions located to the south and the southeast off the main islands of Japan (Fig. 8-1-1). These regions are (1) the Southern Kyushu-Palau Ridge region, (2) the Minami-Io To Island region, (3) the Mogi Seamount region, (4) the Ogasawara Plateau region, (5) the Minami-Tori Shima Island region, (6) the Southern Oki-Daito Ridge region, and (7) the Shikoku Basin region (Executive Summary, Japan's Submission to the Commission on the Limits of the Continental Shelf, 2009).

8-1-2. Role of JAMSTEC in the continental shelf survey

The Japan Agency for Marine-Earth Science and Technology (JAMSTEC) joined a team to prepare all the documents, maps, charts, and databases and to collect all the sea-based data used in Japan's submission as one of the affiliated agencies. Although the supporting scientific and technical data is composed of sea-bottom topography data, seismic data, geochemical petrologic data, and geophysical data, JAMSTEC was in charge of preparing the seismic data in cooperation with the Japan Coast Guard (JCG).

The objectives of these seismic surveys are to understand the scientific background, including the crustal growth process, and specify the characteristics of the crust, including sedimentary sequences. To determine specification of the reflection/refraction seismic surveys using a multichannel reflection system (MCS) and ocean bottom seismographs (OBSs), and to evaluate the resolution for the obtained structure, JAMSTEC and JCG studied past data qualities using various specifications and also carried out numerical tests. The standard specifications of the seismic surveys was determined as follows: (1) The source capacity for reflection/refraction surveys are over 6000 cu. in.; (2) The channel number of the streamer for reflection surveys is over 150 and the group interval is less than 25 m; (3) OBS interval for the refraction surveys is less than 5 km; (4) Shot intervals for

the reflection and refraction surveys are less than 50 m and 200 m, respectively; (5) Reflection surveys are implemented along all refraction survey lines.

We had mainly experimented in the Izu-Ogasawara island arc region using JAMSTEC's RV *Kairei* and RV *Kaiyo* since 2004. To understand the scientific background and the crustal growth process of this region, distribution of these lines is set for the entire arc. Therefore, the lengths of the lines are mostly over 500 km, and we used approximately 100 OBSs for every refraction survey. Such long offset refraction surveys had not been performed until these continental shelf surveys. We had repeated these surveys five times every year. These seismic data collections are managed by JCG as part of the fundamental data used for the submission.

8-1-3. Scientific results on structural characteristics of the Izu-Ogasawara island arc for the submission

The processing of MCS and OBS data was also basically unified between JAMSTEC and JCG. The tomographic inversion technique for OBS data processing was adopted to keep the objectivity for the velocity models, and checkerboard tests were carried out to confirm the resolution. Moreover, layered structures were also constructed on a case-by-case basis. In particular, layered structures are helpful to identify structural characteristics in the back-arc region with relatively thin crusts. For MCS data processing, although the flow is a conventional one from data conversion to depth conversion through the geometry set, amplitude recovery, trace edit, predictive deconvolution filtering, velocity analysis, dip moveout, normal moveout correction, multiple suppression with radon filters, stacking, band-pass filtering, the Kirchhoff time migration, and depth conversion, the prestack depth migration technique was also used to make clear images for understanding the background tectonics.

As a result, we identified the structural characteristics of the entire Izu-Ogasawara island arc region using obtained velocity models and reflection images. These characteristics are common to the Mariana arc and the West Mariana Ridge. Although it is difficult to show everything here due to limited space, the main supportive outlines for the submission are as follows (See Section 2 for a detailed description): (1) The entire arc commonly has a continental middle crust with a velocity

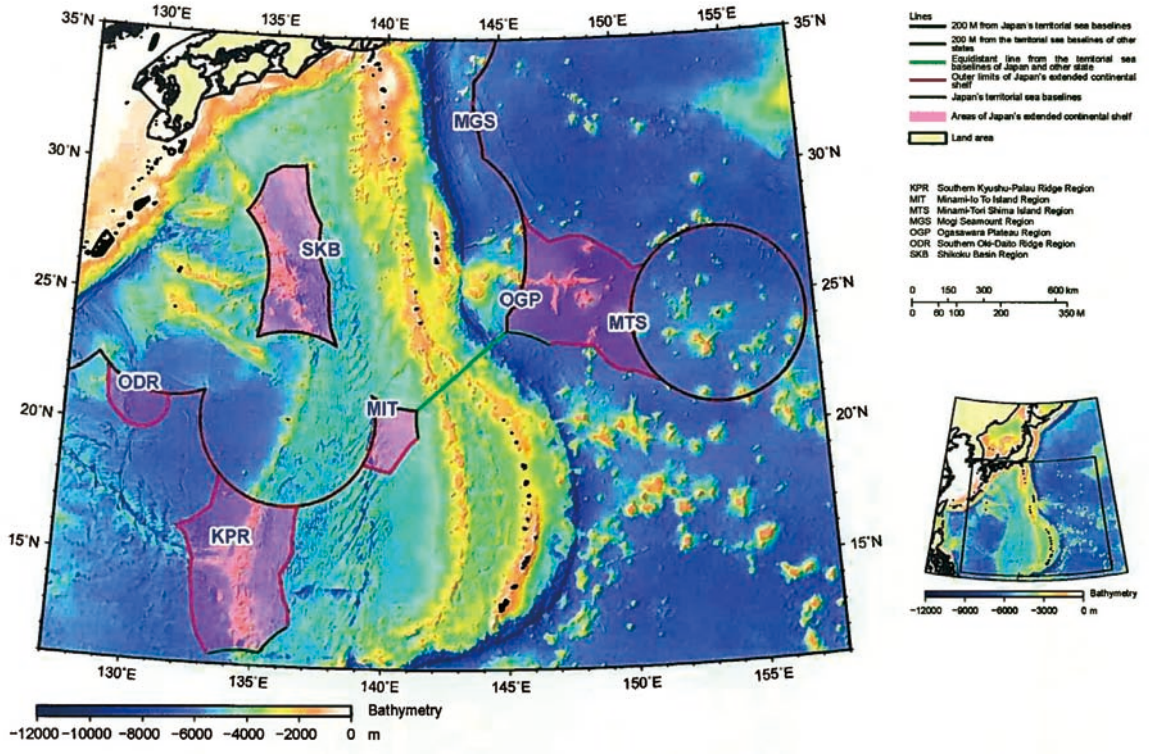

Fig. 8-1-1. Area of Japan's extended continental shelf (Executive Summary, Japan's Submission to the CLCS, 2008, available at the Web site of the Division for Ocean Affairs and the Law of the Sea of the United Nations (www.un.org/Depts/los/clcs_new/submissions_files/submission_jpn.htm).

of 6 km/s, a heterogeneous and thick lower crust beneath the arc regions, a crust-mantle boundary zone beneath the current volcanic front, the remnant arc (Kodaira et al., 2007a, b; Kodaira et al., 2008; Takahashi et al., 2007; Sato et al., 2009); (2) According to these velocity models and petrologic studies, we constructed a scenario of the crustal growth process and found that part of the dense crustal materials are transformed to the uppermost mantle during the process (Tatsumi et al., 2008; Takahashi et al., 2008); (3) The lower crusts beneath the rifted regions, like the Ogasawara Trough and the eastern margin of the Shikoku Basin, commonly have relative high velocities of over 7 km/s, and the origin of the high-velocity lower crust is underplating of dense crustal materials (Takahashi et al., submitted). The volcanisms with the high-velocity lower crust at the eastern margin of the Shikoku back-arc basin were confirmed by geochemical studies (e.g., Ishizuka, 2008).

The seismic surveys carried out in the Izu-Ogasawara island arc region were limited until 2004. In particular, the refraction surveys using OBSs across the entire arc are very few except for Suyehiro et al. (1992). Knowledge of the structural characteristics of the Izu-Ogasawara arc has abruptly increased for these continental shelf surveys. These results are supportive as clues to understanding the scientific background and the crustal growth process for the submission regarding Japan's extended continental shelf.

8-2. Contribution to industry through software development for numerical simulations of crustal activities

8-2-1. Introduction

The key role of IFREE research is to understand crustal activities from the past to the future. However, direct observation of crustal activities can be conducted only on its surface, and most of the deeper part of the crust prevents us from observing it directly. In addition to this geometrical problem, the issue of the time scale from 4.6 billion years ago to a few billion years in the future is always a large barrier for IFREE research. How can we discuss Earth's dynamics regarding unobservable phenomena in the crust only from the results of seismic, geophysical, and dating studies? Unfortunately, there is no universal constitutive law to deal with the crustal materials that deform and flow under wide ranges of temperature and pressure with chemical reactions.

Moreover, a large amount of results on geochemical and material sciences in petrologic studies and on seismic structural imaging, which are a part of the advanced results of IFREE in the world, are not fully linked in view of the spatial scale. For example, it is easily inferred that the local characterization of sedimentary rocks forming accretionary prisms has effects on global tectonics of the subduction zone with the accretion and surrounding regions; however, a real theory to surpass this speculation has not been established.

Our numerical simulation scheme based on particle motion is nothing new; it is a relatively orthodox method. We assume attributes of shape, mass, properties, mechanical quantities, and so on for each particle, estimate interaction among these particles and the field force, and trace the evolution of particle motion with time (Fig. 8-2-1). Although the method itself is orthodox, the mechanical behavior of many particle systems under certain condition is very complex, and the strength of the systems changes autonomously. If the local characters of sedimentary rocks can be regarded as the characters among particles, and if the global behavior of accretionary prisms and a subduction zone can be regarded as output for the conglomerate, the numerical simulation becomes a useful tool to estimate petrologic elements for development of accretionary prisms and occurrence of large earthquakes in a subduction zone. This numerical simulation is a helpful tool for issues with unknown equations controlling the entire field, as is the case with crustal activities. Numerical integration using the Newtonian equation of motion, however, is indispensable to simulate a huge number of particles. We have to calculate development with an extremely short time interval; therefore, advanced techniques for fast programming are demanded to finish the simulation quickly.

For the objectives above, the crustal dynamics research group of IFREE at JAMSTEC has developed the Hyperintelligent Discrete Element Method (HiDEM) and applied it to IFREE research. Here we introduce some applications and contributions for industry. The detailed features and the methods can be reviewed in other articles in JAMSTEC-R.

8-2-2. Application of HiDEM to industry

As described above, HiDEM is a code of the discrete element method (DEM) developed for numerical simulations of crustal activities. As commercial codes of DEM, the PFC and UDEC (Cundall and Hart, 1992) series developed by Itasca in the United States has a large share in the world. There are also many other DEM codes developed by researchers and industry, such as the Xerox DEM and the DEMS developed by Dr. Sawada of Kyoto University. The details of these codes, however, are different from each other due to the arbitrariness in the theory, although the theory is very simple compared with other methods such as the Finite Element Method (FEM). The DEM depends strongly on initial and

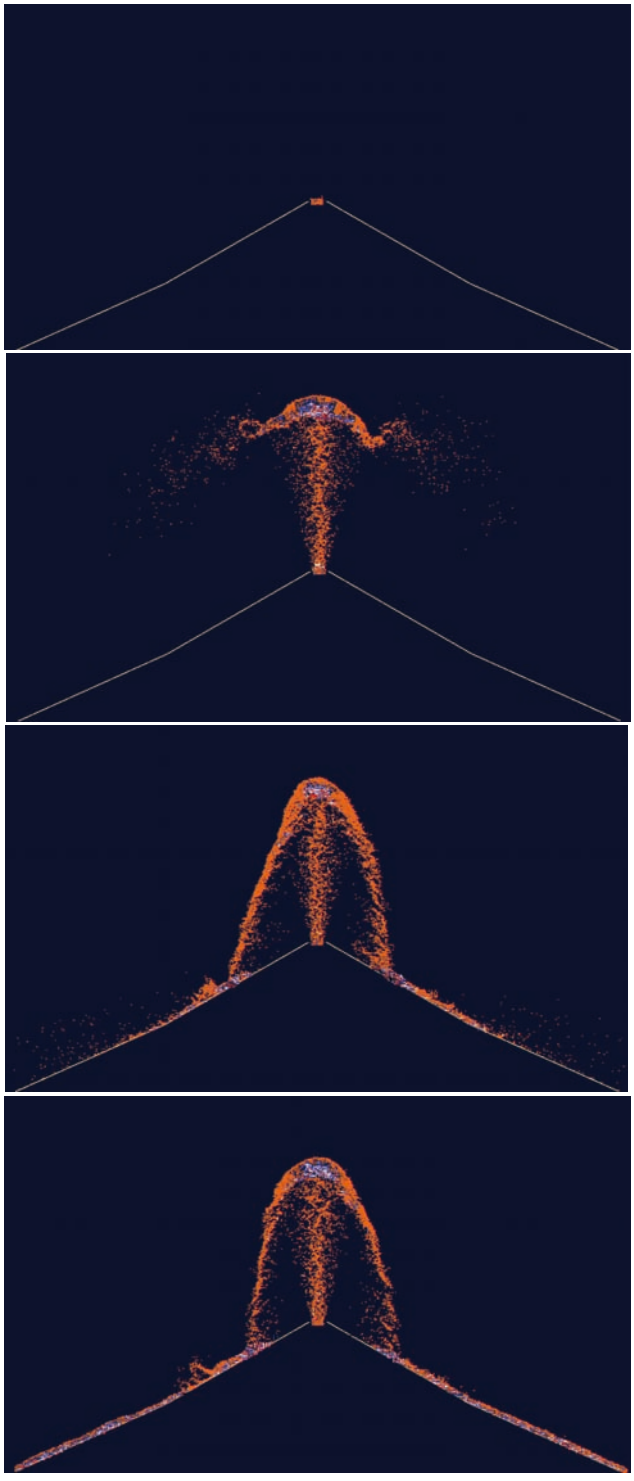

Fig. 8-2-1. DEM simulation for volcanic activities.

boundary conditions (Rotter el al., 1998) due to the large degree of freedom inherent with such a huge number of particles. The generic code for the calculations, including the DEM, is not optimized for specified objectives, and thus the calculation speed is not so fast.

The author has research experience with DEM for over 20 years and developed a DEM code called FastDisc at the Commonwealth Scientific and Industrial Research Organization (CSIRO) in collaboration with Dr. Peter Cundall, who is the pioneer of DEM and developer of the PFC series. Based on this expertise, our group has developed the DEM code for each kind of object-oriented fast computing through special customization. As a result, we completed the ultimate code, which saves occupied-memory size and runs fast calculations on a personal computer/work station, as HiDEM.

HiDEM, which has been developed at JAMSTEC over four years, has been applied to scientific research and industrial utilization by four universities, two public research institutes, and six private companies. After JAMSTEC became an independent agency of the Japanese government, scientific results were released publicly, and income for the intellectual property of HiDEM achieved 4.5 million, 6 million, 3 million, and 14 million yen in fiscal 2005, fiscal 2006, fiscal 2007, and fiscal 2008, respectively. Moreover, we have two patent applications using the subroutine developed for fast computing, which is part of HiDEM. One of the patents, in collaboration with Doshisya University, is utilized for motion analysis of toner particles in electrophotographic machines (printers that use toner, fax machines, and copy machines).

HiDEM is also applied in rubber and ink industries, as recent topics suggest. JAMSTEC is currently studying the application of HiDEM with Sumitomo Rubber Industries and Inctec Inc., and these studies contribute to the development of hyperelastic mechanisms of natural rubbers and high-performance inks (Fig. 8-2-2). HiDEM, moreover, is also used for the development of burial technology for nuclear waste. In addition, many civil companies have already adopted HiDEM for analyses of stable ground and countermeasures to liquefaction.

Thus the demand for numerical simulations using HiDEM is expected to increase further. Our research group has carried out programming development using a GPU that enables high-performance parallel computing at low cost by using normal personal computers and workstations. To date, the author has confirmed that it has high-speed calculation ability over 30 times faster than computing with current CPUs, and he has submitted a new patent application for the special algorithm used for particle calculation on the GPU. Commercial products using the GPU programming will be released in fiscal 2009.

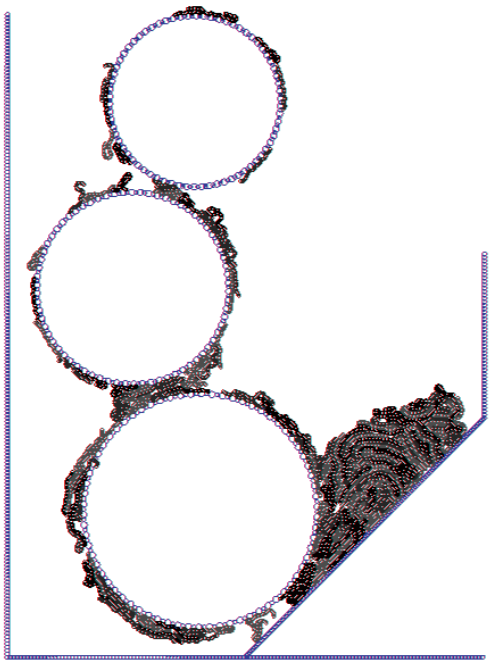

Fig. 8-2-2. HiDEM simulation for transformation in ink to a roller.

Conclusion

This article was written at the end of fiscal 2008 (March 2009). This timing coincided with a reorganization of IFREE that involved substantial changes in the organization's structure and membership. The article, accordingly, may be regarded as the final summary report from IFREE in its present form.

Acknowledgement

We would like to thank Nobuo Ito and Tomomi Iseki for their help in preparing the manuscript.

Publication List

Publications for §1
(Names of the IFREE members underlined)

Araki, E., M. Shinohara, K. Obana, T. Yamada, Y. Kaneda, T. Kanazawa, and K. Suyehiro (2006), Aftershock distribution of the 26 December 2004 Sumatra-Andaman earthquake from ocean bottom seismographic observation, *Earth Planets Space, 58*, 113-119.

Araki, E., M. Shinohara, S. Sacks, A. Linde, T. Kanazawa, H. Shiobara, H. Mikada, and K. Suyehiro (2004), Improvement of Seismic Observation in the Ocean by Use of Seafloor Boreholes, *Bulletin of the Seismological Society of America, 94*, 678-690..

Davis, E. E., K. Becker, K. Wang, K. Obara, Y. Ito and M. Kinoshita (2006), A discrete episode of seismic and aseismic deformation of the Nankai trough subduction zone accretionary prism and incoming Philippine Sea plate, *Earth Planet. Sci. Lett., 242*, 73-84.

Dessa, J.-X., S. Operto, S. Kodaira, A. Nakanishi, G. Pascal, J. Virieux, and Y. Kaneda (2004), Multiscale seismic imaging of the eastern Nankai trough by full waveform inversion, *Geophys. Res. Lett., 31*, L18606, doi:10.1029/2004GL020453.

Dessa, J.-X., S. Operto, S. Kodaira, A. Nakanishi, G. Pascal, K. Uhira and Y. Kaneda (2004), Deep seismic imaging of the eastern Nankai Trough, Japan, from multifold OBS data by combined traveltime tomography and prestack depth migration, *Jour. Geophys. Res., 109*, No. B2, B02111, 10.1029/2003JB002689.

Hori, T. (2009), Mechanisms for variation in size and occurrence interval of interplate earthquakes, *Zisin*.

Hori, T. (2006), Mechanisms of separation of rupture area and variation in time interval and size of great earthquakes along the Nankai Trough, southwest Japan, *J. Earth Simulator, 5*, 8-19.

Hori, T., N. Kato, K. Hirahara, T. Baba and Y. Kaneda (2004), A numerical simulation of earthquate cycles along the Nankai trough, southwest Japan: Lateral variation in frictional property due to the slab geometry controls the nucleation position, *Earth Planet. Sci. Lett., 228*, 215-226.

Kanamatsu, T., Emilio and Herrero-Bervera (2006), Anisotropy of magnetic susceptibility and paleomagnetic studies in relation to the tectonic evolution of the Miocene-Pleistocene accretionary sequence in the Boso and Miura Peninsulas, central Japan, *Tectonophysics, 418*, 1-2, 131-144.

Kasaya, T., T. Goto, H. Mikada, K. Baba, K. Suyehiro, and H. Utada (2005), Resistivity image of the Philippine Sea Plate around the 1944 Tonankai earthquake xone deduced by Marine and Land MT surveys, *Earth Planets Space, 57*, 209-213.

Kato, A., A. Sakaguchi, S. Yoshida, H. Yamaguchi, and Y. Kaneda (2004), Permeability structure around an ancient exhumed subduction-zone fault, *Geophys. Res. Lett., 31*, L06602, doi:10.1029/2003GL019183.

Kimura, G., Y. Kitamura, Y. Hashimoto, A. Yamaguchi, T. Shibata, K. Ujiie, and S. Okamoto (2007), Transition of accretionary wedge structures around the up-dip limit of the seismogenic subduction zone, *Earth Planet Sci. Lett., 255*, 471-484.

Kinoshita, M., T. Kanamatsu, K. Kawamura, T. Shibata, H. Hamamoto, and K. Fujino (2008), Heat flow distribution on the floor of Nankai Trough off Kumano and implications for the geothermal regime of subducting sediments, *JAMSTEC Rep. Res. Dev., 8*, 13-28.

Kinoshita, M., R. Von Huene, G. Moore, H. Tobin, and C. R. Ranero (2006), The seismogenic zone experiment, *Oceanography, 19*, 28-38.

Kodaira, S. (2009), Active Source Seismic Studies in Subduction Zones around Japan - Recent Results from Seismic Surveys in Subduciton Seismogenic Zones and Intra-Oceanic Arcs -, *Zisin*.

Kodaira, S., T. Hori, A. Ito, S. Miura, G. Fujie, J.-O. Park, T. Baba, H. Sakaguchi and Y. Kaneda (2006), A cause of rupture segmentation and synchronization in the

Nankai trough reveled from seismic imaging and numerical simulation, *Jour. Geophys. Res., 111*, B09301, doi:10.1029/2005JB004030.

Kodaira, S., T. Iidaka, A. Nakanishi, J.-O. Park, T. Iwasaki, and Y. Kaneda (2005), Onshore-offshore seismic transect from the eastern Nankai Trough to central Japan crossing a zone of the Tokai slow slip event, *Earth Planets and Space, 57*, 943-959.

Kodaira, S., T. Iidaka, A. Kato, J.-O. Park, T. Iwasaki, and Y. Kaneda (2004), High pore fluid pressure may cause silent slip in the Nankai Trough, *Science, 304*, 1295-1298.

Mukoyoshi, H., A. Sakaguchi, K. Otsuki, T. Hirono, and W. Soh (2006), Co-seismic frictional melting along an out-of-sequence thrust in the Shimanto accretionary complex. Implications on the tsunamigenic potential of splay faults in modern subduction zones, E*arth Planet. Sci. Lett., 245*, 330-343.

Nakanishi, A., E. Kurashimo, Y. Tatsumi, H. Yamaguchi, S. Miura, S. Kodaira, K. Obana, N. Takahashi, T. Tsuru, Y. Kaneda, T. Iwasaki, and N. Hirata (2009), Crustal evolution of the southwestern Kuril Arc, Hokkaido Japan, deduced from seismic velocity and geochemical structure, *Tectonophysics*.

Nakanishi A., S. Kodaira, S. Miura, A. Ito, T. Sato, J.-O. Park, Y. Kido, and Y. Kaneda (2008), Detailed structural image around splay-fault branching in the Nankai subduction seismogenic zone: Results from a high-density ocean bottom seismic survey, *J. Geophys. Res., 113*, B03105, doi:10.1029/2007JB004974.

Nakanishi, A., A. J. Smith, S. Miura, T. Tsuru, S. Kodaira, K. Obana, N. Takahashi, P. R. Cummins and Y. Kaneda (2004), Structural factors controlling the coseismic rupture zone of the 1973 Nemuro-Oki earthquake, the southern Kuril Trench seismogenic zone, *J. Geophys. Res., 109*, doi:10.1029/2003JB002574.

Obana, K., S. Kodaira, and Y. Kaneda (2009), Seismicity at the Eastern End of the 1944 Tonankai Earthquake Rupture Area, *Bulletin of the Seismological Society of America, 99*, 110-122, doi: 10.1785/0120070236.

Obana, K., S. Kodaira, and Y. Kaneda (2006), Seismicity related to heterogeneous structure along the western Nankai trough off Shikoku Island, *Geophys. Res. Lett., 33*, L23310, doi:10.1029/2006GL028179.

Obana, K., S. Kodaira, and Y. Kaneda (2005), Seismicity in the incoming/subducting Philippine Sea plate off the Kii Peninsula, central Nankai trough, *J. Geophysi. Res., 110*, B11311, doi:10.1029/2004JB003487.

Obana, K., S. Kodaira, and Y. Kaneda (2004), Microseismicity around rupture area of the 1944 Tonankai earthquake from ocean bottom seismograph observations, *Earth Planet. Sci. Lett., 222*, 2, 561-572.

Sakai, S., T. Yamada, M. Shinohara, H. Hagiwara, T. Kanazawa, K. Obana, S. Kodaira, and Y. Kaneda (2005), Urgent aftershock observation of the 2004 off the Kii Peninsula earthquake using ocean bottom seismometers, *Earth Planet. Space, 57*, 363-368.

Sawyer, Audrey H., P. Flemings, D. Elsworth, and M. Kinoshita (2008), Response of Submarine Hydrologic Monitoring Instruments to Formation Pressure Changes: Theory and Application to Nankai ACORKs, *J. Geophys. Res., 113*, B01102, doi:10.1029/2007JB005132.

Smith, A.J., P.R. Cummins, T. Baba, S. Kodaira, Y. Kaneda, and H. Yamaguchi (2004), Intraplate Seismicity in the subducting Philippine Sea Plate,Southwest Japan, *Physics Earth Planetary Interiors, 145*, 179-202.

Suyehiro, K., J.-P. Montagner, R. Stephen, E. Araki, T. Kanazawa, J. Orcott, B. Romanowicz, S. Sacks, and M. Shinohara (2006), Ocean Seismic Observatories, *Oceanography, 19*,144-149.

Tobin, H., and M. Kinoshita (2006), NanTroSEIZE: The IODP Nankai Trough Seismogenic Zone Experiment, *Scientific Drilling, 2*, 23-27, doi:10.2204/iodp.sd.2.06.

Ujiie, K., A. Yamaguchi, and S. Taguchi (2008), Stretching of fluid inclusions in calcite as an indicator of frictional heating on faults, *Geology, 36*, 111-114, doi:10.1130/G24263A.1.

Ujiie, K., H. Yamaguchi, A. Sakaguchi, and S. Toh (2007), Pseudotachylytes in an ancient accretionary complex and implications for melt lubrication during subduction zone earthquakes, 2, 599-613.

Publications for §2

(Names of the IFREE members underlined)

Embley, R. W., W. W. Chadwick, E. T. Baker, D. A. Butterfield, J. A. Resing, C. E. J. de Ronde, V. Tunnicliffe, J. E. Lupton, S. K. Juniper, K. H. Rubin, R. J. Stern, G. T. Lebon, K-i. Nakamura, S. G. Merle, J. R. Hein, D. A. Wiens, and Y. Tamura (2006), Long-term eruptive activity at a submarine arc volcano, *Nature, 441*, 7092, 494-497.

Fujiwara, T., Y. Kido, Y. Tamura, and O. Ishizuka (2009), Gravity and magnetic constraints on the crustal structure and evolution of the Horeki seamount in the Izu-Ogasawara (Bonin) arc, *Earth Planets Space*.

Isse, T., H. Shiobara, Y. Tamura, D. Suetsugu, K. Yoshizawa, H. Sugioka, A. Ito, T. Kanazawa, M. Shinohara, K. Mochizuki, E. Araki, K. Nakahigashi, H. Kawakatsu, A. Shito, Y. Fukao, O. Ishizuka, and J. B. Gill (2009), Seismic structure of the upper mantle beneath the Philippine Sea from seafloor and land observation: implications for mantle convection and magma genesis in the Izu-Bonin-Mariana subduction zone, *Earth Planet. Sci. Lett., 278*, 107-119.

Ishizuka, O., R. N. Taylor, M. Yuasa, J. A. Milton, R. W. Nesbitt, K. Uto, I. Sakamoto (2007), Processes controlling along-arc isotopic variation of the southern Izu-Bonin arc., *Geochem. Geophys. Geosyst., 8*, Q06008, doi:10.1029/2006GC001475.

Ishizuka, O., J-I. Kimura, Y. B. Li, R. J. Stern, M. Reagan , R. N. Taylor , Y. Ohara , S. H. Bloomer , T. Ishii, U. Hargrove , S. Haraguchi (2006), Early stages in the evolution of Izu-Bonin arc volcanism: new age, chemical, and isotopic constraints, *Earth Planet. Sci. Lett., 250*, 386-401, doi:10.1016/j.epsl.2006.08.007.

Kodaora, S.., T. Sato, N. Takahashi, M. Yamashita, T. No, and Y. Kaneda (2008), Seismic imaging of a possible paleo-arc in the Izu-Bonin intra-oceanic arc and its implications for arc evolution processes, *Geochem. Geophys. Geosyst*., Q10X01,doi:10.1029/2008GC002073.

Kodaora, S.., T. Sato, N. Takahashi, A. Ito, Y. Tamura, Y. Tatsumi, and Y. Kaneda (2007), Seismological evidence for variable growth of crust along the Izu intra-oceanic arc,, *J. Geophys. Res., 112*, B05104, doi:10.1029/2006JB004593.

Kodaora, S.., T. Sato, N. Takahashi, S. Miura, Y. Tamura, Y. Tatsumi, and Y. Kaneda (2007), New seismological constraints on growth of continental crust in the Izu-Bonin intra-oceanic arc, *Geology, 35*, 11, 1031-1034.

Nishizawa, A., K. Kaneda, A. Nakanishi, N. Takahashi, and S. Kodaora (2006), Crustal structure of the ocean-island arc transition at the mid Izu-Ogasawara(Bonin) arc margin Implementation, *Earth Planet. Space e-lett., 58*, 8, e33-e36.

Sato, T., S. Kodaira, N. Takahashi, Y. Tatsumi, and Y. Kaneda (2009), Amplitude modeling of the seismic reflectors in the crust-mantle transition layer beneath the volcanic front along the northern Izu-Bonin island arc, *Geochem. Geophys. Geosyst., 10*, Q02X04.

Shukuno, H., Y. Tamura, K. Tani, Q. Chang, T. Suzuki, and R. S. Fiske (2006), Origin of silicic magmas and the compositional gap at Sumisu submarine caldera, Izu-Bonin arc, Japan, *J. Volcanol. Geotherm. Res, 156*, 3-4, 187-216.

Stern, R. J., Y. Tamura, R. W. Embley, O. Ishizuka, S. G. Merle, N. K. Basu, H. Kawabata, and S. H. Bloomer (2008), Evolution of West Rota Volcano, an extinct submarine volcano in the southern Mariana Arc: Evidence from sea floor morphology, remotely operated vehicle observations and 40Ar-39Ar geochronological studies., *Island Arc, 17*, 70-89.

Takahashi, N., S. Kodaora, Y. Tatsumi, Y. Kaneda, and K. Suyehiro (2008), Structure and growth of the Izu-Bonin-Mariana arc crust: I. Seismic constraint on crust and mantle structure of the Mariana arc - backarc system, *J. Geophys. Res., 113*, B01104, doi:10.1029/2007JB005120.

Takahashi, N., S. Kodaora, S. L. Klemperer, Y. Tatsumi, Y. Kaneda, and K. Suyehiro (2007), Crustal structure and evolution of the Mariana intra-oceanic island arc, *Geology, 35*, 3, 203-206.

Tamura, Y., J. Nakajima, S. Kodaira, and A. Hasegawa (2008), Tectonic Setting of Volcanic Centers in Subduction Zones: 3D Structure of Mantle Wedge and Arc Crust, *In*: Volcanism, Tectonism and the Siting of Nuclear Facilities, edited by C. Connor, N. Chapman and L. Connor.

Tamura, Y., K. Tani, Q. Chang, H. Shukuno, H. Kawabata, O. Ishizuka, and R. S. Fiske (2007), Wet and dry basalt magma evolution at torishima volcano, izu-bonin arc, japan: the possible role of phengite in the downgoing slab., *J. Petrol., 48*, 10, 1999-2031.

Tamura, Y. and R. Wysoczanski (2006), Silicic volcanism and crustal evolution in oceanic arcs: Introduction, *J. Volcanol. Geotherm. Res., 156*, doi:10.1016/j.jvolgeores.2006.03.001.

Tamura, Y, K. Tani, O. Ishizuka, Q. Chang, H. Shukuno, and R. S. Fiske (2005), Are arc basalts dry, wet, or both? Evidence from the Sumisu caldera volcano, Izu-Bonin arc, Japan, *J. Petrol., 46*, 9, 1769-1803.

Tani, K., R. Fiske, Y. Tamura, Y. Kido, J. Naka, H. Shukuno, and L. Takeuchi (2008), Sumisu volcano, Izu-Bonin arc, Japan: Site of a silicic caldera-forming eruption

from a small openocean island, *Bull. Volcanol., 70*, 547-562.

Tatsumi Y., H. Shukuno, K. Tani, N. Takahashi, S. Kodaira, and T. Kogiso (2008), Structure and growth of the Izu-Bonin-Mariana arc crust: 2. Role of crust-mantle transformation and the transparent Moho in arc crust evolution, *J. Geophys. Res., 113*, B02203, doi:10.1029/2007JB005121.

Tatsumi, Y. (2008), Making continental crust: the sanukitoid connection, *Chinese Sci. Bull., 53*, 2, 1620-1633.

Tatsumi, Y. (2005), The subduction factory: how it operates in the evolving Earth, *GSA Today, 15*, 7, 4-10.

Tatsumi, Y. and R. J. Stern (2006), Manufacturing Continental Crust in the Subduction Factory, *Oceanography, 19*, 4, 104-112.

Wysoczaski, R., K. Tani (2006), Spectroscopic FTIR imaging of water species in silicic volcanic glasses and melt inclusions: An example from the Izu-Bonin arc, *J. Volcanol. Geotherm. Res., 156*, 302-314.

Publications for §3

(Names of the IFREE members underlined)

Chikaraishi, Y., Kashiyama, Y., Ogawa, N. O., Kitazato, H., Satoh, M., Nomoto, S., and Ohkouchi, N. (2008), A compound-specific isotope method for measuring the stable nitrogen isotopic composition of tetrapyrroles. *Organic Geochemistry, 39*, 510-520.

K. Shinotsuka and K. Suzuki (2007), Simultaneous determination of platinum group elements and rhenium in rock samples using isotope dilution ICP-MS after cation exchange followed by solvent extraction, *Anal. Chim. Acta, 603*, 129-139, doi:10.1016/j.aca.2007.09.042

K. Suzuki, Y. Miyata, and N. Kanazawa (2004), Precise Re isotope ratio measurements by negative thermal ionization mass spectrometry (NTI-MS) using total evaporation technique, *Int. J. Mass Spectrom., 235*, no. 1, 97-101.

Kashiyama, Y., N. O. Ogawa, J. Kuroda, H. Kitazato, and N. Ohkouchi (2008), Diazotrophic cyanobacteria as the major photoautotrophs during mid-Cretaceous Oceanic Anoxic Events: nitrogen and carbon isotopic evidence of sedimentary porphyrin, *Organic Geochemistry, 39*, 532-549.

Kashiyama, Y., N. O. Ogawa, R. Tada, H. Kitazato, and N. Ohkouchi (2008), Biogeochemistry and ecology of photoautotrophs reconstructed from nitrogen and carbon isotopic compositions of vanadyl porphyrins from Miocene siliceous sediments, *Biogeosciences, 5*, 797-816.

Kashiyama, Y., R. Tada, N. O. Ogawa, H. Kitazato, and N. Ohkouchi (2007), An improved method for isolation and purification of sedimentary porphyrins by high-performance liquid chromatography for compound-specific isotopic analysis, *Journal of Chromatography A, 1138*, 73-83.

Kashiyama, Y., M. Shiro, R. Tada, and N. Ohkouchi (2007), A novel vanadyl alkylporphyrins from geological samples: a possible derivative of divinylchlorophylls or bacteriochlorophyll a? *Chemistry Letters, 36*, 706-707.

Kashiyama, Y., H. Kitazato, and N. Ohkouchi (2006), An improved method for isolation and purification of sedimentary porphyrins by high-performance liquid chromatography for compound-specific isotopic analysis, *Journal of Chromatography A, 1138*, 73-83.

Kuroda, J., N. O. Ogawa, M. Tanimizu, M. F. Coffin, H. Tokuyama, H. Kitazato, and N. Ohkouchi (2007), Massive volcanism as a causal mechanism for a Cretaceous oceanic anoxic event, *Earth and Planetary Science Letters, 256*, 211-223.

Kuroda, J. and N. Ohkouchi (2006), Implications of spatiotemporal distribution of black shales during Cretaceous Oceanic Anoxic Event-2, *Paleontological Research, 10*, 345-358.

Kuroda, J., N. Ohkouchi, T. Ishii, H. Tokuyama, and A. Taira (2005), Lamina-scale variations in sedimentary components in Cretaceous black shales by chemical compositional mapping: Implications for paleoenvironmental changes during Oceanic Anoxic Events, *Geochimica et Cosmochimica Acta, 69*, 1479-1494.

M. L. G. Tejada, K. Suzuki, J. Kuroda, R. Coccioni, N. Ohkouchi, T. Sakamoto, Y. Tatsumi, and J. J. Mahoney (2009), Ontong Java Plateau and Early Aptian oceanic anoxic event: The Os isotope connection, *Geology*.

Neal, C. R., Coffin, M. F., Duncan, R. A., Eldholm, O., Erba, E., Farnetani, C., Fitton, G., Ingle, S. P., N. Ohkouchi, M. R. Rampino, M. K. Reicow, S. Self, and Y. Tatsumi (2008), Investigating Large Igneous Province formation and associated paleoenvironmental events: A white paper for scientific drilling, *Scientific Drilling Journal, 6*, 4-18.

Ohkouchi, N., Y. Nakajima, N. O. Ogawa, H. Suga, Y.

Chikaraishi, S. Sakai, and H. Kitazato (2008), Carbon isotopic composition of tetrapyrrole nucleus in chloropigments from a saline meromictic lake: A mechanistic view for interpreting isotopic signature of alkyl porphyrins in geological samples, *Organic Geochemistry, 39*, 521-531.

Ohkouchi, N., Y. Kashiyama, J. Kuroda, N. O. Ogawa, and H. Kitazato (2006), The importance of diazotrophic cyanobacteria as primary producers during Cretaceous Oceanic Anoxic Event 2, *Biogeosciences, 3*, 467-478.

Ohkouchi, N., Y. Nakajima, H. Okada, N. O. Ogawa, H. Suga, K. Oguri, and H. Kitazato (2005), Biogeochemical processes in a meronictic lake Kaiike: Implications from carbon and nitrogen isotopic compositions of photosynthetic pigments, *Environmental Microbiology, 7*, 1009-1016.

T. K. Dalai, K. Suzuki and M. Minagawa (2009), Osmium isotopes as a tracer of dust sources: A study from the Shatsky Rise, *Quaternary Science Review*, (submitted).

T.K. Dalai, K. Suzuki, M. Minagawa and Y. Nozaki (2005), Os isotopic record of the Japan Sea sediments over the last glacial-interglacial climate cycle, *Chem. Geol., 220(3-4)*, 303-314.

Kato Y., K. Fujinaga and K. Suzuki (2005), Major and trace element geochemistry and Os isotopic composition of metalliferous umbers from the late Cretaceous Japanese accretionary complex, *Geochemsitry Geophysics Geosystem, 6*, Q07004, doi: 10.1029/2005 GC000920.

Sekine Y., K. Suzuki, R. Senda, E. Tajika, R. Tada, K. Goto, S. Yamamoto, N. Ohkouchi, and N. O. Ogawa (2009), Osmium evidence for correlation between the rise of oxygen and Paleoproterozoic glaciations, *Science*, (submitted).

Publications for §4

(Names of the IFREE members underlined)

Adam, C. and A. Bonneville (2008), No thinning of the lithosphere beneath the Cook-Austral chain, *J. Geophys. Res., 113*, doi:10.1029/2007JB005313.

Adam, C., V. Vidal, and J. Escartin (2007), 80-Myr history of buoyancy and volcanic fluxes along the trails of the Walvis and St. Helena hotspots (South Atlantic), *Earth Planet. Sci. Lett., 261*, 432-442.

Isse, T., D. Suetsugu, H. Shiobara, H. Sugioka, K. Yoshizawa, T. Kanazawa, and Y. Fukao (2006), Shear wave speed structure beneath the South Pacific superswell using broadband data from ocean floor and islands, *Geophys. Res. Lett., 33*, L16303, doi:10.1029/ 2006GL026872.

Kogiso, T. and M. M. Hirschmann (2006), Partial melting experiments of bimineralic eclogite and the role of recycled mafic oceanic crust in the genesis of ocean island basalts, *Earth and Planetary Science Letters, 249*, 188-199.

Kogiso, T., M. M. Hirschmann, and M. Pertermann (2004), High-pressure partial melting of mafic lithologies in the mantle, *Journal of Petrology, 45*, 2407-2422.

Suetsugu, D., H. Shiobara, H. Sugioka, Y. Fukao, and T. Kanazawa (2007), Topography of the mantle discontinuities beneath the South Pacific superswell as inferred from broadband waveforms on seafloor, *Phys. Earth Planet. Inter. 160*, 310-318.

Suetsugu, D., H. Shiobara, H. Sugioka, G. Barruol, F. Schindele, D. Reymond, A. Bonneville, E. Debayle, T. Isse, T. Kanazawa, and Y. Fukao (2005), Probing South Pacific mantle plumes with ocean bottom seismographs, *Eos, Trans. AGU, 86*, 429 and 435.

Suetsugu, D., T. Kogiso, and B. Steinberger (2004), Mantle plumes and hot spots, in *Encyclopedia of Geology*, edited by R.C. Selley, L.R.M. Cocks, and I.R. Plimer, Elsevier.

Suetsugu, D., T. Saita, H. Takenaka, and F. Niu (2004), Thickness of the mantle transition zone beneath the South Pacific as inferred from analyses of ScS reverberated and Ps converted waves, *Phys. Earth Planet. Inter., 146*, 35-46.

Takamasa, A., S. Nakai, Y. V. Sahoo, T. Hanyu, Y. Tatsumi (2009), W isotope compositions of oceanic island basalts from French Polynesia and their meaning for core-mantle interaction, *Chemical Geology*.

Tanaka, S., M. Obayashi, D. Suetsugu, H. Shiobara, H.Sugioka, J. Yoshimitsu, T. Kanazawa, and Y. Fukao (2009), G.Barruol, P-wave tomography of the mantle beneath the South Pacific Superswell revealed by joint ocean floor and islands broadband seismic experiments, *Phys. Earth Planet. Inter., 172*, 268-277.

Yoshida Y. and D. Suetsugu (2004), Lithospheric thickness beneath the Pitcairn hot spot trail as inferred from Rayleigh wave dispersion, *Phys. Earth Planet. Inter., 146*, 75-85.

Publications for §5
(Names of the IFREE members underlined)

Fukao, Y., T. Koyama, M. Obayashi, and H. Utada (2004), Trans-Pacific temperature field in the mantle transition region derived from seismic and electromagnetic tomography, *Earth Planet. Sci. Lett., 217*, 425-434.

Fukao, Yoshio, M. Obayashi, T. Nakakuki and the Deep Slab Project Group (2009), Stagnant slab: A review, *Annu. Rev. Earth Planet. Sci*.

Gorbatov, A. and Y. Fukao (2005), Tomographic search for missing link between the remnant Farallon slab and present Cocos subduction, *Geophys. J. Int., 160*, 849-854.

Hirose K., N. Takafuji, N.Sata, and Y. Ohishi (2005), Phase transition and density of subducted MORB crust in the lower mantle, *Earth Planet. Sci. Lett., 237*, 239-251.

Ichiki M., K. Baba, M. Obayashi, and H. Utada (2006), Water content and geotherm in the upper mantle above the stagnant slab: Interpretation of electrical conductivity and seismic P-wave velocity models, *Phys. Earth Planet. Inter., 155*, 1-15.

Isse, T., H. Shiobara, Y. Tamura, D. Suetsugu, K. Yoshizawa, H. Sugioka, A. Ito, T. Kanazawa, Shinohara M., K. Mochizuki, E. Araki, K. Nakahigashi, A. Shito, Y. Fukao, O. Ishizuka, and J. B. Gill (2009), Seismic structure of the upper mantle beneath the Philippine Sea from seafloor and land observation: implications for mantle convection and magma genesis in the Izu-Bonin-Mariana subduction zone, *Earth. Planet. Sci. Lett*.

Isse, T., K. Yoshizawa, H. Shiobara, M. Shinohara, K. Nakahigashi, K. Mochizuki, H. Sugioka, D. Suetsugu, S. Oki, T. Kanazawa, K. Suyehiro, and Y. Fukao (2006), Three-dimensional shear wave structure beneath the Philippine Sea from land and ocean bottom broadband seismograms, *J. Geophys. Res., 111*, BO6310.

Isse, T., H. Shiobara, Y. Fukao, K. Mochizuki, T. Kanazawa, H. Sugioka, S. Kodaira, R. Hino, and D. Suetsugu (2004), Rayleigh wave phase velocity measurements across the Philippine sea from a broad-band OBS array, *Geophys. J. Int., 158*, 257-266.

Koyama, T., H. Shimizu, H. Utada, M. Ichiki, E. Ohtani, and R. Hae (2006), Water content in the mantle transition zone beneath the North Pacific derived from the electrical conductivity anomaly, *AGU Geophys. Monogr. Ser., 168*, 171-179.

Mibe, K,, M. Kanzaki, T. Kawamoto, K. N. Matsukage, Y. Fei, and S. Ono (2007), Second critical endpoint in the Earth's hydrous mantle, *J. Geophys. Res., 112*, 2, B03201.

Niu F, Levander A, Ham S, Obayashi M. (2005), Mapping the subducting Pacific slab Beneath southwest Japan with Hi-net receiver functions, *Earth Planet. Sci. Lett., 239*, 9 - 17.

Obayashi, M., H. Sugioka, J. Yoshimitsu, and Y. Fukao (2006), High temperature anomalies oceanward of subducting slabs at the 410-km discontinuity, *Earth Planet. Sci. Lett., 243*, 149-158.

Ohta, K., K. Hirose, T. Lay, N. Sata, Y. Ohishi (2007), Phase transitions in pyrolite and MORB at lowermost mantle conditions: Implications for a MORB-rich pile above the core-mantle boundary, *Earth Planet. Sci. Lett., 267*, 1-2, 107-117.

Ono, S. (2008), Experimental constraints on the temperature profile in the lower mantle, *Phys. Earth Planet. Inter., 170*, 3-4, 267-273.

Ono, S. (2007), The Lehmann discontinuity due to dehydration of subducted sediment, *The Open Mineralogy Journal, 1*, 1, 1-4.

Ono S., Y. Ohishi, M. Isshiki, and T. Watanuki (2005), In situ X-ray observations of phase assemblages in peridotite and basalt compositions at lower mantle conditions: implications for density of subducted oceanic plate, *J. Geophys. Res., 110*, BO2208.

Seama, N., K. Baba, H. Utada, H. Toh, N. Tada, M. Ichiki, and T. Matsuno (2007), 1-D electrical conductivity structure beneath the Philippine Sea: Results from an ocean bottom magnetotelluric survey, *Phys. Earth Planet. Inter., 162*, 2-12.

Shiobara, H., K. Baba, H. Utada, and Y. Fukao (2009), Three-year deployment of ocean bottom array to probe the stagnant slab beneath the Philippine Sea, *EOS*.

Shito, A., H. Shiobara, H. Sugioka, A. Ito, Y. Takei, H. Kawakatsu, and T. Kanazawa (2009), Physical properties of subducted slab and surrounding mantle in the Izu-Bonin subduction zone based on Broadband Ocean Bottom Seismograph data, *J. Geophys. Res*., doi:10.1029/2007JB005568.

Suetsugu, D., M. Shinohara, E. Araki, T. Kanazawa, K. Suyehiro, T. Yamada, K. Nakahigashi, H. Shiobara, H.

Sugioka, K. Kawai, and Y. Fukao (2005), Mantle discontinuity depths beneath west Philippine basin from receiver function analysis of deep-sea borehole and seafloor broadband waveforms, *Bull. Seism. Soc. Am., 95*, 1947-1956.

Suetsugu D, Inoue T, Yamada A, Zhao D, and M. Obayashi (2006), Towards mapping the three-dimensional distribution of water in the transition zone from P-velocity tomography and 660-km discontinuity depths, *AGU Geophys. Monogr. Ser., 168*, 237-249.

Tateno, S., K. Hirose, N. Sata, and Y. Ohishi (2009), Determination of post-perovskite phase transition boundary up to 4400 K and implications for thermal structure in D" layer, *Earth Planet. Sci. Lett., 277*, 130-136.

Tono, Y., T. Kunugi, Y. Fukao, S. Tsuboi, K. Kanjo, and K. Kasahara (2005), Mapping of the 410- and 660-km discontinuities beneath the Japanese islands, *J. Geophys. Res*., B03306, 10.1029/2004JB003194.

Yanagisawa, T. and Y. Yamagishi (2005), Rayleigh-Benard Convection in Spherical Shell with Infinite Prandtl Number at High Rayleigh Number, *Journal of Earth Simulator, 4*, 11-17.

Yoshida, M. and T. Nakakuki (2009), Effects on the long-wavelength geoid anomaly of lateral viscosity variations caused by stiff subducting slabs, weak plate margins and lower mantle rheology, *Phys. Earth Planet. Inter., 172*, 3-4, 278-288.

Yoshida, M. (2008), Mantle convection with longest-wavelength thermal heterogeneity in a 3-D spherical model: Degree one or two?, *Geophys. Res. Lett., 35*, L23303, doi:10.1029/2008GL036059- 2008a.

Yoshida, M. (2008), Core-mantle boundary topography estimated from numerical simulations of instantaneous mantle flow, *Geochem. Geophys. Geosyst., 9*, Q07002, doi:10.1029/2008GC002008- 2008b.

Publications for §6
(Names of the IFREE members underlined)

Asanuma, H., E. Ohtani, T. Sakai, H. Terasaki, N. Hirao, N. Sata, and Y. Ohishi (2008), Phase relations of Fe-Si alloy up to core conditions: Implications for the Earth's inner core, *Geophys. Res. Lett., 35*, doi:10.1029 /2008GL033863-2008.

Fujino, K., K. Suzuki, D. Nishio-Hamane, Y. Seto, T. Nagai, and N. Sata (2008), High pressure phase relation of $MnSiO_3$ up to 85 GPa: Existence of $MnSiO_3$ perovskite, *Am. Mineral., 93*, 653-657.

Hirose, K., N. Sata, T. Komabayashi, and Y. Ohishi (2008), Simultaneous volume measurements of Au and MgO to 140 GPa and thermal equation of state of Au based on the MgO pressure scale, *Phys. Earth Planet. Inter., 167*, 149-154.

Hirose, K., R. Sinmyo, N. Sata, and Y. Ohishi (2006), Determination of post-perovskite phase transition boundary in MgSiO3 using Au and MgO pressure standards, *Geophys. Res. Lett., 33*, L01310, doi:10.1029/2005GL024468-2006.

Hirose, K., K. Kawamura, Y. Ohishi, S. Tateno, and N. Sata (2005), Stability and equation of state of $MgGeO_3$ post-perovskite phase, *Am. Mineral., 90*, 262-265.

Ichikawa, H., K. Kurita, Y. Yamagishi, and T. Yanagisawa (2006), Cell pattern of thermal convection induced by internal heating, *Physics of Fluids, 18*, 038101.

Ishibashi, I., K. Hirose, N. Sata, and Y. Ohishi (2007), Dissociation of CAS phase in the uppermost lower mantle, *Phys. Chem. Mineral., 35*, 197-200.

Komabayashi, T., K. Hirose, E. Sugimura, N. Sata, Y. Ohishi, and L. S. Dubrovinsky (2008), Simultaneous volume measurements of post-perovskite and perovskite in $MgSiO_3$ and their thermal equations of state, *Earth Planet. Sci. Lett., 265*, 3-4, 515-524.

Komabayashi, T., K. Hirose, N. Sata, Y. Ohishi, and L. S. Dubrovinsky (2007), Phase transition in $CaSiO_3$ perovskite, *Earth Planet. Sci. Lett., 260*, 3-4, doi:10.1016/j.epsl.2007.06.015-2007.

Kuwayama, Y., K. Hirose, N. Sata, and Y. Ohishi (2008), Phase relations of iron and iron, *Earth Planet. Sci. Lett., 273*, 379-385.

Kuwayama, Y., K. Hirose, N. Sata, and Y. Ohishi (2005), The pyrite-type high-pressure form of silica, *Science, 309*, 923-925.

Mibe, K., M. Kanzaki, T. Kawamoto, K. N. Matsukage, Y. Fei, and S. Ono (2007), Second critical endpoint in the Earth's hydrous mantle, *J. Geophys. Res., 112*, B03201.

Mibe, K., T. Fujii, A. Yasuda, and S. Ono (2006), Mg-Fe partitioning between olivine and ultramafic melts at high pressures, *Geochim. Cosmocim. Acta., 70*, 757-766.

Murakami, M., S. V. Sinogeikin, J. D. Bass, N. Sata, Y. Ohishi, and K. Hirose (2007), Sound velocity of

$MgSiO_3$ post-perovskite phase: A constraint on the D" discontinuity, *Earth Planet. Sci. Lett., 259*, 18-23.

Murakami, M., K. Hirose, N. Sata, and Y. Ohishi (2005), Post-perovskite phase transition and mineral chemistry in the pyrolitic lowermost mantle, *Geophys. Res. Lett., 32*, L03304- 2005.

Nishiyama, N., T. Yagi, S. Ono, H. Gotou, and T. Harada (2007), Effect of incorporation of iron and aluminum on the thermoelastic properties of magnesium silicate perovskite, *Phys. Chem. Mineral, 34,* 131-143.

Oganov, A. R., S. Ono, Y. Ma, C. W. Glass, and A. Garcia (2008), Novel Phases of $MgCO_3$, $CaCO_3$ and CO_2 and their role in the Earth's mantle, *Earth Planet. Sci. Lett., 273*, 38-47.

Oganov, A. R., C. W. Glass, and S. Ono (2006), High-pressure phases of $CaCO_3$: crystal structure prediction and experiment, *Earth Planet. Sci. Lett. 241*, 95-103.

Oganov, A. R. and S. Ono (2005), The high pressure phase of alumina and implications for Earth's D" layer, *Proc. Natl. Acad. Sci., 102*, 31, 10828-10831.

Oganov, A. R. and S. Ono (2004), Theoretical and experimental evidence for a post-perovskite phase of $MgSiO_3$ in Earth's D" layer, *Nature, 430*, 445-448.

Ohfuji, H., N. Sata, H. Kobayashi, Y. Ohishi, and K. Hirose (2007), T. Irifune, A new high-pressure and high-temperature polymorph of FeS, *Phys. Chem. Mineral., 34*, 5, 335-343.

Ohishi, Y., N. Hirao, N. Sata, K. Hirose, and M. Takata (2008), Highly intense monochromatic X-ray diffraction facility for high-pressure research at SPring-8, *High Pressure Res., 28*, doi:10.1080/08957950802208910-2008.

Ohishi, Y., A Sakuraba, and Y. Hamano (2007), Numerical method for geodynamo simulations based on Fourier expansion in longitude and finite difference in meridional plane, Phys. *Earth Planet. Inter., 164*, 208-220.

Ohta, K., S. Onoda, K. Hirose, R. Sinmyo, K. Shimizu, N. Sata, Y. Ohishi, and A. Yasuhara (2008), The Electrical Conductivity of Post-Perovskite in Earth's D" Layer, *Science, 320*, 89-91.

Ohta, K., S. Onoda, K. Hirose, R. Sinmyo, K. Shimizu, N. Sata, Y. Ohishi, and A. Yasuhara (2008), The Electrical Conductivity of Post-Perovskite in Earth's D" Layer, *Science, 320*, 89-91.

Ohta, K., K. Hirose, T. Lay, N. Sata, and Y. Ohishi (2007), Phase transitions in pyrolite and MORB at lowermost mantle conditions: Implications for a MORB-rich pile above the core-mantle boundary, *Earth Planet. Sci. Lett., 267*, 1-2, 107-117.

Ono, S. (2008), Experimental constraints on the temperature profile in the lower mantle, *Phys. Earth Planet. Inter., 170*, 3-4, 267-273.

Ono, S., J. P. Brodholt, and G. D. Price (2008), First-principles simulation of high-pressure polymorphs in $MgAl_2O_4$, *Phys. Chem. Mineral., 35*, 7, 381-386.

Ono, S., J. P. Brodholt, G. D. Price (2008), Phase transitions of $BaCO_3$ at high pressures, *Mineralogical Mag., 72*, 659-665.

Ono, S., J. P. Brodholt, G. D. Price (2008), Structural phase transitions in IrO_2 at high pressures, *J. Phys. Condens. Matter, 20*, 045202.

Ono, S. (2007), The Lehmann discontinuity due to dehydration of subducted sediment, *The Open Mineralogy Journal, 1*, 1-4.

Ono, S. (2007), High-pressure phase transformation in $MnCO_3$: a synchrotron XRD study, *Mineral. Mag., 71*, 105-111.

Ono, S., T. Kikegawa, and Y. Ohishi (2007), High-Pressure Transition of $CaCO_3$, *Am. Mineral., 92*, 1246-1249.

Ono, S., Y. Nakajima, and K. Funakoshi (2007), In situ observations of decomposition of kyanite at high pressures and high temperatures, *Am. Mineral., 92*, 1624-1629.

Ono, S. (2007), New high-pressure phases in $BaCO_3$, *Phys. Chem. Minerals, 34*,215-221.

Ono, S., A.R. Oganov, T. Koyama, and H. Shimizu (2006), Stability and compressibility of the high-pressure phases of Al_2O_3 up to 200 GPa: implications for the electrical conductivity of the base of the lower mantle, *Earth Planet. Sci. Lett., 246*, 3, 326-335.

Ono, S., T. Kikegawa, and Y. Ohishi (2006), The Stability and compressibility of $MgAl_2O_4$ high-pressure polymorphs, *Phys. Chem. Mineral., 33*, 3, 200-206.

Ono, S., T. Kikegawa, Y. Ohishi (2006), Structural properties of $CaIrO_3$-type $MgSiO_3$ up to 144 GPa, *Am. Mineral., 91*, 1, 475-478.

Ono, S., Y. Ohishi, M. Isshiki, and T. Watanuki (2005), In situ x-ray observations of phase assemblages in peridotite and basalt compositions at lower mantle conditions, *J. Geophys. Res., 110*, doi:10.1029/2004JB003196-2005.

Ono, S., K. Funakoshi, Y. Ohishi, and E. Takahashi (2005),

In situ X-ray observation of phase transition between hematite-perovskite structures in Fe_2O_3, *J. Physics: Condensed Matter, 17*, 269-276.

Ono, S., T. Iizuka, and T. Kikegawa (2005), Compressibility of the calcium aluminosilicate, CAS, phase to 44 GPa, *Phys. Earth Planet. Inter., 150*, 4, 331-338.

Ono, S., and A. R. Oganov (2005), In situ observations of phase transition between perovskite and $CaIrO_3$-type phase in $MgSiO_3$ and pyrolitic mantle composition, *Earth Planet. Sci. Lett., 236*, 3, 914-932.

Ono, S., and Y. Ohishi (2005), Phase transformation of perovskite structure in Fe_2O_3 at high pressures and high temperatures, *J. Phys. Chem. Solid, 66*, 10, 1714-1720.

Ono, S., T. Kikegawa, Y. Ohishi, and J. Tsuchiya (2005), Post-aragonite phase transformation in $CaCO_3$ at 40 GPa, *Am. Mineral., 90*, 667-671.

Ono, S., T. Kikegawa, and Y. Ohishi (2005), High-pressure and high-temperature synthesis of a cubic IrO_2 polymorph, *Physica B, 363*, 140-145.

Ono, S., K. Funakoshi, A. Nozawa and T. Kikegawa (2005), High-pressure phase transitions in SnO_2, *J. Appl. Phys., 97*, 073523.

Ono, S., T. Kikegawa, and Y. Ohishi (2004), High-pressure phase transition of hematite, Fe_2O_3, *J. Phys. Chem. Solid., 65*, 1527-1530.

Ono, S., T. Kikegawa, and T. Iizuka (2004), The equation of state of orthorhombic perovskite in a peridotitic mantle composition to 80 GPa: Implications for chemical composition of the lower mantle, *Phys. Earth Planet. Inter., 145*, 9-17.

Ono, S., Y. Ohishi, and K. Mibe (2004), Phase transition of Ca-parovskite and stability of Al-bearing Mg-perovskite in the lower mantle, *Am. Mineral., 89*, 1480-1485.

Ono, S., A. R. Oganov, J. P. Brodholt, L. Vo_adlo, I. G. Wood, A. Lyakhov, C. W. Glass, A. S. Côté, G. D. Price (2008), High-pressure phase transformations of FeS: novel phases at conditions of planetary cores, *Earth Planet. Sci. Lett., 272*, 481-487.

Ono, S., Y. Ohishi, T. Kikegawa (2007), High-pressure study of rhombohedral iron oxide, FeO, at pressures between 41 and 142 GPa, *J. Phys. Condens. Matter, 19*, 036205.

Ono, S., T. Kikegawa, Y. Ohishi (2007), Static compression of high-pressure phase FeSi, *Eur. J. Mineral., 19*, 183-187.

Ono, S., T. Kikegawa (2006), High-pressure study of FeS, between 20 and 120 GPa, using synchrotron X-ray powder diffraction, *Am. Mineral., 91*, 1941-1944.

Ozawa, O., K. Hirose, M. Mitome, Y. Bando, N. Sata, and Y. Ohishi (2008), Chemical equilibrium between ferropericlase and molten iron to 134 GPa and implications for iron content at the bottom of the mantle, *Geophys. Res. Lett., 35*, doi:10.1029/2007GL032648-2008.

Sakuraba, A., and Y. Hamano (2007), Turbulent structure in Earth's fluid core inferred from time series of geomagnetic dipole moment, *Geophys. Res. Lett., 34*, L15308, doi:10.1029/2007GL029898.

Sano, A., E. Ohtani, T. Kondo, N. Hirao, T. Sakai, N. Sata, Y. Ohishi, and T. Kikegawa (2007), Aluminous hydrous mineral δ-AlOOH as a carrier of hydrogen into the core mantle boundary, *Geophys. Res. Lett., 35*, L03303, doi:10.1029/2007GL031718.

Sata, N., H. Ohfuji, K. Hirose, H. Kobayashi, Y. Ohishi, and N. Hirao (2008), New high-pressure B2 phase of FeS above 180 GPa, *Am. Mineral., 93*, 492-494.

Shieh, S. R., T. S. Duffy, A. Kubo, G. Shen, V. B. Prakapenka, N. Sata, K. Hirose, and Y. Ohishi (2006), Equation of state of the postperovskite phase synthesized from a natural $(Mg,Fe)SiO_3$ orthopyroxene, *Proceedings of the National Academy of Sciences of the United States of America, 103*, 9, doi:10.1073/pnas.0506811103-2006.

Shimizu, H., T. Iitaka, T. Fukushima, T. Kume, S. Sasaki, N. Sata, Y. Ohishi, H. Fukuoka, and S. Yamanaka (2007), Raman and x-ray diffraction studies of Ba doped germanium clathrate Ba_8Ge_{43} at high pressure, *J. Appl. Phys., 101*, doi:10.1063/1.2713354-2007.

Sinmyo, R., K. Hirose, D. Nishio-Hamane, Y. Seto, K. Fujino, N. Sata, and Y. Ohishi (2008), Partitioning of iron between perovskite/postperovskite and ferropericlase in the lower mantle, *J. Geophys. Res., 113*, doi:10.1019/2008JB005730-2008.

Sinmyo, R., H. Ozawa, K. Hirose, A. Yasuhara, N. Endo, N. Sata, and Y. Ohishi (2008), Ferric iron content in $(Mg,Fe)SiO_3$ perovskite and postperovskite at deep lower mantle conditions, *Am. Mineral., 93*, doi:10.2138/am.2008.2806-2008.

Stebbins, J. F., L-S. Du, K. Kelsey, H. Kojitani, M. Akaogi, and S. Ono (2006), Aluminum substitution in stishovite and $MgSiO_3$ perovskite: High-resolution ^{27}Al NMR, *Am. Mineral., 91*, 337-343.

Sugimura, E., T. Iitaka, K. Hirose, Kawamura, N. Sata, and

Y. Ohishi (2008), Compression of H_2O ice to 126 GPa and implications for hydrogenbond symmetrization: Synchrotron x-ray diffraction measurements and density-functional calculations, *Phys. Rev. B, 77*, doi:10.1103/PhysRevB.77.214103-2008.

Tange, T., E. Takahashi, Y. Nishihara, K-i. Funakoshi, and N. Sata (2008), Phase relations in the system MgO-FeO-SiO_2 to 50 GPa and 2000 degree C: An application of experimental techniques using multianvil apparatus with sintered diamond anvils, *J. Geophys. Res*.

Tasaka, Y., Y. Takeda, and T. Yanagisawa (2008), Ultrasonic visualization of thermal convective motion in a liquid gallium layer, *Flow Measurement and Instrumentation, 19*, 131-137.

Tasaka, Y., K. Yonekura, Y. Takeda, and T. Yanagisawa (2008), Dilatation and Pattern Formation of Cells in Internally Heated Convection, *Journal of Visualization, 11*, 213-220.

Tasaka, Y., Y. Kudoh, Y. Takeda, and T. Yanagisawa (2005), Experimental investigation of natural convection induced by internal heat generation, *Journal of Physics: Conference Series 14*, 168-179.

Tateno, S., K. Hirose, N. Sata, and Y. Ohishi (2008), Determination of post-perovskite phase transition boundary up to 4400 K and implications for thermal structure in D" layer, *Earth Planet. Sci. Lett., 277*, 1-2, 130-136.

Tateno, S., K. Hirose, N. Sata, and Y. Ohishi (2007), Solubility of FeO in (Mg,Fe)SiO_3 perovskite and the postperovskite phase transition, *Phys. Earth Planet. Inter., 160*, 319-325.

Tateno, S., K. Hirose, N. Sata, and Y. Ohishi (2005), Phase relations in $Mg_3Al_2Si_3O_{12}$ to 180 GPa: Effect of Al on post-perovskite phase transition, *Geophys. Res. Lett., 32*, doi:10.1029/2005GL023309-2005.

Tateno, S., K. Hirose, N. Sata, and Y. Ohishi (2005), High-pressure behavior of $MnGeO_3$ and $CdGeO_3$ perovskites and the post-perovskite phase transition, *Phys. Chem. Mineral., 32*, doi:10.1007/s00269-005-0049-7-2005.

Y. Hamano, T. Yanagisawa, Y. Yamagishi (2005), Geodynamo and Mantle Dynamics, *Journal of Geography, 114(2)*, 142-150. (in Japanese)

Y. Tasaka, T. Yanagisawa, Y. Yamagishi, M. Yoshida, Y. Takeda, (2006) Measurement of Liquid Metal Flow using Ultrasonic Velocity Profiler : 2nd Report, Visualization of Thermal Convective Motion in Liquid Gallium Layer, Transactions of the Japan Society of Mechanical Engineers. B, 72, 1559-1565. (in Japanese)

Yanagisawa, T., Y. Yamagishi, A. Sakuraba, Y. Tasaka, K. Yano, Y. Takeda, and Y. Hamano (2008), Measurement of turbulent thermal convection in liquid metal under uniform magnetic field, *Proceedings of the 6th International Symposium on Ultrasonic Doppler Methods for Fluid Mechanics and Fluid Engineering*, 175-178.

Yanagisawa, T., and Y. Yamagishi (2005), Rayleigh-Benard convection in spherical shell with infinite Prandtl number at high Rayleigh number, *Journal of the Earth Simulator, 4*, 11-17.

Yano, K., Y. Tasaka, Y. Murai, Y. Takeda, and T. Yanagisawa (2008), Ultrasonic investigation on coupling of flows between liquid and liquid metal layers, *Proceedings of the 6th International Symposium on Ultrasonic Doppler Methods for Fluid Mechanics and Fluid Engineering*, 179-182.

Yusa, H., T. Tsuchiya, J. Tsuchiya, N. Sata, and Y. Ohishi (2008), alpha-Gd_2S_3-type structure in In_2O_3: Experiments and theoretical confirmation of a high-pressure polymorph in sesquioxide, *Phys. Rev. B, 78*, doi:10.1103/PhysRevB.78.092107.

Yusa, H., T. Tsuchiya, N. Sata, and Y. Ohishi(2008), Rh_2O_3(II)-type structures in Ga_2O_3 and In_2O_3 under high pressure: Experiment and theory, *Phys. Rev. B, 77*, doi:10.1103/PhysRevB.77.064107.

Yusa, H., N. Sata, and Y. Ohishi (2007), Rhombohedral (9R) and hexagonal (6H) perovskites in barium silicatesunder high pressure, *Am. Mineral., 92*, 648-654.

Yusa, H., M. Akaogi, N. Sata, H. Kojitani, R. Yamamoto, and Y. Ohishi (2006), High-pressure transformations of ilmenite to perovskite, and lithium niobate to perovskite in zinc germanate, *Phys. Chem. Mineral., 33*, 217-226.

Yusa, H., M. Akaogi, N. Sata, H. Kojitani, Y. Kato, and Y. Ohishi (2005), Unquenchable hexagonal perovskite in high pressure polymorphs of strontium silicates, *Am. Mineral., 90*, 1017-1020.

Publications for §7

(Names of the IFREE members underlined)

Fujiwara, T., N. Hirano, N. Abe and K. Takizawa (2007), Subsurface structure of the "petit-spot" volcanoes on

the northwestern Pacific Plate, *Geophysical Research Letters, 34*, L13305, doi:10.1029/2007GL030439.

Gooday, A. J., Y. Todo, K. Uematsu, and H. Kitazato (2008), New organic-walled Foraminifera (Protista) from the ocean's deepest point, the Challenger Deep (western Pacific Ocean), *The Zoological Journal to the Linnean Society, 153*, 399-423

Gooday, A.J., O.E. Kamenskaya and H. Kitazato (2008), The enigmatic, deep-sea, organic-walled foraminiferal genera Chitinosiphon, Nodellum and Resigella (Protists): a taxonomic re-evaluation, Systematics and Biodiversity, 6, 3, 385-404.

Gooday, A. J., H. Nomaki and H. Kitazato (2008), Modern deep-sea benthic foraminifera: a brief review of their morphology-based biodiversity and trophic diversity, edited by Austin, W.E.N. and R.H. James, *Biogeochemical Controls on paleoceanographic environmental proxie*, Geol. Soc. London, Special Publications, 303, 97-119.

Hirano, N., A. A. P. Koppers, A. Takahashi, T. Fujiwara, and M. Nakanishi (2008), Seamounts, knolls and petit spot monogenetic volcanoes on the subducting Pacific Plate, *Basin Research, 20(4)*, 543-553, doi:10.1111/j.1365-2117.2008.00363.x.

Hirano, N., E. Takahashi, J. Yamamoto, N. Abe, S. P. Ingle, I. Kaneoka, J. Kimura, T. Hirata, T. Ishii, Y. Ogawa, S. Machida, and K. Suyehiro (2006), Volcanism in response to plate flexure, *Science, 313(5792)*, 1426-1428, doi:10.1126/science.1128235.

Hirano, N., J. Yamamoto, H. Kagi, and T. Ishii (2004), Young, olivine xenocryst-bearing alkali-basalt from the oceanward slope of the Japan Trench, *Contributions to Mineralogy and Petrology, 148(1)*, 47-54, doi:10.1007/s00410-004-0593-z.

K. Baba, N. Abe, N. Hirano, T. Fujiwara, M. Ichiki, S. Machida, A. Takahashi, J. Yamamoto, M. Yamano, H. Hamamoto, H.Sugioka, A. Shito (2007), プチスポット総合調査, *月刊地球*, *29(9)*, 548-553

Kitazato, H., K. Uematsu, Y. Todo, and A.J. Gooday (2009), New species of *Leptohalysis* (Rhizaria, Foraminifera) from an extreme hadal site in the western Pacific Ocean, *Zootaxa*.

Machida, S., N. Hirano, and J. Kimura (2009), Evidence for recycled plate material in Pacific upper mantle unrelated to plumes, *Geochimica et Cosmochimica Acta*, doi:10.1016/j.gca.2009.01.026.

Nozawa, F., H. Kitazato, M. Tsuchiya and A. J. Gooday (2006), Benthic foraminifera at three abyssal sites in the equatorial Pacific nodule province: abundance, diversity and taxonomic composition, *Deep-sea Research, I, 53*, 1406-1422.

Szarek, R.T., H. Nomaki, and H. Kitazato (2007), Living deep-sea benthic foraminifera from the warm and oxygen-depleted environment of the Sulu Sea, *Deep-sea Research, II, 54*, 145-176.

Todo, Y., H. Kitazato, A. J. Hashimoto and A. J. Gooday (2005), Simple foraminifera flourish at the ocean's deepest point, *Science, 307*, 68

Toh, H., Y. Hamano, M. Ichiki, and H. Utada (2004), Geomagnetic observatory operates at the seafloor in the Northwest Pacific Ocean, *Eos, Trans. Am. Geophys. Union, 85*, 467-473.

Toh, H., Y. Hamano and M. Ichiki (2006), Long-term seafloor geomagnetic station in the northwest Pacific: A possible candidate for a seafloor geomagnetic observatory, *Earth Planets Space, 58*, 697-705.

Publications for §8
(Names of the IFREE members underlined)

Ishizuka, O. (2008), Study of age stratigraphy usinf the Daisuishin-Kiso-Tyosa data, *Report on the Daisuishin-Kiso-Tyosa collaborative study in 2007*, (in Japanese).

Japanese government(2009), *Executive summary: Japan's Submission to the Commission on the Limits of the Continental Shelf.*

Kodaira, S., T. Sato, N. Takahashi, M. Yamashita, T. No and Y. Kaneda (2008), Seismic imaging of a possible paleoarc in the Izu-Bonin intraoceanic arc and its implications for arc evolution processes, *Geochem. Geophys. Geosyst., 9*, Q10X01, doi:10.1029/2008GC002073.

Kodaira, S., T. Sato, N. Takahashi, S. Miura, Y. Tamura, Y. Tatsumi and Y. Kaneda (2007), New seismological constraints on growth of continental crust in the Izu-Bonin intra-oceanic arc, *Geology, 35*, 11, doi: 10.1130/G23901A, 1031-1034.

Kodaira, S., T. Sato, N. Takahashi, A. Ito, Y. Tamura, Y. Tatsumi and Y. Kaneda(2007), Seismological evidences for variation of continental growth along the Izu intra-oceanic arc and its implication for arc volcanism, *J. Geophys. Res., 112*, B05104, doi: 10.1029/2006JB004593.

Sato, T., S. Kodaira, N. Takahashi, Y. Tatsumi and Y. Kaneda (2008), Amplitude modeling of the seismic reflectors in the crust-mantle transition layer beneath the volcanic front along the northern Izu-Bonin island arc, *Geochem. Geophys. Geosyst., 10*, Q02X04, doi:10.1029/2008GC001990.

Suyehiro, K., N. Takahashi, Y. Ariie, Y. Yokoi, R. Hino, M. Shinohara, T. Kanazawa, N. Hirata, H. Tokuyama, and A. Taira (1996), Continental crust, crustal underplating, and low-Q upper mantle beneath an oceanic island arc, *Science, 272*, 390-392.

Takahashi, N., S. Kodaira, Y. Tatsumi, M. Yamashita, T. Sato, Y. Kaiho, S. Miura, T. No, K. Takizawa and Y. Kaneda, Structural variations of arc crusts and rifted margins in southern Izu-Ogasawara arc-backarc system, *Geochem. Geophys. Geosyst*., (submitted).

Takahashi, N., S. Kodaira, Y. Tatsumi, Y. Kaneda, and K. Suyehiro (2008), Structure and growth of the Izu-Bonin-Mariana arc crust: 1. Seismic constraint on crust and mantle structure of the Mariana arc?back-arc system, *J. Geophys. Res., 113*, B01104, doi:10.1029 /2007JB005120.

Takahashi, N., S. Kodaira, S. Klemperer, Y. Tatsumi, Y. Kaneda and K. Suyehiro (2007), Crustal structure and evolution of the Mariana intra-oceanic island arc, *Geology, 35*, 3, 203-206, doi:10.1130/G23212A.

Tatsumi, Y., K. Tani, T. Kogiso, N. Takahashi and S. Kodaira (2008), Structure and growth of the Izu-Bonin-Mariana arc crust: II. Arc evolution, continental crust formation. and crust-mantle transformation, *J. Geophys. Res., 113*, B02203, doi:10.1029/2007JB005121.